

UNIVERSITÀ
DEGLI STUDI
DI PADOVA

Sede Amministrativa: Università degli Studi di Padova
Dipartimento di *Scienze Biomediche*

SCUOLA DI DOTTORATO DI RICERCA IN BIOSCIENZE E BIOTECNOLOGIE
INDIRIZZO: GENETICA E BIOLOGIA MOLECOLARE DELLO SVILUPPO
CICLO XXIV

Unraveling the role of collagen VI in the central and peripheral nervous system

Direttore della Scuola: Ch.mo Prof. Giuseppe Zanotti

Coordinatore d'indirizzo: Ch.mo Prof. Paolo Bonaldo

Supervisore: Ch.mo Prof. Paolo Bonaldo

Dottoranda: Matilde Cescon

Abstract	I
Part I	
1. Introduction	1
1.1 The ECM in the skeletal muscle	1
1.2 Collagen VI	3
1.3 Collagen VI null mouse model	5
1.4 The autophagic pathway in skeletal muscle	7
1.5 Study of autophagy in collagen VI null mice	10
Part II	
1. Introduction	23
1.1 The ECM in the nervous system	23
1.2 Collagen VI in PNS and CNS	25
1.3 Autophagy in the nervous tissue	27
1.4 <i>In vitro</i> models to study neural processes	30
2. Methods	33
2.1 Mice	33
2.2 Behavioural tests	33
2.3 CNS analysis	34
2.3.1 Brain and spinal cord sections	34
2.3.2 Primary neural cultures	36
2.4 PNS analysis	38
2.4.1 Sciatic nerve sections	38
2.4.2 Analysis on teased fibers	39
2.5 Microscopy analysis	39
2.6 Statistical analysis	39
3. Results	41
3.1 Collagen VI detection in the nervous system	41
3.2 Analysis of the role of collagen VI in the CNS	41

3.2.1	Establishment and characterization of primary neural cell cultures in wild-type and <i>Col6a1</i> ^{-/-} mice.	41
3.2.2	Production of collagen VI by neural cell cultures	42
3.2.3	Lack of collagen VI affects the neuronal fraction and causes increased apoptosis in neural cell cultures	42
3.2.4	Lack of collagen VI causes alterations of the mitochondrial network in neural cell cultures	43
3.2.5	The autophagic flux is impaired in <i>Col6a1</i> ^{-/-} neural cell cultures	44
3.2.6	<i>Col6a1</i> ^{-/-} neural cell cultures are more vulnerable to oxidative damage	46
3.2.7	Neurodegeneration hallmarks in aged <i>Col6a1</i> ^{-/-} mice.	47
3.3	Analysis of the role of collagen VI in the PNS	49
3.3.1	Lack of collagen VI leads to hypermyelination and alterations in Remak bundles	49
3.3.2	<i>Col6a1</i> ^{-/-} mice display abnormalities in motor and sensory functions	50
4.	Discussion	53
5.	Figures	67
	References	97

Abstract

Collagen VI is an extracellular matrix protein expressed in different tissues, such as skin, peripheral nerves, cartilages and skeletal muscle. It consists of three alpha chains encoded by separate genes. Mutations of collagen VI genes in humans cause several muscle diseases, including Bethlem myopathy and Ullrich congenital muscular dystrophy. Collagen VI null (*Col6a1*^{-/-}) mice display an early onset myopathic phenotype characterized by organelle defects, mitochondrial dysfunction and spontaneous apoptosis.

During my first PhD year, I was involved in a large project aimed at elucidating collagen VI patho-molecular defects in muscle disorders. This led to demonstrate that the persistence of altered organelles and apoptosis in collagen VI deficient muscles is due to defective regulation of autophagy in myofibers. In particular, I performed experiments aimed at assessing the relationships between autophagy and apoptosis in wild-type and *Col6a1*^{-/-} muscles, either in basal condition or after different genetic, nutritional and pharmacological treatments.

During the second part of my PhD study, I decided to focus the study of collagen VI in another compartment, the nervous tissue. Indeed, alterations of the autophagic clearance machinery are known to cause detrimental effects in several organs, particularly in the central nervous system. Moreover, recent findings showed that collagen VI can protect neurons from the toxicity of A β peptides, a critical step in the pathogenesis of Alzheimer's disease, and from UV-irradiation-induced apoptosis. To investigate the role of collagen VI in the central nervous system, I established cortical and hippocampal primary cultures from brains of neonatal wild-type and *Col6a1*^{-/-} mice and analyzed some cellular processes and molecular pathways, which we previously found to be altered in the skeletal muscle in the absence of collagen VI. In wild-type cultures, collagen VI was found to be localized on the surface of both neurons and glial cells. *Col6a1*^{-/-} neural cultures displayed a significant increase of spontaneous apoptosis, that could be rescued by plating them onto purified collagen VI. Biochemical analysis of autophagic markers revealed a noticeable increase of p62 levels in *Col6a1*^{-/-} neural cell extracts and a reduced level of LC3-II in basal conditions. Further experiments, carried out by directly monitoring LC3 lipidation and by measuring fluorescent autophagy puncta in neural cell cultures from transgenic GFP-LC3;*Col6a1*^{+/+} and GFP-LC3;*Col6a1*^{-/-} under different conditions, allowed establishing that the autophagic flux of neural cultures is impaired in the absence of collagen VI. Furthermore, *Col6a1*^{-/-} neural cell cultures displayed higher vulnerability to oxidative stress. These *in vitro* findings indicate that lack of collagen VI leads to increased apoptosis and to defective autophagic regulation

in neural cells. Further *in vivo* studies carried out in brain sections from wild-type and *Col6a1*^{-/-} mice of different ages showed that known autophagic regulators are altered, apoptosis is higher and rotarod test performance is reduced in aged *Col6a1*^{-/-} mice, thus suggesting a protective role for collagen VI in the central nervous system during aging.

Finally, during the last year, I carried out some studies also in the peripheral nervous system of wild-type and *Col6a1*^{-/-} mice, considering previous work from our laboratory showing that Schwann cells express collagen VI during development. These studies showed that the protein is abundant in the endoneurium of sciatic nerves and that lack of collagen VI causes structural defects, including increased myelin thickness and abnormalities of Remak bundles, as well as motor and sensory functional defects.

Altogether, these findings reveal an unforeseen new role for collagen VI in both central and peripheral nervous system compartments, where it seem to exert different structural and functional effects, thus opening the field for further investigations in patients.

Riassunto

Il collagene VI è una proteina della matrice extracellulare espressa in diversi tessuti come pelle, nervi periferici, cartilagine e muscolo scheletrico. La proteina è costituita dalle catene polipeptidiche, $\alpha 1(VI)$, $\alpha 2(VI)$ ed $\alpha 3(VI)$, codificate da tre geni distinti. Mutazioni a carico di tali geni causano nell'uomo disordini muscolari come la miopatia di Bethlem e la distrofia muscolare congenita di Ullrich. I topi privi di collagene VI (*Col6a1*^{-/-}) mostrano un fenotipo miopatico, caratterizzato dalla presenza, nei muscoli scheletrici, di difetti ultrastrutturali a carico di organelli cellulari, come mitocondri e reticolo sarcoplasmatico, di una disfunzione mitocondriale ed dall'insorgenza di apoptosi spontanea.

Durante il primo anno del mio dottorato, ho partecipato ad un progetto volto alla comprensione dei meccanismi pato-molecolari alla base del difetto muscolare, in assenza del collagene VI. Questo lavoro ha dimostrato che nei topi *Col6a1*^{-/-} la ritenzione di organelli disfunzionali è dovuta ad una regolazione inefficiente del flusso autofagico nelle fibre muscolari. In particolare, in tale contesto, mi sono occupata degli esperimenti istologici e relativi all'analisi dell'apoptosi nei muscoli di topi *wild-type* e *knockout* in condizioni di controllo e sottoposti a diversi approcci di tipo genetico, nutrizionale e farmacologico.

In seconda battuta, nel corso del periodo di dottorato ho focalizzato il mio interesse sullo studio del collagene VI in un tessuto diverso, quello nervoso. Infatti recentemente è stato dimostrato che questa proteina è in grado di proteggere specificamente i neuroni dalla tossicità degli A β -peptidi, agenti critici nell'insorgenza della malattia di Alzheimer, e dalla morte cellulare indotta da radiazioni UV. Inoltre, alterazioni a carico dell'apparato autofagico sono note essere particolarmente dannose nel sistema nervoso centrale (SNC). Al fine di comprendere il ruolo del collagene VI nel SNC ho allestito colture primarie da corteccia ed ippocampo di topi neonati *wild-type* e *Col6a1*^{-/-} ed ho analizzato *in vitro* i segnali dimostratisi alterati nel muscolo scheletrico in assenza della proteina in esame. Nelle colture *wild-type* il collagene VI è localizzato sulla superficie delle cellule neuronali e gliali. Le cellule *knockout* mostrano un aumento significativo dell'apoptosi, effetto recuperato quando le colture sono piastrate su collagene VI purificato, come substrato. L'analisi biochimica di marcatori autofagici ha rivelato un alto livello di p62 ed una minore lipidazione della proteina LC3 in estratti da colture *Col6a1*^{-/-} in condizioni basali. Osservazioni condotte in colture primarie neurali derivate da topi transgenici GFP-LC3;*Col6a1*^{+/+} e GFP-LC3;*Col6a1*^{-/-} e analisi biochimiche svolte in condizioni inducenti autofagia, hanno rivelato, inoltre, un'alterazione nel flusso autofagico in assenza di collagene VI. Infine, risultati preliminari indicano una maggiore vulnerabilità delle cellule *Col6a1*^{-/-} allo stress ossidativo. Queste

osservazioni *in vitro* suggeriscono che la mancanza di collagene VI induce morte cellulare ed un'alterata risposta autofagica in cellule primarie di derivazione nervosa. Di maggior interesse è quindi la dimostrazione *in vivo* di un ruolo protettivo del collagene VI nel SNC. Analisi condotte sul cervello di topi dell'età di 23 mesi, diversamente da quanto accade in topi più giovani, hanno mostrato la presenza di aumentata apoptosi, maggiore stress ossidativo, alterati livelli di marcatori autofagici e ridotta coordinazione motoria in assenza di collagene VI, confermando l'importanza della proteina nel SNC e suggerendone un'implicazione durante il processo di invecchiamento.

Infine nell'ultimo anno, vista l'alta espressione del collagene VI nel sistema nervoso periferico (SNP), sono state condotte anche analisi a livello del nervo sciatico, volte alla comprensione del ruolo della proteina in questo tessuto. Precedenti studi, inoltre, dimostravano l'espressione della proteina durante il differenziamento delle cellule di Schwann. Le analisi finora condotte mostrano che la mancanza del collagene VI nel nervo sciatico inducono un ispessimento della mielina, alterazioni a livello ultrastrutturale nelle fibre nervose e deficit sia motori che sensoriali.

Queste evidenze nell'insieme, dimostrano una crescente importanza del collagene VI sia nel sistema nervoso centrale che periferico, in cui la proteina svolge ruoli specifici, apparentemente differenti.

1. Introduction

1.1 The extracellular matrix in skeletal muscle

In multicellular organisms the space between cells consists of a complex network of locally secreted macromolecules, called extracellular matrix (ECM), that combine to build up the characteristic structural and functional properties of the different tissues and contributing to the regulation of cell homeostasis. The ECM is able to activate specific signal transduction pathways and to modulate different functions, such as cell proliferation, migration and differentiation, by binding different receptors on the plasma membrane (Hynes, 2009). Finally, the ECM in many tissues provides the proper microenvironment, or niche, to support stem or progenitor cells in maintaining their regenerative potential (Tsang *et al.*, 2010). Many of the functions performed by the ECM thus require transmembrane adhesion receptors that bind different matrix components and interact with the cytoskeleton through adaptor proteins.

The three major groups of macromolecules particularly abundant in the ECM of all tissues are:

- proteoglycans, macromolecular complexes that bind a wide variety of extracellular molecules;
- fibrous proteins, typically collagens, that provide mechanical strength and resistance to the cells and tissues;
- multifunctional adhesive proteins, able to connect plasma membrane receptors with elements of the ECM.

Proteoglycans are a specific group of proteins bound to complex chains of polysaccharides, called glycosaminoglycans. They are ubiquitous proteins, acting as tissue organizers. Due to their charged chemical groups, proteoglycans generate a water-filled compartment, keeping the ECM hydrated. They are able to influence the differentiation and growth of specialized tissues and to modulate the activity of growth factors, by enhancing or inhibiting their action. Proteoglycans can exclude or attract other molecules and retain the permeability to lower molecular weight solutes. This can affect the concentration of some macromolecules, modulating reaction rates and promoting all interactions that are concentration dependent (Hardingham *et al.*, 1992). Proteoglycans are also involved in tumour cell growth and progression (Iozzo *et al.*, 2011).

Fibrous proteins have both structural and adhesive functions in the ECM. Some participate directly to the reinforcement of ECM, defining tightly its shape and creating a layer to which cells can attach. Collagens are the most abundant structural components of the ECM, mainly produced by fibroblasts. Made of three different polypeptide subunits, called α chains, they form triple helical structures. Each α chain is characterized by the presence of a region containing repeated Gly-Xaa-Yaa amino acid sequences, called the collagenic domain. The three α chains can assemble as homotrimers or heterotrimers, giving rise to different combinations. Collagens can be divided in different subgroups: (i) fibrillar collagens (types I, II, III, V, and XI), (ii) fibril associated collagens with interrupted triple helix (types IX, XII, XIV, XVI and XIX), (iii) beaded microfilaments (type VI); (iv) multiplexin family (types VII, XV and XVIII), (v) network forming (types IV and VII which form respectively basal lamina and anchoring fibrils). The alignment and density of collagens are the primary determinants of the tensile strength of the ECM (Goody and Henry, 2010).

A specialized form of ECM adjacent to or surrounding a large variety of cells is called basement membrane, whose major components are laminins, collagen IV, nidogens and the heparan sulphate proteoglycan perlecan. Laminins and collagen IV form independent networks that are connected by nidogens and perlecan. The basement membrane is associated with cells through interactions with plasma membrane receptors, such as integrins and dystroglycan (Carmignac and Durbeej, 2012).

Although the skeletal muscle is mostly studied according to its properties related to the major component of contractile fibers, this tissue is also made of connective tissue, blood vessels and nerves that strongly influence its function. In particular, evidence indicates that the ECM affects muscle normal function, its ability to adapt and the biological reservoir of muscle stem cells including satellite cells (Gillies *et al.*, 2011). Skeletal muscle fibers are coated by a layer of ECM in the form of a basement membrane. Each skeletal muscle contains different portions of specialized connective tissue layers called endomysium, perimysium and epimysium, which correspond to the structures enwrapping a single muscle fiber, a fiber bundle, and the entire muscle, respectively. The endomysial basement membrane is made of a basal lamina (BL) and a fibroreticular lamina (FL) consisting of a network of collagen fibrils embedded in a ground substance (Campbell and Stull, 2003). The FL is characterized by the presence of a microfilamentous network of collagen VI, which guarantees the connection between the BL and the interstitial connective tissue (Kuo *et al.*, 1997).

In the BL the most abundant protein is collagen IV, whose subunits have terminal non-collagenous domains. Specific laminin isoforms are differentially expressed in BL during

myogenesis; in the adult muscle, the predominant isoforms are laminin-211 ($\alpha 2\beta 1\gamma 1$) and laminin-221 ($\alpha 2\beta 2\gamma 1$), known together as merosin. The networks of collagen IV and laminin are able to self-assemble and are linked to each other by nidogen glycoprotein. These core components bear a number of sites that bind other BL components and serve as ligands for transmembrane receptors, such as integrins and dystroglycans, which in turn interact with the cell cytoskeleton (Gullberg *et al.*, 1999; Sanes, 2003). Hence, the whole system allows myofibers to be tightly anchored to the BM, in turn connected to the surrounding connective tissues. This provides a mechanical support to contraction and an efficient communication between the intracellular and the extracellular environments (Kovanen, 2002; Campbell and Stull, 2003).

Considering the complex architecture of the BM and the variety of key roles played by muscle ECM, it is implicit that mutations in genes encoding its proteins and their receptors account for several types of muscular dystrophies (Carmignac and Durbeej, 2012).

1.2 Collagen VI

Collagen VI is a protein largely found in the ECM of several organs, such as skeletal muscle, tendons, skin, lungs, heart, adipose tissue, cartilages, intervertebral disks and peripheral nerves (Kuo *et al.*, 1997). Collagen VI is composed of three genetically distinct polypeptide α chains, namely $\alpha 1(\text{VI})$ (140 kDa), $\alpha 2(\text{VI})$ (130 kDa) and $\alpha 3(\text{VI})$ (250-350 kDa), which assemble into a triple helical monomer in a 1:1:1 stoichiometric ratio (Colombatti and Bonaldo, 1987; Colombatti *et al.*, 1995).

The $\alpha 1(\text{VI})$ and $\alpha 2(\text{VI})$ chains are encoded by *COL6A1* and *COL6A2* genes, which are organized in a head-to-tail fashion on chromosome 21q22.39, while the *COL6A3* gene encodes the $\alpha 3(\text{VI})$ chain and maps to 2q37 chromosome (Lampe and Bushby, 2005). All three chains contain a central short triple helical domain of 335-336 amino acids flanked by large N- and C-terminal globular domains mostly consisting of motifs of 200 amino acids sharing similarity with the von Willebrand factor type A (vWF-A) module. The $\alpha 1(\text{VI})$ and $\alpha 2(\text{VI})$ chains contain one N-terminal- and two C-terminal vWF-A modules (N1, C1 and C2, respectively), while the $\alpha 3(\text{VI})$ chain displays larger globular domains, with ten N-terminal vWF-A modules (N1-N10) and five C-terminal modules (C1-C5), where C1 and C2 are vWF-A like, C3 is a proline-rich domain, C4 is a fibronectin type III domain and C5 is a Kunitz-like domain (Bonaldo and Colombatti, 1990) (Fig. 1). Moreover, *COL6A3* transcripts undergo

extensive alternative splicing, generating multiple polypeptides with a different number of vWF-A modules (Saitta *et al.*, 1990; Doliana *et al.*, 1998).

The assembly of collagen VI is a complex multistep process. Association of the three $\alpha 1(\text{VI})$, $\alpha 2(\text{VI})$ and $\alpha 3(\text{VI})$ chains to form a triple helical monomer is followed by the assembly into disulfide-bonded antiparallel dimers, which then align to form tetramers, also stabilised by disulfide bonds. Outside the cell, tetramers, the secreted form of collagen VI, associate end-to-end by non-covalent bonds to form the characteristic beaded microfilaments (Bernardi and Bonaldo, 2008).

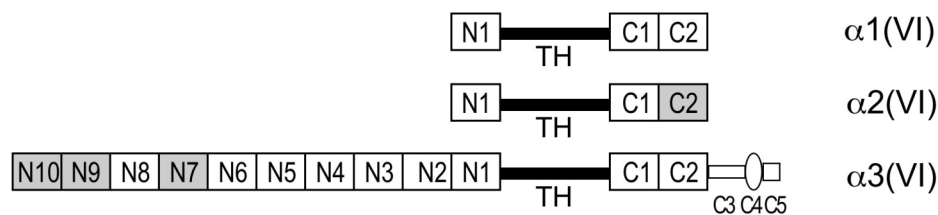


Figure 1. Primary structure of the $\alpha 1(\text{VI})$, $\alpha 2(\text{VI})$, $\alpha 3(\text{VI})$ chains. Grey squares highlight domains that can undergo alternative splicing. TH, triple helical region.

Given its complex structure and variety of domains, collagen VI is able to bind different components of the ECM, not only bridging cells to the surrounding connective tissue, but also being involved in intracellular signalling since it can interact with several membrane receptors. For instance, by binding basal lamina collagen IV and decorin, collagen VI allows the formation of a physical connection between muscle cells and ECM (Kuo *et al.*, 1997). Moreover, interactions with other ECM components, including collagen I, collagen II and fibronectin, were reported. Different membrane receptors, such as $\alpha_1\beta_1$ and $\alpha_2\beta_1$ integrins and NG2 proteoglycan, were found to bind collagen VI and transduce intracellular signals by acting on the cytoskeleton (Sabatelli *et al.*, 2001; Burg *et al.*, 1996; Stallcup *et al.*, 2002). Recent studies demonstrated that the absence of collagen VI in skeletal muscle has a dramatic impact on muscle fibers and alters molecular signals and cell viability, but the nature of the cell receptor(s) accountable for these effects and thus mediating collagen VI signals in muscle are still unknown (Irwin *et al.*, 2003; Grumati *et al.*, 2010).

The critical role of collagen VI in skeletal muscle is witnessed by the fact that mutations in the genes encoding collagen VI chains were shown to be responsible for several forms of inherited human skeletal muscle diseases, including Bethlem myopathy (BM), Ullrich congenital muscular dystrophy (UCMD) and myosclerosis myopathy (Lampe and

Bushby, 2005; Bönnemann, 2011). UCMD represents the second most frequent form of congenital muscular dystrophy and it is characterized by a severe early-onset muscle weakness with proximal limb contractures, distal hyperlaxity, rigid spine and a rapid progression of symptoms leading to respiratory distress (Brinas *et al.*, 2010). BM usually follows a relatively mild course characterized by proximal muscle weakness and joint contractures mainly involving the elbows, ankles, and fingers, with limited or no progression of symptoms (Lampe and Bushby, 2005). Myosclerosis myopathy is characterized by early and diffuse contractures resulting in severe limitation of movement of axial, proximal, and distal joints, and in a “woody” consistence of muscles (Merlini *et al.*, 2008b).

1.3 Collagen VI null mouse model

To investigate the function of collagen VI *in vivo*, a knockout null mouse was produced by targeted inactivation of the second exon of the *Col6a1* gene. The generated mutation causes an interruption of the coding sequence of the *Col6a1* gene just below the translation start codon and the signal peptide sequence, thus leading to the complete absence of the $\alpha 1(\text{VI})$ chain in homozygous null (*Col6a1*^{-/-}) mice. Although $\alpha 2(\text{VI})$ and $\alpha 3(\text{VI})$ chains are normally transcribed, the absence of $\alpha 1(\text{VI})$ prevents the formation of collagen VI monomers, so that the assembly and secretion of collagen VI do not occur, and *Col6a1*^{-/-} mice completely lack the protein in their tissues (Bonaldo *et al.*, 1998).

Despite the widespread distribution of collagen VI in different tissues during embryonic and postnatal development, *Col6a1*^{-/-} mice undergo normal development, are fertile and do not display any obvious anatomical alteration, thus suggesting that the lack of collagen VI can be at least in part compensated by other ECM components. Nonetheless, *Col6a1*^{-/-} mice are affected by a early onset myopathic disease characterized by muscle weakness, decreased strength and structural defects of skeletal muscles (Bonaldo *et al.*, 1998). Histological analysis of *Col6a1*^{-/-} mice muscles shows the presence of degenerating myofibers, centrally nucleated myofibers and variability of myofiber cross-sectional areas, all hallmarks of myopathy. Ultrastructural analysis of *Col6a1*^{-/-} muscles revealed the presence of abnormal mitochondria and dilated sarcoplasmic reticulum (SR) cisternae; in addition, electrondense nuclei were found in some myofibers, suggesting activation of apoptosis (Irwin *et al.*, 2003) (Fig. 2).

Further studies confirmed that lack of collagen VI has a remarkable impact on myofiber homeostasis. Indeed, TUNEL analysis, showed a marked increase of spontaneous apoptosis *Col6a1*^{-/-} diaphragms when compared to the corresponding wild-type muscles.

Experiments on *ex vivo* myofibers isolated from *flexor digitorum brevis* (FDB) muscle revealed the presence of a latent mitochondrial dysfunction (Irwin *et al.*, 2003). Mitochondrial membrane potential was monitored by fluorescence microscopy using tetramethylrhodamine-methyl-ester (TMRM), a lipophilic positively charged fluorescent probe that loads energized mitochondria and is released upon mitochondria depolarization. The addition of oligomycin, a drug inhibiting the mitochondrial F₁F₀ ATP-synthase, unmasked a latent mitochondrial dysfunction in *Col6a1*^{-/-} myofibers, which rapidly showed mitochondrial depolarization, differently from wild-type ones. This defect was linked to an increased opening of the permeability transition pore (PTP), a large channel localized in the inner membrane of mitochondria (Irwin *et al.*, 2003). PTP opening leads to mitochondria depolarization, also causing the release of cytochrome *c*, thus triggering apoptosis (Bernardi and Bonaldo, 2008).. Addition of cyclosporin A, a drug able to bind mitochondrial cyclophilin D and desensitize PTP opening, rescued both mitochondrial and apoptotic phenotypes of isolated *Col6a1*^{-/-} myofibers. The same effect was achieved when myofibers were grown onto purified native collagen VI used as substrate. Remarkably, *in vivo* administration of cyclosporin A for four days to *Col6a1*^{-/-} mice rescued the apoptotic and mitochondrial defects and led to a marked recovery from the myopathic phenotype (Irwin *et al.*, 2003).

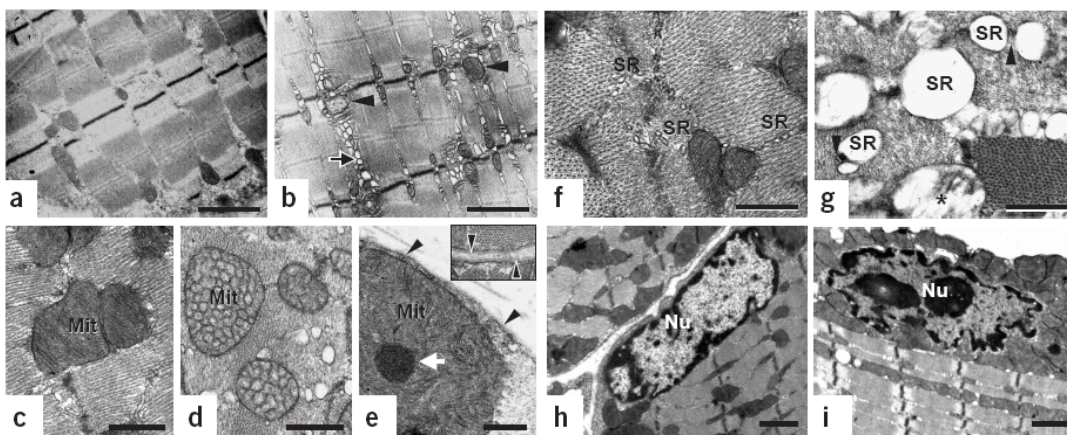


Figure 2. Ultrastructural defects in *Col6a1*^{-/-} muscles. Electron microscopy of wild-type (a,c,f,h) and *Col6a1*^{-/-} muscles (b,d,e,g,i). Mit: mitochondria, Nu: nucleus, SR: sarcoplasmic reticulum (Irwin *et al.*, 2003).

Since the phenotypic features displayed by *Col6a1*^{-/-} mice are similar to those detected in BM and UCMD patients, these pioneering studies carried out in mice led to the understanding of the pathophysiological defects underlying BM and UCMD. Indeed, muscle biopsies from BM/UCMD patients also revealed the presence of a high incidence of apoptosis when

compared to non-affected donors, and myoblasts derived from BM/UCMD biopsies displayed remarkably similar defects to *Col6a1*^{-/-} myofibers, with latent mitochondrial dysfunction and spontaneous apoptosis. As for the mouse model, these defects were recovered by treatment with cyclosporin A or adhesion onto collagen VI (Angelin *et al.*, 2007). Based on these findings, a pilot clinical trial with cyclosporin A was carried out on some UCMD and BM patients, and after one month of drug treatment a significant reduction of the mitochondrial/apoptotic phenotype was achieved (Merlini *et al.*, 2008a).

More recently, further studies were carried out in *Col6a1*^{-/-} mice in order to get a better understanding of the pathogenic mechanisms and of the molecular pathways involved in the onset of the myopathic disease caused by collagen VI deficiency. In particular, a critical role for the autophagic pathway was addressed (Grumati *et al.*, 2010).

1.4 The autophagic pathway in skeletal muscle

Autophagy is a complex process leading to bulk lysosomal degradation mainly of long-lived proteins and damaged organelles. Different types of autophagy were defined so far, including microautophagy, macroautophagy and chaperone-mediated autophagy, which differ between each other based on their mechanisms and functions. Microautophagy permits the degradation of small amounts of cytoplasm, directly enwrapped by the lysosomal membrane. Macroautophagy (often simply referred to as “autophagy”) is deputed to the degradation of higher amounts of cytoplasm, in order to recycle proteins or aged organelles, through the formation of a new temporary cellular compartment, called autophagosome, which is targeted to lysosomal digestion. Differently from these two types of autophagy, which mediate both selective and non-selective degradation, the chaperone-mediated autophagy process degrades only soluble proteins in a selective manner (Mizushima *et al.*, 2008).

The ability that the cells display to get rid of materials that could become harmful for survival and to recycle them, thus obtaining new useful metabolites for energy sources, is important for cellular and tissue homeostasis. On the other hand, unregulated degradation could carry a certain risk. Therefore, autophagy is tightly regulated through a complex network of interacting components (Fig. 3).

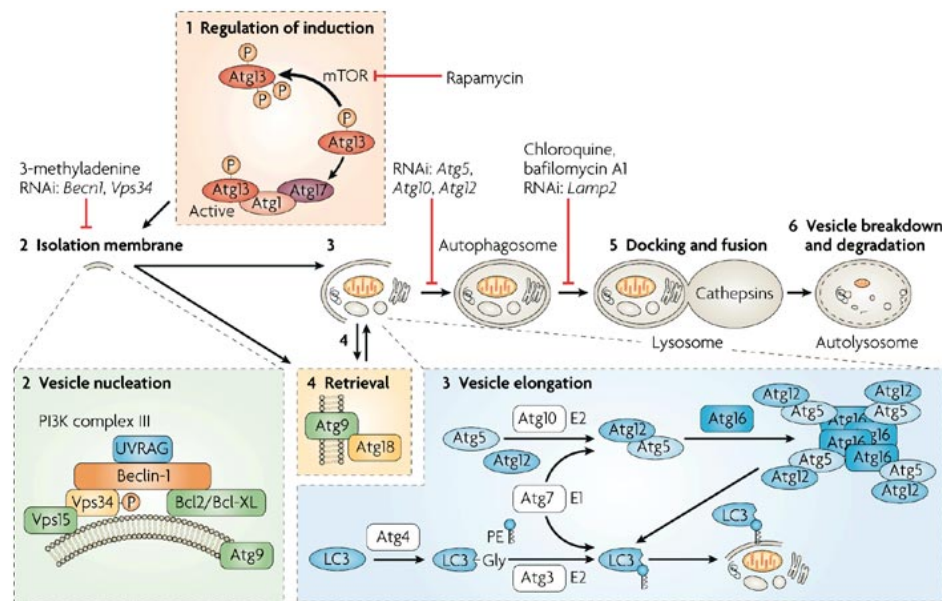


Figure 3: Autophagy is a process made of different steps: autophagy induction (1), autophagic membrane nucleation (2), vesicular membrane elongation (3), retrieval mechanisms (4), lysosome to autophagosome fusion (5), and autophagosome degradation (6) (Maiuri *et al.*, 2007).

The autophagic process involves a set of evolutionary conserved proteins, known as Atg proteins, required in particular for the formation of the autophagosome. Autophagosome formation involves two major steps: *i*) nucleation, and *ii*) elongation of the so-called isolation membrane, able to sequester material in double membrane vesicles. In many cellular settings, a major regulatory step involves the mTOR (mammalian Target Of Rapamycin) Ser/Thr kinase, which inhibits autophagy by phosphorylating Atg13. This event leads to the dissociation of Atg13 from a protein complex containing Atg1 kinase and Atg17. When mTOR is inhibited, the re-association of dephosphorylated Atg13 with Atg1 stimulates its catalytic activity thus inducing autophagy (Maiuri *et al.*, 2007). ULK/Atg1 kinase complex and phosphatidylinositol-3-phosphate (PI3P) effectors are critical for the membrane nucleation step (Mizushima *et al.*, 2010). Vps34 activation, a class III phosphatidylinositol-3-kinase, is necessary for vesicle nucleation and depends on the formation of a multiprotein complex that includes Beclin-1 (Becn1/Atg6), UVRAG, Ambra-1 and Atg15.

The subsequent steps require two ubiquitin-like conjugation systems, Atg12-Atg5 and Atg8 (LC3)-PE (phosphatidyl-ethanolamine) (Fig. 3). Atg12 is first activated by Atg7 (working like an ubiquitin-activating E1 enzyme) and then transferred to Atg10 (similar in function to an E2 enzyme). After this, Atg7 is released and Atg12 covalently binds to Atg5. Atg10 is also released and the binding of Atg16L to this complex allows the elongation of the pre-autophagosomal membrane. Finally, the Atg12-Atg5 complex dissociates from the mature

autophagosome (Ferraro *et al.*, 2007). The second ubiquitin-like molecule essential for the autophagy process completion is LC3. LC3 is cleaved by Atg4 to produce the active cytosolic form LC3-I. Subsequent modifications are mediated by Atg7, which transfers LC3-I to Atg3 and induces its binding to PE, generating a lipidated membrane-bound form of LC3 called LC3-II. The two conjugation systems are tightly related to each other: if the first one is defective, the second one cannot target the pre-autophagosomal structures (Ferraro *et al.*, 2007). LC3-II remains inserted in the membrane of autophagosomes until their degradation by lysosomal hydrolases. Because of this, LC3 is currently considered the best marker to monitor the autophagic flux from its beginning to completion. A LC3-GFP transgenic mouse strain was generated, which allows monitoring autophagy induction in living tissues by fluorescence microscopy (Mizushima *et al.*, 2004; Mizushima, 2004). LC3 also binds p62 (a protein also known as sequestosome-1 or SQSTM1), which is characterized by an ubiquitin-binding domain, thus serving as a crossroad for poly-ubiquitinated proteins to be targeted to lysosomal degradation. Several studies reported that p62 is accumulated when autophagy is impaired (Moscat and Diaz-Meco, 2009; Jaeger and Wyss-Coray, 2009). Other Atg proteins are involved in specific steps of autophagy. Among them is Atg9, a membrane-bound protein localized in the preautophagosomal membrane and playing an essential role in the closure of the autophagosome (Maiuri *et al.*, 2007).

Autophagy regulation is mainly based on the phosphorylation/de-phosphorylation of some Atg proteins. The major upstream actor in these intracellular pathways is the mTOR kinase, which inhibits autophagy by regulating Atg genes transcription and translation and by directly or indirectly modifying Atg proteins. Often described as a sensor for nutrients, mTOR can control the activity of proteins regulating protein translation, such as the initiation factor 4E binding protein (4E-BP1) and the ribosomal protein S6 kinase and acts a major role in regulating switches between anabolic and catabolic metabolism (Di Bartolomeo *et al.*, 2010). Moreover, in high presence of nutrients, active mTOR induces Atg13 hyperphosphorylation, thus preventing Atg13-Atg1 interaction.

Autophagy is generally active at a basal level in most of cell types. In this manner, autophagy fulfills a critical regulative role in protein turnover and in the degradation of damaged structures. Autophagy can be stimulated by different stress conditions, such as starvation, thus maintaining the essential metabolism for cell survival. Autophagy is also involved in several pathologies, such as cancer, neurodegenerative diseases, pathogen invasion, and muscular disorders (Mizushima *et al.*, 2008). In skeletal muscle, macroautophagy is a constitutively active process, by which myocytes can adapt their

metabolism according to different conditions such as nutrients depletion or the absence of growth signals like insulin. Autophagy is rapidly induced in the post-natal age, when autophagosomes full of glycogen are frequently detected. The importance of the autophagy-lysosomal pathway for the skeletal muscle tissue is also demonstrated by different human myopathies, the so-called *autophagic vacuolar myopathies* (AVM), which are caused by deficiencies in critical proteins for lysosome function. Among them, the most well-known are Danon disease, a inherited disease caused by deficiency of LAMP-2 (lysosome-associated membrane protein-2), a lysosomal membrane-associated protein, and Pompe disease, which is caused by the absence of acid maltase, a lysosomal acid α -1,4-glucosidase able to hydrolyze glycogen into glucose. In both Pompe and Danon diseases, as well as in the X-linked myopathy with excessive autophagy (XMEA), the lysosomal impairment causes an increase in autophagic vacuoles within the myofibers, leading to the disruption of myofibrillar structures and ultimately to myofiber breakdown and loss of muscle function (Malicdan *et al.*, 2008).

Several studies demonstrated that starvation-induced autophagy in skeletal muscle is mediated by the mTOR kinase. The process is inhibited by mTOR, which in turn is directly regulated based on the levels of intracellular amino acids. mTOR is also regulated by some extracellular growth factors, such as insulin and IGF1, through the Akt kinase and according to the energy status of the cell, thorough the AMPK kinase. mTOR can activate different transcription factors, in particular the class of forkhead box O (FoxO). In basal conditions, FoxOs transcription factors are phosphorylated and inactivated by Akt, but in the absence of nutrients, the Akt pathway is inhibited and FoxOs are free to translocate into the nucleus where they bind the activate the transcription of several genes, such as Bnip3, a key protein involved in autophagy regulation (Mammuccari *et al.*, 2007).

1.5 Study of autophagy in collagen VI null mice

During my PhD, I was engaged in a large project aimed at understanding the molecular pathways underlying the myopathic phenotype of *Col6a1*^{-/-} mice. We found that lack of collagen VI leads to an impairment of the autophagic flux in skeletal muscles, due to inappropriate regulation of Beclin-1 and Bnip3 proteins, causing the accumulation of damaged organelles and leading to the apoptotic degeneration of muscle fibers. To understand the basis of the autophagy impairment, we forced autophagy activation in *Col6a1*^{-/-} mice by different nutritional and pharmacological approaches. Toward this aim, we put mice under food starvation for 24 and 30 hours, to evaluate short-term responses, and we also fed mice

for four weeks with a low protein diet, in order to study long-term results. Besides this, we treated mice with rapamycin, a well-known drug able to induce autophagy induction through mTOR inhibition. Finally, we carried out a genetic approach, by transfecting a Beclin-1-EGFP cDNA construct in muscle *in vivo*. To evaluate the responses to these different approaches, the RNA and protein levels of several autophagy-related molecules were estimated. TUNEL, histology, electron microscopy and quantitative measurement of muscle strength were also performed, to assess for muscle structural and functional features. I contributed to this work by carrying out a careful histological analysis and a quantification of myofiber apoptosis in diaphragms and tibialis anterior muscles of *Col6a1*^{-/-} and wild-type mice in all the different control and test conditions (Grumati *et al.*, 2010).

Autophagy is defective in collagen VI muscular dystrophies, and its reactivation rescues myofiber degeneration

Paolo Grumati^{1,8}, Luisa Coletto^{2,8}, Patrizia Sabatelli³, Matilde Cescon¹, Alessia Angelin⁴, Enrico Bertaglia², Bert Blaauw⁵, Anna Urciuolo¹, Tania Tiepolo¹, Luciano Merlini⁶, Nadir M Maraldi^{3,7}, Paolo Bernardi⁴, Marco Sandri^{2,4} & Paolo Bonaldo¹

Autophagy is crucial in the turnover of cell components, and clearance of damaged organelles by the autophagic-lysosomal pathway is essential for tissue homeostasis. Defects of this degradative system have a role in various diseases, but little is known about autophagy in muscular dystrophies. We have previously found that muscular dystrophies linked to collagen VI deficiency show dysfunctional mitochondria and spontaneous apoptosis, leading to myofiber degeneration. Here we demonstrate that this persistence of abnormal organelles and apoptosis are caused by defective autophagy. Skeletal muscles of collagen VI-knockout (*Col6a1*^{-/-}) mice had impaired autophagic flux, which matched the lower induction of beclin-1 and BCL-2/adenovirus E1B-interacting protein-3 (Bnip3) and the lack of autophagosomes after starvation. Forced activation of autophagy by genetic, dietary and pharmacological approaches restored myofiber survival and ameliorated the dystrophic phenotype of *Col6a1*^{-/-} mice. Furthermore, muscle biopsies from subjects with Bethlem myopathy or Ullrich congenital muscular dystrophy had reduced protein amounts of beclin-1 and Bnip3. These findings indicate that defective activation of the autophagic machinery is pathogenic in some congenital muscular dystrophies.

Macroautophagy (hereafter referred to as autophagy) is a dynamic process in which portions of cytoplasm are sequestered within double-membraned vesicles called autophagosomes and delivered to lysosomes for degradation and subsequent recycling¹⁻³. The autophagic machinery is highly conserved and has key roles in tissue homeostasis, participating in the clearance of damaged organelles, misfolded proteins and pathogens¹⁻⁴. Furthermore, autophagy is crucial for cell survival during nutrient deprivation, but it is detrimental when massively activated or inhibited². Likewise, mitochondria are essential for energy conservation, but, if damaged, they become a source of proapoptotic factors and reactive oxygen species^{5,6}. Selective removal of dysfunctional mitochondria via autophagy (mitophagy) is a key mechanism to not only preserve cell viability but also rejuvenate mitochondrial function⁷.

Congenital muscular dystrophies represent a large and heterogeneous group of inherited muscle disorders with a severe and progressive clinical course. Mutations in any of the three genes coding for collagen VI, a major extracellular matrix protein of the endomysium of skeletal muscles, cause multiple muscle diseases, including Bethlem myopathy and Ullrich congenital muscular dystrophy (UCMD)⁸. We have previously demonstrated that muscles of *Col6a1*^{-/-} mice and humans with UCMD or Bethlem myopathy have a latent mitochondrial dysfunction accompanied by ultrastructural alterations of mitochondria

and the sarcoplasmic reticulum and spontaneous apoptosis of muscle fibers^{9,10} (see also **Supplementary Fig. 1a**). However, in our previous study we did not uncover the reason for the occurrence of dysfunctional organelles. Here we show that the accumulation of abnormal mitochondria and sarcoplasmic reticulum is caused by a defect of autophagy and that restoration of a proper autophagic flux in *Col6a1*^{-/-} muscles ameliorates these alterations.

RESULTS

Autophagy is impaired in *Col6a1*^{-/-} muscles

To explore the relationship between organelle defects and muscle pathology of collagen VI muscular dystrophies *in vivo*, we examined several skeletal muscle types of *Col6a1*^{-/-} mice for the main molecular pathways linked with mitochondrial function and cell survival. We chose the diaphragm and tibialis anterior as examples of oxidative and glycolytic muscles, respectively. We did not find any substantial difference between wild-type and *Col6a1*^{-/-} muscles in the protein amounts of B cell leukemia/lymphoma-2 (Bcl-2), Bcl-2-associated X protein (Bax) and Bcl-X_L and in the phosphorylation of Akt, suggesting no major alterations in pro- or antiapoptotic pathways. However, the amount of the active form of AMP-activated protein kinase (AMPK) was increased in *Col6a1*^{-/-} muscles (**Supplementary Fig. 1b,c**). AMPK acts as an energy sensor, being activated under

¹Department of Histology, Microbiology & Medical Biotechnology, University of Padova, Padova, Italy. ²Dulbecco Telethon Institute, Venetian Institute of Molecular Medicine, Padova, Italy. ³Institute of Medical Genetics—National Research Council, Bologna, Italy. ⁴Department of Biomedical Sciences, University of Padova, Padova, Italy. ⁵Department of Human Anatomy & Physiology, University of Padova, Padova, Italy. ⁶Department of Experimental and Diagnostic Medicine, University of Ferrara, Ferrara, Italy. ⁷Department of Anatomical Sciences, University of Bologna, Bologna, Italy. ⁸These authors contributed equally to this work. Correspondence should be addressed to P. Bonaldo (bonaldo@bio.unipd.it) or M.S. (marco.sandri@unipd.it).

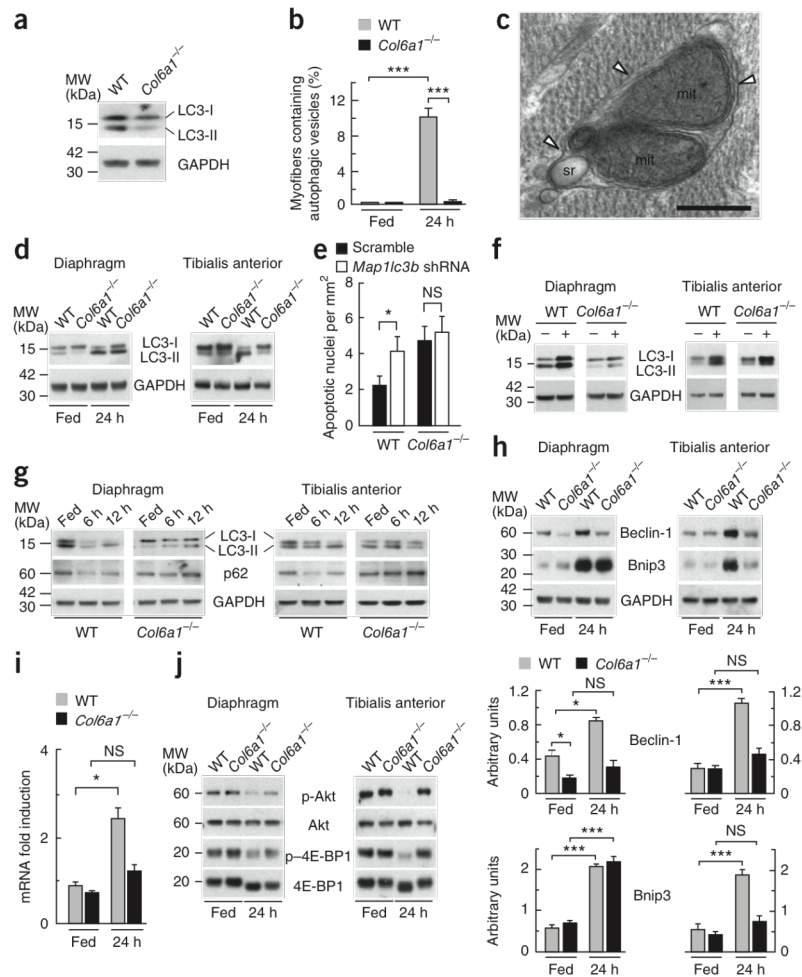
metabolic stress¹¹. These data indicate an energy imbalance in *Col6a1*^{-/-} muscles, which is readily explained by the observed mitochondrial dysfunction. Indeed, it was previously shown that *Col6a1*^{-/-} flexor digitorum brevis (FDB) myofibers have an increased incidence of dysfunctional mitochondria⁹. The presence of abnormal mitochondria with disorganized cristae (Supplementary Fig. 1d) prompted us to check whether the autophagic system was affected. Compared to wild-type mice, muscles from *Col6a1*^{-/-} mice had less of the lipidated form of microtubule-associated protein-1 light chain 3 (LC3)-II (Fig. 1a and Supplementary Fig. 1e), which is generated during autophagosome formation^{1,2}. The decreased conversion of LC3-I to LC3-II suggested an alteration of basal autophagy in *Col6a1*^{-/-} muscles and led us to investigate the autophagic process.

We next subjected mice to starvation for 24 h, a well-characterized stimulus able to induce the formation of autophagosomes in various organs including muscles¹². Fasting for 24 h prompted massive autophagosome formation in wild-type but not *Col6a1*^{-/-} muscles, as revealed by the appearance of LC3-positive puncta in tibialis anterior transfected with YFP-LC3 (Supplementary Fig. 1h) and by electron microscopy of diaphragm (Fig. 1b,c). Notably, the few autophagosomes present in *Col6a1*^{-/-} diaphragm contained mitochondria with abnormal cristae (Supplementary Fig. 1i). Moreover,

diaphragm and tibialis anterior showed reduced LC3-I to LC3-II conversion in fasted *Col6a1*^{-/-} mice compared to fasted wild-type mice (Fig. 1d and Supplementary Fig. 1j). Tibialis anterior was completely resistant to autophagy induction, whereas diaphragm showed a partial LC3 conversion after 24-h starvation (Fig. 1d). The differential response of these two muscles probably reflects differences in metabolic properties and fiber types¹². These results obtained with fasted mice confirm that *Col6a1*^{-/-} muscles have an abnormal response to a physiological autophagic stimulus.

The decreased amount of autophagosomes and the reduced LC3 lipidation in *Col6a1*^{-/-} muscles could be caused by either defective autophagy induction or excessive vesicle exhaustion. Because autophagy is a dynamically regulated process, we used a combination of *in vivo* tools for reliably monitoring the autophagic flux^{13,14}. First, we used a genetic approach to knock down mRNA encoding LC3 (*Map1lc3b*) and thus inhibit autophagosome formation. To achieve this knockdown *in vivo*, we transfected adult myofibers with a bicistronic vector encoding *Map1lc3b*-targeting shRNA and GFP¹⁵. Knockdown of *Map1lc3b* led to a significant increase in the number of TUNEL-positive nuclei in wild-type myofibers, but it did not affect the TUNEL-positive nuclei of *Col6a1*^{-/-} myofibers (Fig. 1e). Next, we treated mice with chloroquine¹⁶, a lysosomal

Figure 1 Autophagy is impaired in *Col6a1*^{-/-} mice. (a) Western blot for LC3 lipidation in diaphragm of fed wild-type and *Col6a1*^{-/-} mice. MW, molecular weight; WT, wild-type; GAPDH, glyceraldehyde 3-phosphate dehydrogenase. (b) Electron-microscopic quantification of myofibers containing autophagic vesicles in diaphragms of fed and 24-h-fasted mice (****P* < 0.001; *n* = 5, each group). Error bars indicate s.d. (c) Electron micrograph of a double-membrane autophagosome (arrowheads) containing mitochondria (mit) and sarcoplasmic reticulum (sr) in diaphragms of 24-h-fasted wild-type mice. Scale bar, 400 nm. (d) Western blot for LC3 lipidation in diaphragm (left) and tibialis anterior (right) of fed and 24-h-fasted mice. (e) Quantification of TUNEL-positive nuclei in tibialis anterior transfected with vector expressing either scrambled or *Map1lc3b*-targeting shRNA (**P* < 0.05; NS, not significant; *n* = 5, each group). Error bars indicate s.e.m. (f) Western blot for LC3 lipidation in diaphragm (left) and tibialis anterior (right) of untreated mice (-) or mice treated with chloroquine diphosphate at 50 mg per kg body weight per day for 10 d (+). (g) Western blot for LC3 and p62 in diaphragm (left) and tibialis anterior (right) of fed, 6-h-fasted and 12-h-fasted mice. (h) Western blot for beclin-1 and Bnip3 in diaphragm (left) and tibialis anterior (right) of fed and 24-h-fasted mice (top) and densitometric quantification of beclin-1 (middle) and Bnip3 (bottom) (****P* < 0.001; **P* < 0.05; *n* = 3). Error bars indicate s.e.m. (i) Quantitative RT-PCR (qRT-PCR) analysis of *Bnip3* mRNA in tibialis anterior of fed and 24-h-fasted mice (**P* < 0.05; *n* = 7). Error bars indicate s.e.m. (j) Western blot for Akt and 4E-BP1 phosphorylation (p-Akt and p-4E-BP1, respectively) in diaphragm (left) and tibialis anterior (right) of fed or 24-h-fasted mice.



inhibitor that blocks the degradation of autophagosome content, including LC3 (refs. 13,17), and investigated its effect on LC3 protein abundance. Chloroquine treatment led to a marked increase in LC3 bands in both diaphragm and tibialis anterior of wild-type mice, but the increase was much smaller in the corresponding samples of *Col6a1*^{-/-} mice (Fig. 1f and Supplementary Fig. 2a). Finally, we assessed during fasting the variations in protein amounts of p62, a well-known substrate of the autophagy-lysosome system^{13,14,18}. Both diaphragm and tibialis anterior showed a decrease in p62 during the first 6–12 h of fasting in wild-type mice but not in *Col6a1*^{-/-} mice (Fig. 1g and Supplementary Fig. 2b). Together, these data show an impairment of autophagy induction in *Col6a1*^{-/-} muscles, which explains their lower incidence of autophagosomes and defective LC3 lipidation.

Beclin-1 and Bnip3 are defective in *Col6a1*^{-/-} muscles

Bnip3 has a key role in the autophagic removal of mitochondria^{19,20}, and induction of Bnip3 is crucial for autophagosome formation in muscle during starvation¹⁵. In contrast to the case in wild-type mice, Bnip3 protein and mRNA expression was not induced in tibialis anterior of 24-h-fasted *Col6a1*^{-/-} mice (Fig. 1h,i). Conversely, diaphragm of 24-h-fasted *Col6a1*^{-/-} mice showed Bnip3 induction, which matched the partial LC3 lipidation reported above (Fig. 1h). Other Bcl-2 family members, including Bax and Bcl-X_L, did not

differ in expression between fed and fasted mice as well as between control and knockout mice, whereas Bcl-2 protein abundance was increased only in fasted *Col6a1*^{-/-} tibialis anterior (Supplementary Fig. 2e). Bcl-2 has been shown to inhibit the autophagic function of beclin-1, a component of the class III phosphoinositide 3-kinase (PI3K) complex necessary for autophagosome formation^{2,21}. Because beclin-1 plays a key part in autophagy², we investigated its expression in wild-type and knockout muscles. Under fed conditions, beclin-1 protein amounts were lower in *Col6a1*^{-/-} diaphragm when compared to wild-type diaphragm (Fig. 1h). Starvation led to a marked increase of beclin-1 protein levels in both diaphragm and tibialis anterior of wild-type animals (Fig. 1h). Notably, the levels of mRNA encoding for beclin-1 (*Becn1*) were similar in fed and starved tibialis anterior (Supplementary Fig. 2f), suggesting that variations of beclin-1 levels in muscle may primarily rely on protein stability. Conversely, *Col6a1*^{-/-} diaphragm and tibialis anterior did not show any substantial increase of beclin-1 protein after 24-h fasting (Fig. 1h). Vps34 protein, the class III PI3K of the PI3K–beclin-1 complex¹⁻³, was upregulated in *Col6a1*^{-/-} diaphragm but not in *Col6a1*^{-/-} tibialis anterior after 24-h fasting (Supplementary Fig. 2g,h). These data indicate that *Col6a1*^{-/-} muscles have an imbalance of proteins actively involved in the autophagic process and suggest that complete activation of autophagy requires a proper induction of beclin-1 and Bnip3.

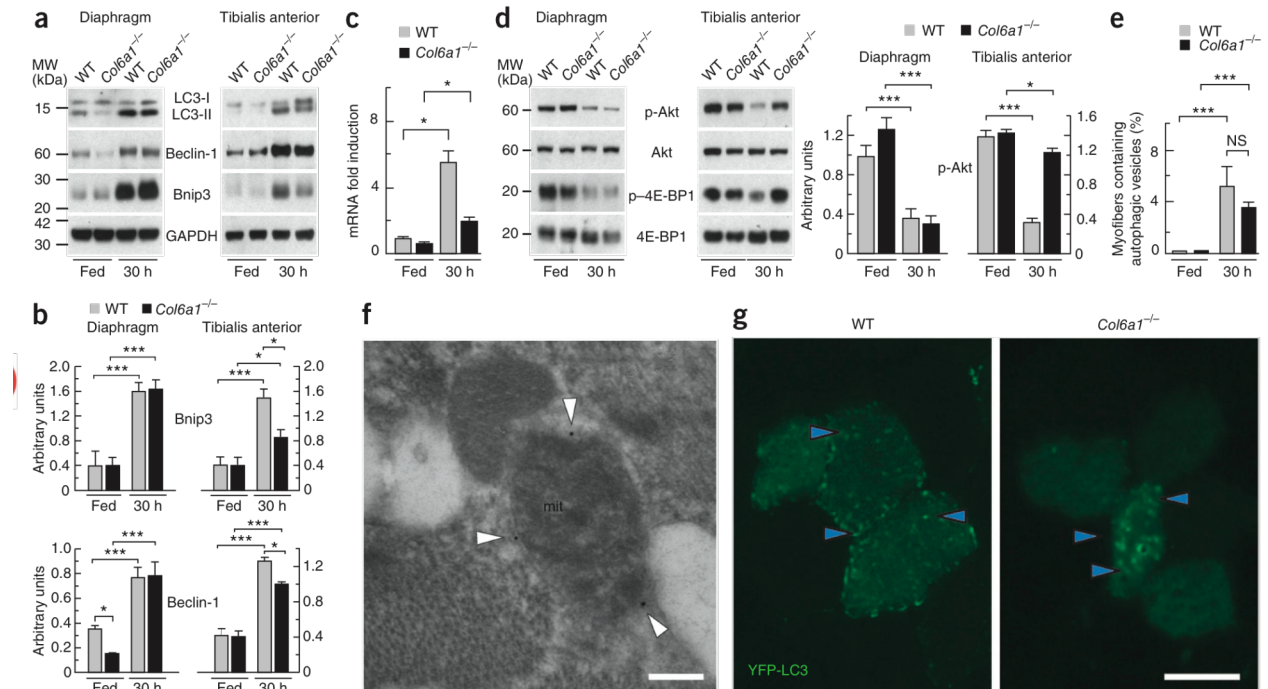


Figure 2 Prolonged starvation induces autophagy in *Col6a1*^{-/-} mice. (a) Western blot for LC3, beclin-1 and Bnip3 in diaphragm (left) and tibialis anterior (right) of fed and 30-h-fasted mice. (b) Densitometric quantification of Bnip3 (top) and beclin-1 (bottom) after western blotting of diaphragm (left) and tibialis anterior (right) (****P* < 0.001; **P* < 0.05, *n* = 3). Error bars indicate s.e.m. (c) qRT-PCR analysis of *Bnip3* mRNA in tibialis anterior of fed and 30-h-fasted mice (**P* < 0.05; *n* = 7). Error bars indicate s.e.m. (d) Immunoblot analysis for Akt and 4E-BP1 phosphorylation in diaphragm (left) and tibialis anterior (right) of fed and 30-h-fasted mice. The right graphs show the densitometric quantification of the western blots for p-Akt. (****P* < 0.001; **P* < 0.05; *n* = 3). Error bars indicate s.e.m. (e) Quantification of myofibers containing autophagic vesicles in diaphragms of 30-h-fasted mice (****P* < 0.001; *n* = 5, each group). Error bars indicate s.d. (f) Immunogold labeling of LC3 in 30-h-fasted *Col6a1*^{-/-} diaphragm. LC3 labeling (black dots marked by arrowheads) is associated with the membrane of an autophagosome containing a mitochondrion (mit). Scale bar, 300 nm. (g) Fluorescence microscopy of tibialis anterior cryosections from wild-type and *Col6a1*^{-/-} mice transfected with YFP-LC3 and starved for 30 h. LC3 puncta (arrowheads) are indicated. Scale bar, 50 μm.

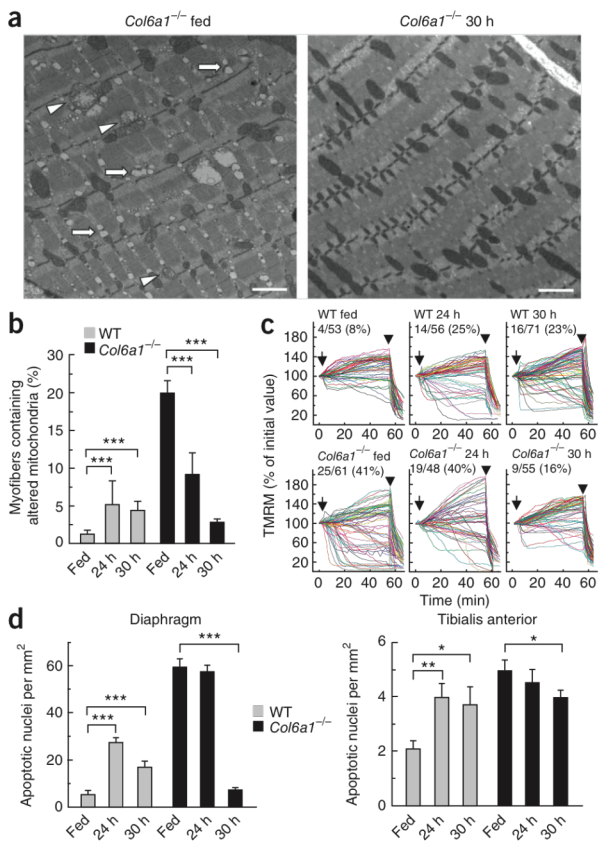


Figure 3 Induction of autophagy ameliorates the dystrophic phenotype. (a) Electron micrographs of diaphragm from *Col6a1*^{-/-} mice in fed conditions (left) and after 30 h starvation (right). Abnormal mitochondria (arrowheads) and dilated sarcoplasmic reticulum cisternae (arrows) in myofibers of the fed *Col6a1*^{-/-} mice are indicated. Scale bar, 1 μ m. (b) Percentage of myofibers with morphologically altered mitochondria in diaphragm of fed, 24-h-fasted and 30-h-fasted mice (*** $P < 0.001$; $n = 5$, each group). Error bars indicate s.d. (c) Mitochondrial response to oligomycin in myofibers isolated from FDB muscles of fed and fasted mice. Where indicated, 6 μ M oligomycin (arrow) or 4 μ M of the protonophore carbonylcyanide-*p*-trifluoromethoxyphenyl hydrazone (FCCP) (arrowhead) were added. Each trace represents the tetramethylrhodamine methyl ester (TMRM) fluorescence of a single fiber. The fraction of myofibers with depolarizing mitochondria is indicated for each condition, where fibers are considered as depolarizing when they lose more than 10% of initial value of TMRM fluorescence after oligomycin addition ($n = 5$, each group). (d) Quantification of TUNEL-positive nuclei in diaphragm (left) and tibialis anterior (right) of fed, 24-h-fasted and 30-h-fasted mice (*** $P < 0.001$, ** $P < 0.01$, * $P < 0.05$; $n = 5$, each group). Error bars indicate s.e.m.

wild-type mice led to decreased Bnip3 and beclin-1 protein amounts and resulted in a dystrophic phenotype characterized by p62 aggregates, vacuolated fibers and centrally located myonuclei (Supplementary Fig. 3). These findings support a role for the persistence of Akt activation in autophagy inhibition and in the development of the dystrophic phenotype in *Col6a1*^{-/-} mice.

Because 24-h fasting was not sufficient to trigger a robust Akt dephosphorylation and full activation of autophagy in *Col6a1*^{-/-} muscles, we investigated whether prolonged starvation could reactivate the autophagic process and confer some beneficial effects on the dystrophic phenotype. Starvation for 30 h triggered LC3 lipidation and increased beclin-1 and Bnip3 protein amounts in both diaphragm and tibialis anterior of *Col6a1*^{-/-} mice (Fig. 2a,b and Supplementary Fig. 4a,b). Bnip3 mRNA levels were also increased by 30-h fasting, whereas Becn1 transcripts were unaffected (Fig. 2c and Supplementary Fig. 4c). Similarly, Vps34 was induced in *Col6a1*^{-/-} muscles (Supplementary Fig. 4d,e). As with 24-h fasting, Bcl-X_L and Bax expression did not change between wild-type and *Col6a1*^{-/-} muscles, whereas the Bcl-2 protein amount was increased in 30-h-fasted *Col6a1*^{-/-} tibialis anterior (Supplementary Fig. 4f). Therefore, high expression of Bcl-2 did not prevent reactivation of autophagy in *Col6a1*^{-/-} mice. Prolonged starvation attenuated the differences between wild-type and *Col6a1*^{-/-} muscles in the phosphorylation of Akt (Fig. 2d). Atrogin-1 mRNA expression was induced in 30-h-fasted *Col6a1*^{-/-} mice (Supplementary Fig. 4g). Detection of LC3-positive vesicles by fluorescence microscopy in YFP-LC3-transfected fibers and by immunoelectron microscopy confirmed that 30-h fasting elicited substantial autophagosome formation in both wild-type and *Col6a1*^{-/-} myofibers (Fig. 2e-g and Supplementary Fig. 4h).

Prolonged starvation resulted in the amelioration of myofiber abnormalities in *Col6a1*^{-/-} mice (Fig. 3a). Indeed, *Col6a1*^{-/-} diaphragms showed a significant rescue of ultrastructural alterations of mitochondria and sarcoplasmic reticulum (Fig. 3a,b and Supplementary Fig. 4h-j). Moreover, the percentage of FDB myofibers showing mitochondrial depolarization was substantially lower, and the amount of TUNEL-positive-nuclei in *Col6a1*^{-/-} muscles became close to that of control muscles (Fig. 3c,d). Wild-type mice showed some degree of muscle alterations after fasting (Fig. 3b-d and Supplementary Fig. 4h,j), in keeping with the observation that excessive autophagy contributes to muscle wasting^{15,24}.

Next, we investigated the signaling pathways involved in autophagy regulation. In skeletal muscle, autophagy and Bnip3 expression are regulated by the Akt–forkhead box protein O3 axis, a pathway that also regulates the atrophy-related ubiquitin ligase atrogin-1 (ref. 22). Similarly to Bnip3, upregulation of atrogin-1 was impaired in fasted *Col6a1*^{-/-} tibialis anterior, whereas induction of muscle RING-finger protein-1, another atrophy-related ubiquitin ligase that is under nuclear factor- κ B control, was unaffected (Supplementary Fig. 2i). These findings suggest there is abnormal Akt signaling in fasted *Col6a1*^{-/-} muscles, and, indeed, starvation induced dephosphorylation of Akt in wild-type but not *Col6a1*^{-/-} tibialis anterior (Fig. 1j and Supplementary Fig. 2j). In agreement with the abnormal Akt phosphorylation, the mammalian target of rapamycin pathway, which negatively regulates autophagy^{2,23}, remained active in fasted *Col6a1*^{-/-} tibialis anterior, as indicated by the persistent phosphorylation of eukaryotic translation initiation factor 4E-binding protein-1 (4E-BP1), a downstream target of this signaling axis (Fig. 1j). Fasted *Col6a1*^{-/-} diaphragm showed dephosphorylation of Akt and 4E-BP1, albeit to a lesser extent than starved wild-type muscles, and this explains why autophagy is partially activated in diaphragm after 24-h fasting (Fig. 1j and Supplementary Fig. 2j).

Recent studies have shown that constitutive Akt expression in wild-type muscle inhibits autophagosome formation¹⁵. To get further evidence of the impact of abnormal Akt signaling, we investigated the phenotype of mice expressing a muscle-specific, inducible Akt transgene, resulting in chronic Akt activation. In agreement with our findings in *Col6a1*^{-/-} mice, chronic Akt activation in otherwise

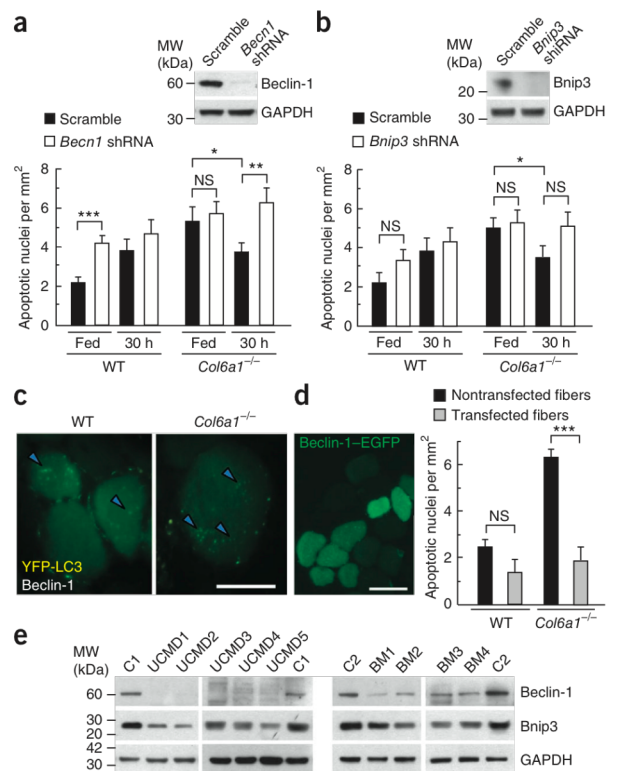
Figure 4 Beclin-1 protein abundance is decreased in muscle biopsies of subjects with UCMD or Bethlem myopathy, and its expression counteracts muscle apoptosis in *Col6a1*^{-/-} mice. **(a,b)** Quantification of TUNEL-positive nuclei in wild-type and *Col6a1*^{-/-} tibialis anterior transfected with a vector expressing scramble or *Becn1* shRNA **(a)** or *Bnip3* shRNA **(b)**. Western blot confirmation of RNAi-mediated knockdown of *Becn1* and *Bnip3* in tibialis anterior of wild-type mice is included above each set of graphs ($***P < 0.001$; $**P < 0.01$; $*P < 0.05$; $n = 10$, each group). Error bars indicate s.e.m. **(c)** Fluorescence microscopy of tibialis anterior cryosections from wild-type and *Col6a1*^{-/-} mice transfected with beclin-1 and YFP-LC3 expression vectors and maintained in fed condition. LC3 puncta (arrowheads) are indicated. Scale bar, 50 μm . **(d)** Right, quantification of TUNEL-positive nuclei in transfected and nontransfected myofibers of wild-type and *Col6a1*^{-/-} tibialis anterior muscle after *in vivo* transfection with beclin-1-EGFP expression vector. Transfected fibers were revealed by fluorescence microscopy (left). Scale bar, 50 μm ($***P < 0.001$; $n = 10$, each group). Error bars indicate s.e.m. **(e)** Western blot for beclin-1 and Bnip3 in protein lysates of human muscle biopsies from two healthy (normal) controls (C1, C2), five individuals with UCMD (UCMD1-5) and four individuals with Bethlem myopathy (BM1-4). Data are representative of three independent experiments.

Restoration of beclin-1 ameliorates muscle phenotype

To further investigate the contribution of beclin-1 and Bnip3 in the pathogenesis of *Col6a1*^{-/-} muscles, we performed *in vivo* loss-of-function experiments. Adult tibialis anterior was transfected with expression plasmids encoding shRNAs targeting *Becn1* and *Bnip3* transcripts²⁴. *Becn1* knockdown for 2 weeks led to a marked increase in apoptotic nuclei in myofibers of wild-type mice and completely prevented the significant decrease of TUNEL-positive nuclei observed in 30-h-fasted *Col6a1*^{-/-} mice (**Fig. 4a**). Conversely, *Bnip3* knockdown for 2 weeks did not substantially impinge on the incidence of TUNEL-positive nuclei of wild-type mice and had a minor effect on 30-h-starved *Col6a1*^{-/-} mice when compared to *Becn1* knockdown (**Fig. 4b**). Together with the above findings showing that autophagy flux is impaired in *Col6a1*^{-/-} muscles, these data indicate that the inefficient autophagy and subsequent muscle apoptosis observed in these mice is due to beclin-1 inhibition.

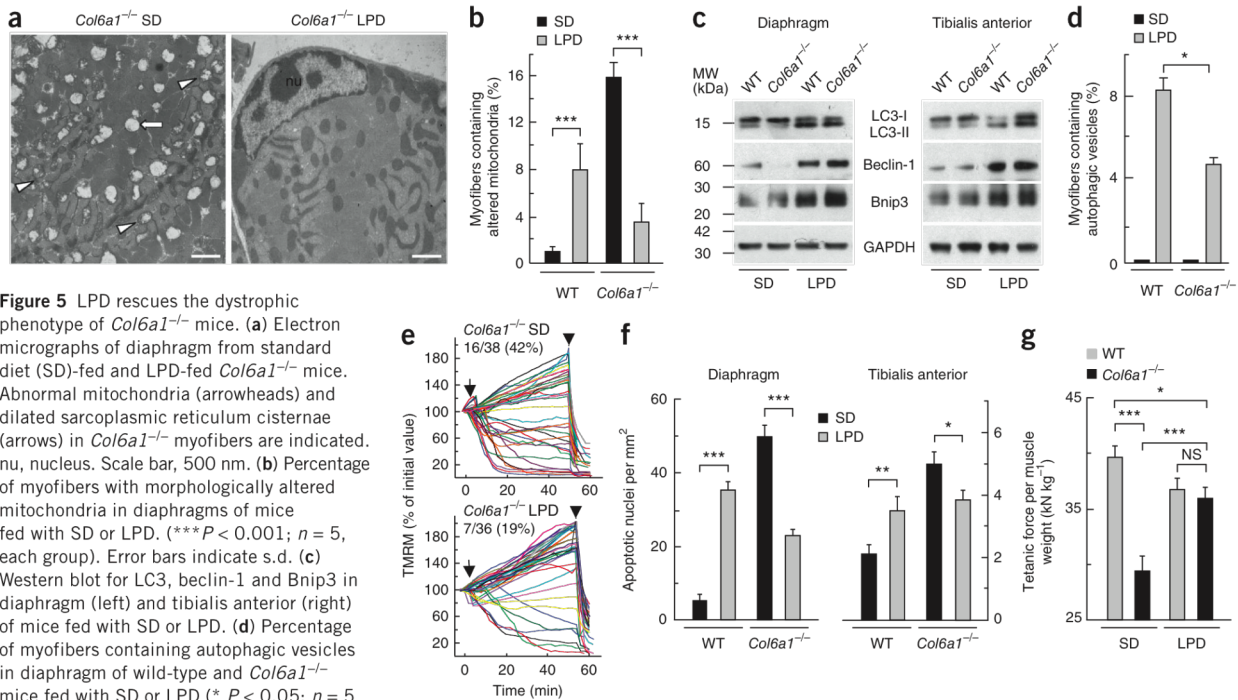
To support the pathogenetic role of beclin-1 deficiency in myofiber degeneration, we carried out *in vivo* transfection of tibialis anterior with an expression construct coding for beclin-1. Transfection of the beclin-1 construct was able to activate autophagy in both wild-type and *Col6a1*^{-/-} muscles, as revealed by concurrent transfection of YFP-LC3 and formation of LC3-positive puncta (**Fig. 4c**). Moreover, beclin-1 overexpression led to a marked decrease of TUNEL-positive nuclei in myofibers of *Col6a1*^{-/-} mice, whereas it did not affect wild-type muscles (**Fig. 4d**). Therefore, correction of beclin-1 levels in *Col6a1*^{-/-} muscle fibers is sufficient to reactivate autophagy and thus prevent apoptotic degeneration.

To assess whether the findings obtained in the *Col6a1*-null mouse model also apply to human collagen VI disorders, we investigated muscle biopsies derived from five subjects with UCMD and four subjects with Bethlem myopathy (**Supplementary Table 1**). The amounts of both beclin-1 and Bnip3 proteins were decreased in subjects with UCMD and Bethlem myopathy when compared to healthy (normal) controls. Individuals with UCMD had very low beclin-1 levels, whereas individuals with Bethlem myopathy, whose dystrophic phenotype is milder, showed a less prominent decrease in the amount of beclin-1, which seemed closer but not identical to amounts in controls. Bnip3 protein abundance was also lower in samples from UCMD and Bethlem myopathy individuals compared to those in controls, albeit the reductions are much less prominent than that seen for beclin-1 abundance between disease samples and controls (**Fig. 4e** and **Supplementary Fig. 5a**).



Autophagy reactivation ameliorates muscle pathology

Given that prolonged starvation reactivated autophagy and blocked apoptotic degeneration in *Col6a1*^{-/-} muscles, we investigated whether milder and long-lasting dietary regimens were able to activate autophagy and ameliorate muscle morphology and function. Depletion of amino acids strongly induces autophagy²⁵⁻²⁷. Conversely, supplementation of protein-free diets with amino acids suppresses muscle protein degradation through inhibition of autophagy²⁸. To allow for a long-term response, we fed mice with a specifically designed low-protein diet (LPD) (**Supplementary Table 2**). Four weeks of LPD was able to ameliorate the dystrophic features of *Col6a1*^{-/-} mice (**Fig. 5a,b** and **Supplementary Fig. 6**). LPD induced autophagy and did not have any significant effect on the ubiquitin-proteasome system as shown by atrogin-1 expression (**Supplementary Fig. 6c**). Diaphragm and tibialis anterior of both wild-type and *Col6a1*^{-/-} LPD-fed mice showed LC3 lipidation and increased beclin-1 and Bnip3 protein amounts, consistent with the formation of autophagosomes (**Fig. 5c,d** and **Supplementary Fig. 6a,b**). Activation of autophagy by LPD led to removal of structurally abnormal organelles (**Fig. 5b** and **Supplementary Fig. 6e**). Similarly to prolonged starvation, induction of autophagy by LPD led to a marked recovery of the dystrophic alterations of *Col6a1*^{-/-} mice and produced some muscle alterations in wild-type mice (**Fig. 5e,f** and **Supplementary Fig. 6e-g**). The percentages of myofibers showing mitochondrial depolarization and TUNEL positivity were significantly lower in LPD-fed *Col6a1*^{-/-} mice compared to *Col6a1*^{-/-} mice fed with normal diet and were similar to (or lower than) those observed in LPD-fed wild-type mice (**Fig. 5f** and **Supplementary Fig. 6g**). Autophagy reactivation also ameliorated the histological features of *Col6a1*^{-/-} muscles, resulting in a more uniform myofiber size (**Supplementary Fig. 6h**). Moreover, long-term induction of autophagy by LPD also



improved muscle strength of *Col6a1*^{-/-} mice, as indicated by the significant increase of specific force measured in gastrocnemius muscle (**Fig. 5g** and **Supplementary Fig. 6i**). Thus, reactivation of autophagy by dietary approaches is sufficient to improve both morphology and function of *Col6a1*^{-/-} dystrophic muscles.

Drugs inducing autophagy rescue the dystrophic phenotype

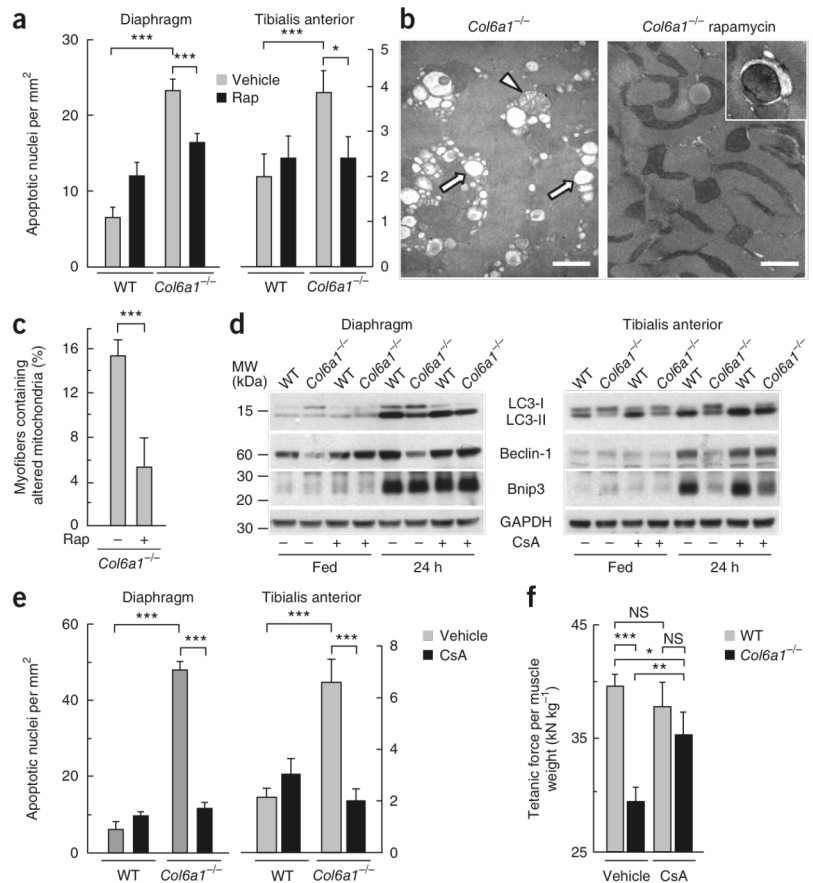
As reactivation of autophagy by dietary restriction showed a therapeutic potential in *Col6a1*^{-/-} mice, we further explored this possibility with pharmacological tools. Rapamycin is a well-known inducer of autophagy that can be used for *in vivo* treatments¹⁷. Treatment of *Col6a1*^{-/-} mice with rapamycin for 15 d decreased myofiber degeneration and removed abnormal organelles (**Fig. 6a–c** and **Supplementary Fig. 7a**). Cyclosporin A has been reported to modulate autophagy^{7,29,30}, and we previously demonstrated that this drug rescues the dystrophic phenotype of *Col6a1*^{-/-} mice by desensitizing the mitochondrial permeability transition pore⁹. Because reactivation of autophagy in *Col6a1*^{-/-} mice led to a marked amelioration of the phenotype, we investigated whether treatment with cyclosporin A would have any effect on autophagy. Notably, cyclosporin A induced autophagy in *Col6a1*^{-/-} muscles, with a concomitant block of apoptotic degeneration and recovery of muscle strength (**Fig. 6d–g** and **Supplementary Fig. 7b–d**). Moreover, cyclosporin A treatment restored beclin-1 and Bnip3 induction, LC3 lipidation and Akt dephosphorylation in 24-h-fasted *Col6a1*^{-/-} muscles (**Fig. 6d** and **Supplementary Fig. 7e**). These data suggest that the robust beneficial effect of cyclosporin A in collagen VI-deficient mice is linked to both restoration of mitochondrial function⁹ and autophagy induction.

DISCUSSION

Previous studies have shown that the muscle pathology of collagen VI-null mice and humans with UCMD or Bethlem myopathy is strictly related to ultrastructural alterations of organelles, mitochondrial dysfunction and spontaneous apoptosis in skeletal muscles^{9,10}. Here we show that autophagy is impaired in *Col6a1*^{-/-} muscles and that the failure of this process has a major role in the pathogenesis of the dystrophic phenotype, causing accumulation of abnormal organelles and apoptotic degeneration of muscle fibers. Forced induction of autophagy is able to reactivate the process, achieving a beneficial response in *Col6a1*^{-/-} mice. Thus, prompt elimination of defective organelles is essential to protect *Col6a1*^{-/-} myofibers from the harmful consequences of dysfunctional mitochondria and excessive apoptosis (**Supplementary Fig. 8a**). Indeed, accumulation of abnormal mitochondria in *Col6a1*^{-/-} muscles is associated with oxidative stress and increased production of reactive oxygen species, which contribute to trigger apoptotic response³¹. Our findings indicate that a proper autophagic flux is crucial for the clearance of damaged organelles and the maintenance of muscle homeostasis. Moreover, we also point out that both defective and excessive autophagy lead to muscle degeneration, in keeping with the intricate interplay between autophagic and apoptotic pathways shown in different systems^{1–3,32} (**Supplementary Fig. 8b**). In agreement with our model, muscle-specific inactivation of autophagy genes results in muscle atrophy with abnormal organelles^{33,34}.

In certain storage diseases and vacuolar myopathies, a reduced 'off-rate' of autophagy results from mutations of genes coding for proteins involved in lysosomal function, leading to accumulation of autophagic vesicles^{1,3,35,36}. Conversely, our findings suggest that the impaired

Figure 6 Pharmacological treatments induce autophagy and ameliorate the myopathic phenotype of *Col6a1*^{-/-} mice. (a) Quantification of TUNEL-positive nuclei in diaphragm (left) and tibialis anterior (right) of wild-type and *Col6a1*^{-/-} mice treated with vehicle (ethanol) or with rapamycin (Rap) for 15 d (***P* < 0.001; **P* < 0.05; *n* = 5, each group). Error bars indicate s.e.m. (b) Representative micrographs of a transverse section of diaphragm from untreated (left) and rapamycin-treated (right) *Col6a1*^{-/-} mice. Abnormal mitochondria (white arrowheads) and dilated sarcoplasmic reticulum (white arrows) in the muscle of untreated mice are indicated, as is autophagosome formation in the treated mice (inset). Scale bar, 500 nm. (c) Percentage of myofibers with morphologically altered mitochondria in the diaphragm of *Col6a1*^{-/-} mice treated with rapamycin (+) or left untreated (-) for 15 d (***P* < 0.001; *n* = 5 each group). Error bars indicate s.d. (d) Western blot analysis for LC3, beclin-1 and Bnip3 in diaphragm (left) and tibialis anterior (right) of wild-type and *Col6a1*^{-/-} mice treated with vehicle (olive oil) (-) or with cyclosporin A (CsA) (+) for 4 d and maintained in fed or 24-h-fasting conditions. (e) Quantification of TUNEL-positive nuclei in diaphragm (left) and tibialis anterior (right) of wild-type and *Col6a1*^{-/-} mice treated with vehicle or with cyclosporin A for 4 d (***P* < 0.001; *n* = 4, each group). Error bars indicate s.e.m. (f) *In vivo* tetanic force measurements in the gastrocnemius muscle of mice treated with vehicle or with cyclosporin A for 10 d (***P* < 0.001; ***P* < 0.01; **P* < 0.05; *n* = 8, each group). Error bars indicate s.e.m.



autophagic flux of collagen VI dystrophic muscles results from a decreased 'on-rate', with defective formation of autophagosomes. Indeed, we have found that amounts of two major autophagic effector proteins, beclin-1 and Bnip3, are reduced in *Col6a1*^{-/-} muscles. Although Bnip3 induction is sufficient to trigger autophagy¹⁵, our data suggest that the concomitant beclin-1 upregulation is required for a proper autophagy induction. Thus, beclin-1 seems to be necessary and sufficient for basal autophagy and for its correct induction, whereas Bnip3 is able to trigger autophagy in the presence of appropriate protein levels of beclin-1.

The demonstration that muscles of *Col6a1*^{-/-} mice are characterized by inefficient autophagy has a major impact on the understanding of the pathogenesis of collagen VI muscular dystrophies. Muscle biopsies of subjects with UCMD and Bethlem myopathy show reduced protein amounts of beclin-1 and Bnip3. Notably, forced reactivation of autophagy in the mouse model by nutritional and pharmacological approaches is able to rescue the morphological and functional aspects of the dystrophic phenotype. This opens new possibilities for targeted therapeutic approaches aimed at combating muscle loss in UCMD and Bethlem myopathy that add to desensitization of the mitochondrial permeability transition pore through cyclophilin D inhibition^{10,37,38}.

In more general terms, our results support a view that points at the activators of autophagic process and at clearance systems as new therapeutic targets for avoiding accumulation of toxic molecules and damaged organelles in skeletal muscle. Moreover, the finding

that modulation of autophagy through various nutritional and pharmacological treatments is beneficial for collagen VI dystrophic muscles paves the way for investigating autophagy defects in other muscular dystrophies.

METHODS

Methods and any associated references are available in the online version of the paper at <http://www.nature.com/naturemedicine/>.

Note: Supplementary information is available on the Nature Medicine website.

ACKNOWLEDGMENTS

We thank N. Bergamin for her involvement in the initial study, P. Braghetta for help with mouse manipulations, E. Rizzo and S. Castagnaro for histology, S. Cogliati for assistance with mitochondria isolation and F. Gualandi for muscle biopsies. We are grateful to N. Heintz (Rockefeller University) for supplying the beclin-1-EGFP expression construct and E. Kominami (Juntendo University School of Medicine) for the YFP-LC3 construct. This work was supported by the Telethon Foundation (GGP08107 and TCP04009), the Italian Ministry of University and Research, Association Francaise contre les Myopathies and the EU (BIO-NMD and MYOAGE).

AUTHOR CONTRIBUTIONS

P.G. performed biochemical analyses, autophagy assays, mouse treatments, analysis and interpretation of data, and contributed to manuscript preparation. L.C. carried out RNA analysis, muscle transfections, molecular biology, analysis and interpretation of data, and contributed to manuscript preparation. P.S. performed electron microscopy. M.C. performed TUNEL and histology. A.A. performed tetramethylrhodamine methyl ester (TMRM) analysis. E.B. carried out muscle transfections and mitochondria isolation. B.B. analyzed muscle mechanics. A.U. performed TUNEL analysis. T.T. genotyped and maintained mice. L.M.,

P. Bernardi and N.M.M. were involved in data analysis. P. Bonaldo and M.S. designed the study, analyzed data and wrote the paper. All authors discussed the results and commented on the manuscript.

COMPETING FINANCIAL INTERESTS

The authors declare no competing financial interests.

Published online at <http://www.nature.com/naturemedicine/>.

Reprints and permissions information is available online at <http://npg.nature.com/reprintsandpermissions/>.

- Levine, B. & Kroemer, G. Autophagy in the pathogenesis of disease. *Cell* **132**, 27–42 (2008).
- Maiuri, M.C., Zalckvar, E., Kimchi, A. & Kroemer, G. Self-eating and self-killing: crosstalk between autophagy and apoptosis. *Nat. Rev. Mol. Cell Biol.* **8**, 741–752 (2007).
- Mizushima, N., Levine, B., Cuervo, A.M. & Klionsky, D.J. Autophagy fights disease through cellular self-digestion. *Nature* **451**, 1069–1075 (2008).
- Nakai, A. *et al.* The role of autophagy in cardiomyocytes in the basal state and in response to hemodynamic stress. *Nat. Med.* **13**, 619–624 (2007).
- Green, D.R. & Kroemer, G. The pathophysiology of mitochondrial cell death. *Science* **305**, 626–629 (2004).
- Bernardi, P. *et al.* The mitochondrial permeability transition from in vitro artifact to disease target. *FEBS J.* **273**, 2077–2099 (2006).
- Kim, I., Rodriguez-Enriquez, S. & Lemasters, J.J. Selective degradation of mitochondria by mitophagy. *Arch. Biochem. Biophys.* **462**, 245–253 (2007).
- Lampe, A.K. & Bushby, K.M. Collagen VI related muscle disorders. *J. Med. Genet.* **42**, 673–685 (2005).
- Irwin, W.A. *et al.* Mitochondrial dysfunction and apoptosis in myopathic mice with collagen VI deficiency. *Nat. Genet.* **35**, 367–371 (2003).
- Angelin, A. *et al.* Mitochondrial dysfunction in the pathogenesis of Ullrich congenital muscular dystrophy and prospective therapy with cyclosporins. *Proc. Natl. Acad. Sci. USA* **104**, 991–996 (2007).
- Long, Y.C. & Zierath, J.R. AMP-activated protein kinase signaling in metabolic regulation. *J. Clin. Invest.* **116**, 1776–1783 (2006).
- Mizushima, N., Yamamoto, A., Matsui, M., Yoshimori, T. & Ohsumi, Y. *In vivo* analysis of autophagy in response to nutrient starvation using transgenic mice expressing a fluorescent autophagosome marker. *Mol. Biol. Cell* **15**, 1101–1111 (2004).
- Mizushima, N., Yoshimori, T. & Levine, B. Methods in mammalian autophagy research. *Cell* **140**, 313–326 (2010).
- Klionsky, D.J. *et al.* Guidelines for the use and interpretation of assays for monitoring autophagy in higher eukaryotes. *Autophagy* **4**, 151–175 (2008).
- Mammucari, C. *et al.* FoxO3 controls autophagy in skeletal muscle *in vivo*. *Cell Metab.* **6**, 458–471 (2007).
- Schmalbruch, H. The early changes in experimental myopathy induced by chloroquine and chlorpheniramine. *J. Neuropathol. Exp. Neurol.* **39**, 65–81 (1980).
- Rubinsztein, D.C., Gestwicki, J.E., Murphy, L.O. & Klionsky, D.J. Potential therapeutic applications of autophagy. *Nat. Rev. Drug Discov.* **6**, 304–312 (2007).
- Bjørkøy, G. *et al.* p62/SQSTM1 forms protein aggregates degraded by autophagy and has a protective effect on huntingtin-induced cell death. *J. Cell Biol.* **171**, 603–614 (2005).
- Hamacher-Brady, A. *et al.* Response to myocardial ischemia/reperfusion injury involves Bnip3 and autophagy. *Cell Death Differ.* **14**, 146–157 (2007).
- Sandoval, H. *et al.* Essential role for Nix in autophagic maturation of erythroid cells. *Nature* **454**, 232–235 (2008).
- Pattingre, S. *et al.* Bcl-2 antiapoptotic proteins inhibit beclin-1-dependent autophagy. *Cell* **122**, 927–939 (2005).
- Sandri, M. *et al.* FoxO transcription factors induce the atrophy-related ubiquitin ligase atrogin-1 and cause skeletal muscle atrophy. *Cell* **117**, 399–412 (2004).
- Shintani, T. & Klionsky, D.J. Autophagy in health and disease: a double-edged sword. *Science* **306**, 990–995 (2004).
- Romanello, V. *et al.* Mitochondrial fission and remodelling contributes to muscle atrophy. *EMBO J.* **29**, 1774–1785 (2010).
- Codogno, P. & Meijer, A.J. Autophagy and signaling: their role in cell survival and cell death. *Cell Death Differ.* **12** Suppl 2, 1509–1518 (2005).
- Mizushima, N. Autophagy: process and function. *Genes Dev.* **21**, 2861–2873 (2007).
- Mortimore, G.E. & Poso, A.R. Intracellular protein catabolism and its control during nutrient deprivation and supply. *Annu. Rev. Nutr.* **7**, 539–564 (1987).
- Sugawara, T., Ito, Y., Nishizawa, N. & Nagasawa, T. Regulation of muscle protein degradation, not synthesis, by dietary leucine in rats fed a protein-deficient diet. *Amino Acids* **37**, 609–616 (2009).
- Yoo, Y.M. & Jeung, E.B. Melatonin suppresses cyclosporine A-induced autophagy in rat pituitary GH3 cells. *J. Pineal Res.* **48**, 204–211 (2010).
- Pallet, N. *et al.* Autophagy protects renal tubular cells against cyclosporine toxicity. *Autophagy* **4**, 783–791 (2008).
- Menazza, S. *et al.* Oxidative stress by monoamine oxidases is causally involved in myofiber damage in muscular dystrophy. *Hum. Mol. Genet.* published online, doi:10.1093/hmg/ddq339 (17 August 2010).
- Boya, P. *et al.* Inhibition of macroautophagy triggers apoptosis. *Mol. Cell. Biol.* **25**, 1025–1040 (2005).
- Masiero, E. *et al.* Autophagy is required to maintain muscle mass. *Cell Metab.* **10**, 507–515 (2009).
- Wu, J.J. *et al.* Mitochondrial dysfunction and oxidative stress mediate the physiological impairment induced by the disruption of autophagy. *Aging* **1**, 425–437 (2009).
- Ramachandran, N. *et al.* VMA21 deficiency causes an autophagic myopathy by compromising V-ATPase activity and lysosomal acidification. *Cell* **137**, 235–246 (2009).
- Malicdan, M.C., Noguchi, S., Nonaka, I., Saftig, P. & Nishino, I. Lysosomal myopathies: an excessive build-up in autophagosomes is too much to handle. *Neuromuscul. Disord.* **18**, 521–529 (2008).
- Palma, E. *et al.* Genetic ablation of cyclophilin D rescues mitochondrial defects and prevents muscle apoptosis in collagen VI myopathic mice. *Hum. Mol. Genet.* **18**, 2024–2031 (2009).
- Merlini, L. *et al.* Cyclosporin A corrects mitochondrial dysfunction and muscle apoptosis in patients with collagen VI myopathies. *Proc. Natl. Acad. Sci. USA* **105**, 5225–5229 (2008).

ONLINE METHODS

Mice. We backcrossed *Col6a1*^{+/-} mice in the inbred C57BL/6J strain (Charles River) for eight generations⁹. We performed all experiments in 16- to 24-week-old mice and compared age-matched *Col6a1*^{-/-} (collagen VI-null) and *Col6a1*^{+/+} (wild-type) mice. We housed mice in individual cages in an environmentally controlled room (23 °C, 12-h light-dark cycle) and provided food and water *ad libitum*. For starvation experiments, we removed chow in the morning and maintained mice for 6–30 h with no food but free access to water. We fed mice with either SD (Laboratorio Dottori Piccioni) or LPD (TestDiet) (**Supplementary Table 2**). Muscle-specific inducible Akt-ER-Cre transgenic mice were previously described¹⁵, and we achieved transgene activation by tamoxifen administration in the chow (Harlan). Mouse procedures were approved by the Ethics Committee of the University of Padova and authorized by the Italian Ministry of Health.

Drug treatments. We subjected wild-type and *Col6a1*^{-/-} mice to intraperitoneal injection with either chloroquine diphosphate (50 mg per kg body weight; Sigma) every 24 h for 10 d; cyclosporine A (5 mg per kg body weight; Novartis) every 12 h for 4 d or 10 d or rapamycin (2 mg per kg body weight; LC Laboratories) every 24 h for 15 d.

Muscle *in vivo* transfection. We performed *in vivo* transfection experiments by intramuscular injection of expression plasmids in tibialis anterior followed by electroporation as previously described²². We used the following expression constructs: YFP-LC3 (ref. 39), beclin-1-EGFP⁴⁰ and beclin-1. For the preparation of the beclin-1 expression construct, we amplified *Becn1* cDNA by PCR from the beclin-1-EGFP plasmid using primers 5'-CTATGGAGGGTCTAAGGC-3' (forward) and 5'-TCACTTGTATAGAAGTGTGAGG-3' (reverse) and cloned the amplified sequence into the HindIII and XbaI sites of the pcDNA3.1 (Invitrogen) expression vector. We carried out RNAi-mediated knockdown by transfection of shRNA constructs targeting *Map1lc3b* (ref. 15), *Bnip3* (ref. 15) and *Becn1*. For *Becn1*, we used a commercial kit containing oligonucleotides against *Becn1* target sequences and the BLOCK-IT Pol II miR RNAi expression vector (Invitrogen).

Gene expression analyses. We prepared total RNA from skeletal muscle with the Promega SV Total RNA Isolation kit. We generated cDNA products with SuperScript III reverse transcriptase (Invitrogen) and analyzed them by qRT-PCR with the QuantiTect SYBR Green PCR kit (Qiagen). We normalized all data to *Gapdh* expression. Oligonucleotide primers used for qRT-PCR are listed in **Supplementary Table 3**.

Fluorescence microscopy and transmission electron microscopy. We fixed muscle cryosections with ice-cold 4% paraformaldehyde, mounted the samples with Fluorescence Mounting Medium (DAKO) and examined them on a Leica DM5000B fluorescence microscope. For electron microscopy, we fixed and stained stretched diaphragms as previously described⁹. For statistical analysis, we studied at least 1,000 muscle fibers, obtained from two levels of three different tissue blocks for each diaphragm. We considered positive fibers presenting at least one mitochondrion with abnormal cristae or a portion of dilated sarcoplasmic reticulum. We performed immunoelectron microscopy according to previously published protocols⁴¹. We etched ultrathin sections with 3% sodium alcholate, treated them with 10% H₂O₂ and incubated them overnight with LC3-specific antibody (LB 100-2220, Novus Biologicals). We visualized the antibody binding by incubation with 15-nm colloidal gold-conjugated secondary antibody (Amersham).

Western blotting. We pulverized mouse frozen muscles and human muscle biopsies by grinding in liquid nitrogen, and we lysed and immunoblotted the samples as previously described²². When needed, we stripped and reprobed

membranes. We used antibodies from Cell Signaling Technologies specific for the following proteins: 4E-BP1 (9452), phospho-4E-BP1 (Thr37 and Thr46) (2855), AMPK (2532), phospho-AMPK (Thr172) (2531), Akt (9272), phospho-Akt (Ser473) (4058), Bcl-X_L (2764), beclin-1 (3738), caspase-3 (9665), caspase-9 (9504), LC3 (2775), S6 (2212), phospho-S6 (Ser240 and Ser244) (2215). Antibodies to Bnip3 (B7931) and Vps34 (V9764) were from Sigma. Antibodies to Bax (sc-493) and TOM20 (sc-11415) were from Santa Cruz. Antibodies to Bcl-2 (610539) and calnexin (610523) were from BD Transduction Laboratories. Antibody to p62 (GP62-C) was from Progen. Antibody to GAPDH (MAB374) was from Chemicon International. We performed western blots in at least three independent experiments. We carried out densitometric quantification by the ImageJ software (US National Institutes of Health).

Isolation of skeletal myofibers and measure of mitochondrial membrane potential. We isolated muscle fibers from FDB muscle, and we measured mitochondrial membrane potential by epifluorescence microscopy on the basis of the accumulation of TMRM fluorescence, as previously described^{9,37}. We considered fibers as depolarizing when they lost more than 10% of the initial value of TMRM fluorescence. We performed imaging with a Zeiss Axiovert 100 TV inverted microscope equipped with a 12-bit digital cooled charge-coupled device camera (Micromax, Princeton Instruments). We analyzed the data with MetaFluor imaging software (Universal Imaging).

Terminal deoxynucleotidyl transferase dUTP nick end labeling. We prepared sections (7- μ m thick) from diaphragm, after fixation with 4% paraformaldehyde and paraffin embedding, and from tibialis anterior muscles frozen in isopentane. We performed TUNEL assays with the ApopTag peroxidase *in situ* apoptosis detection system (Chemicon)^{9,37}. For transfected muscles, we determined the number of TUNEL-positive nuclei in randomly selected fields by considering, separately, transfected and nontransfected fibers.

Muscle mechanics. We carried out *in vivo* determination of force and contraction kinetics of gastrocnemius muscle as previously described⁴².

Human samples. We froze muscle biopsies of children and adults in isopentane. Details on subjects included in the study are provided in **Supplementary Table 1**. All subjects provided informed consent and were previously diagnosed with UCMD and Bethlem myopathy according to the criteria of the European NeuroMuscular Center⁴³ and by genetic analysis, which showed mutations in any of the *COL6A1*, *COL6A2* and *COL6A3* genes.

Statistical analyses. We expressed data as means \pm s.e.m. or as means \pm s.d. We determined statistical significance by unequal variance Student's *t* test (for TUNEL assay), equal variance Student's *t* test (for qRT-PCR and muscle mechanics) and Mann-Whitney test (for electron microscopy). A *P* value of less than 0.05 was considered statistically significant.

39. Tanida, I. *et al.* HsAtg4B/HsApg4B/autophagin-1 cleaves the carboxyl termini of three human Atg8 homologues and delipidates microtubule-associated protein light chain 3- and GABAA receptor-associated protein-phospholipid conjugates. *J. Biol. Chem.* **279**, 36268–36276 (2004).

40. Zhong, Y. *et al.* Distinct regulation of autophagic activity by Atg14L and Rubicon associated with beclin-1-phosphatidylinositol-3-kinase complex. *Nat. Cell Biol.* **11**, 468–476 (2009).

41. Degrossi, A. *et al.* Transfer of HIV-1 to human tonsillar stromal cells following cocultivation with infected lymphocytes. *AIDS Res. Hum. Retroviruses* **10**, 675–682 (1994).

42. Blaauw, B. *et al.* Akt activation prevents the force drop induced by eccentric contractions in dystrophin-deficient skeletal muscle. *Hum. Mol. Genet.* **17**, 3686–3696 (2008).

43. Pepe, G. *et al.* Bethlem myopathy (BETHLEM) and Ullrich scleroatonic muscular dystrophy: 100th ENMC international workshop, 23–24 November 2001, Naarden, The Netherlands. *Neuromuscul. Disord.* **12**, 984–993 (2002).

1. Introduction

1.1 The ECM in the nervous system

For a long time the existence of an extracellular matrix (ECM) in the nervous system, particularly in the central nervous system (CNS) was neglected. In the 1970s, neurobiologists started recognizing the presence of a matrix characterized by the paucity of otherwise frequent ECM molecules, such as fibronectin or collagens. Nonetheless, the structure and function of the ECM is much more elucidated in the peripheral nervous system (PNS) rather than in the CNS (Zimmermann and Dours-Zimmermann, 2008).

The ECM in the brain is predominantly made of chondroitin sulfate proteoglycans (CSPGs) of the lectican/hyalactan family, hyaluronan, link proteins, tenascins and basement membrane (BM) components (collagen IV, laminins, fibronectin). Actually a true BM exists around all cerebral blood vessels and the *glial limitans externa*, separating astrocytic foot processes from pia-arachnoid cells (Rutka et al., 1988). Proteoglycans are glycoproteins bound to a variable numbers of N- and O-linked glycosaminoglycan (GAG) side chains, covalently linked to a core protein. Hyaluronan (also known as hyaluronic acid) is the only unsulfated GAG and is present in the ECM as a core protein-free molecule. The main hyaluronan binding proteins in the nervous system are lecticans, such as brevican, neurocan, aggrecan and versican. Besides these large aggregating proteoglycans of the lectican family, phosphacan, whose RNA precursor can alternatively give rise to a receptor type tyrosine phosphatase, is able to bind the secreted glycoproteins tenascin-R and tenascin-C (Novak and Kaye, 2000). Phosphacan also interacts with various cell adhesion molecules of the Ig-superfamily, including N-CAM, Ng-CAM, axonin-1 and contactin, and it binds to the extracellular portion of voltage-gated sodium channels. The hyaluronan and lectican interactions are reinforced by a group of small link proteins collectively named HAPLNs (hyaluronan and proteoglycan binding link proteins) (Zimmermann and Dours-Zimmermann, 2008). Even if the amount of collagens and fibrous protein is extremely low in the CNS, these proteins are well expressed in several stages of CNS development and in several pathophysiological conditions. Some collagens, such as types I, IV, IX, XVII and XVIII, are involved in directioning axonal cone growth (Hubert *et al.*, 2009); collagen type IV is important for synapse stabilization (Fox, 2008); collagen types I and IV are involved in neurogenesis and stem cell niche adaptation; finally, collagen types I, III and V can support axonal regeneration after damage (Hubert *et al.*, 2009).

In the nervous system, the ECM is involved in the maintenance of the normal structure and supports its functions. Furthermore, the ECM fulfills important roles during embryonic development (e.g., it is required for regulating the migration and differentiation of neural crest cells), in adult neurogenesis, and in some pathological processes such as repair and neoplasia (Rutka *et al.*, 1988; Wojcik-Stanaszek *et al.*, 2011).

Within the central nervous system, a peculiar specialized ECM consists in perineuronal nets (PNNs), lattice-like structures found in particular population of neurons, which enwrap the cell soma and proximal neurites and embed, with the exception of the synaptic clefts, the presynaptic boutons. PNNs were first described as reticular networks by Golgi and Cajal in the 1890s. At first dismissed as an artefact due to the staining techniques, PNNs are now recognized and increasingly studied as structures with specific features and functions (Celio *et al.*, 1998). They can be stained through the binding with agglutinins from *Wisteria floribunda*, *Vicia villosa* and soy bean, which can bind with high affinity N-acetylgalactosamine residues (Karetko and Skangiel-Kramsa, 2009).

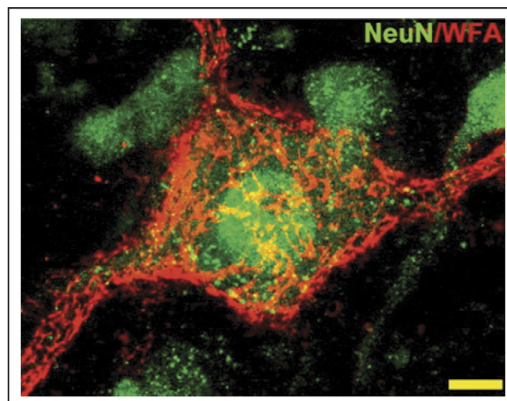


Figure 1. CSPGs in a perineuronal net enveloping a neuron. CSPGs are labeled by *Wisteria floribunda* agglutinin (WFA) staining (in red). Neurons are labeled by staining for the neuron-specific nuclear protein (NeuN, in green). Scale bar, 10 μm (Busch and Silver, 2007).

PNNs consist of extracellular proteoglycans of the lectican class, which are complexed with hyaluronan through specific link proteins and colocalize with tenascins (Fig. 1). Most of the PNN constituents seem to be expressed by the ensheathed neurons themselves, but contributions from surrounding glial cells cannot be excluded. PNNs can be observed in many areas of the CNS including the cerebral cortex, the hippocampus, the thalamus, the cerebellum, the brain stem and the spinal cord (Zimmermann and Dours-Zimmermann, 2008). PNNs develop postnatally during the period of synaptic refinement and myelination, indicating the beginning of mature physiological properties of neurons (Brückner and Grosche, 2001). Possible roles for the immature PNNs are the formation of a link between the

extracellular space and the intracellular cytoskeleton, and the capability of attracting and trapping neurotrophic factors, thus regulating neuronal maturation and axonal growth. As postnatal maturation of CNS proceeds, PNNs become more complex thus stabilizing synaptic contacts, supporting the electrical activity of neurons and modulating their plasticity (Karetko and Skangiel-Kramsa, 2009).

The PNS mainly consists of motor and sensory neurons (axons) and Schwann cells. Fibroblasts constitute roughly 10% of total cells within the PNS (Alovskaya et al., 2007). The myelinated axons of motor and large sensory neurons, as well as the unmyelinated nerves of small sensory and autonomic neurons, are bundled into fascicles within the connective tissue layer of the epineurium. Each fascicle is surrounded by the perineurium (the level of the blood-nerve barrier) and each nerve fiber is contained within the endoneurium (Wood et al., 2011). The ECM composing this connective tissue is mostly produced by Schwann cells during nerve development, and it is made of a tubular basal lamina sheet that surrounds the individual axon/Schwann cell unit and by a fibrillar matrix consisting of collagen-based fibrils that lie external to the basal lamina in mature nerves. When Schwann cell function is perturbed, basal lamina fails to form and nerve function is impaired. Therefore, in the PNS therefore the ECM has different key roles in nerve fiber outgrowth, proliferation of Schwann cells and myelination of nerves (Rutka et al., 1988). It is known that laminin, fibronectin and collagen types I, IV and XVIII secreted from Schwann cells can promote cell adhesion and support their migration, while tenascin and fibrin, ECM proteins abundantly expressed in the developing PNS, can inhibit Schwann cell migration on fibronectin, likewise decorin and versican proteoglycans (McGarvey *et al.*, 1984; Probstmeier *et al.*, 2001; Braunewell *et al.*, 1995). Moreover, several ECM proteins can be involved in the regulation of neurite outgrowth and axon fasciculation. Thus, laminin can induce axonal growth, while studies on NG2 proteoglycan, tenascin-R and collagen V revealed that they have an inhibitory action (Probstmeier *et al.*, 2001; Ughrin *et al.*, 2003). Thus increasing evidence underlines the importance of ECM in supporting PNS development, and in maintaining structural properties and functions, with implications on proper regeneration after injury.

1.2 Collagen VI in PNS and CNS

The first studies that showed collagen VI presence in the nervous system considered solely PNS. The reasons stand in the fact that analysis on collagen VI expression during mouse embryogenesis and postnatal development showed no presence of transcripts and protein in CNS, while in the PNS the expression was evident mostly in the distal portion of

nerves as a sheath around axon bundles (Marvulli *et al.*, 1996). Collagen VI is indeed abundant in peripheral nerves, where it is produced both by Schwann cells and by endo- and perineurial cells (Jaakkola *et al.*, 1989).

During development, neural crest cells migrate to reach differentiation sites, and collagen VI is a primary component of the ECM deposited along the migratory pathways of neural crest cells, suggesting that the protein participates to the regulation of their movement (Perris *et al.*, 1993). Using a transgenic mouse line expressing the *lacZ* reporter under the control of a regulatory region of the *Col6a1* gene, Vitale and co-workers managed to demonstrate when neural crest cells start expressing collagen VI and showed that the induction of collagen VI expression in these Schwann cell precursors is neuregulin-dependent, although this dependence is lost as soon as collagen VI expression is elicited (Vitale *et al.*, 2001). Activation of the *Col6a1* gene corresponds to the time in which immature Schwann cells start differentiating into myelinating cells, and once they acquire their mature phenotype Schwann cell cease to express collagen VI (Vitale *et al.*, 2001). The same regulation must occur in postnatal and adult nerves, given the persistent presence of collagen VI in the ECM of peripheral nerves until adulthood.

Collagen VI presence in the CNS was initially revealed in a study investigating the interactions between meningeal cells and glia limitans, highlighting the importance of ECM molecules in the interspace between these two structures in the proper glia limitans organization (Sievers *et al.*, 1994). Subsequent immunohistochemical studies in goat demonstrated the presence of collagen VI in the connective compartments of the pars distalis, intermedia and lobus nervosus of hypophysis (Nishimura *et al.*, 2004). Other works demonstrated the *in vitro* expression of collagen VI by glial cells. Thus, the U-87 MG glioblastoma cell line, which exhibits properties of glial precursor cells, expresses collagen VI, suggesting that it may be involved in tumour cell infiltration and invasion of healthy brain in rats (Han *et al.*, 1994; Han *et al.*, 1995).

More recently, Cheng and co-workers demonstrated a connection between collagen VI expression and Alzheimer disease. They analyzed hippocampal *Col6a1* expression in wild-type mice and in transgenic mice with neuronal expression of familial Alzheimer's disease-mutant human APP (hAPP), as well as in humans with or without Alzheimer's disease, and found that both mRNA and protein levels were higher in the affected samples (Cheng *et al.*, 2009). By *in situ* hybridization, dentate gyrus granule cells were identified as the main source of collagen VI expression in the affected samples. The pyramidal layer of the hippocampal subregions CA1 and CA3 and the neocortex also showed some collagen VI expression but at

lower levels. In a different set of experiments, these authors showed a dose-dependent increase in *Col6a1* mRNA and protein in primary cultured neurons treated with A β -peptides, but not in cultured astrocytes. Moreover, neuronal cultures derived from *Col6a1*^{-/-} mice displayed increased apoptosis than wild-type cultures when treated with A β -peptides, thus indicating a neuroprotective role for collagen VI against A β -peptides toxicity (Cheng *et al.*, 2009).

A neuroprotective effect for collagen VI was also suggested by studies on UV irradiation in cultured neurons. Expression of *Col6a1*, *Col6a2* and *Col6a3* genes was increased in primary neurons after UV irradiation. Moreover, addition of soluble collagen VI to the culture medium could rescue UV-induced apoptosis and limit dendrite shrinkage, by acting through the Akt and JNK pathways (Cheng *et al.*, 2011).

These recent observations threw new light on the presence and function of collagen VI in the CNS and opened new perspectives on the potential role of this ECM component in regulating neuronal survival processes.

1.3 Autophagy in the nervous tissue

Neurons display specific features in intracellular communication provided by highly specialized structures like axons, dendrites and synapses. In particular, along the axon, proteins and organelles are transferred over significant distances in the nervous system. Neurons are more susceptible to the consequences of dysfunctional autophagy (Fig. 2). In addition, since neurons are post-mitotic cells and do not replicate, they result more prone to accumulate toxic proteins and damaged mitochondria and other organelles than replicating cells that could dilute all this through cell divisions (Son *et al.*, 2012). Autophagy has been suggested to be associated with axonal dystrophy and swellings following axotomy or excitotoxic insults, leading to chromatolysis, a condition where cytoplasm is devoid of organelles and filled with vesicles including autophagosomes. Synapses represent regions of high-energy demand and protein turnover. In agreement with this, increasing or decreasing autophagy in synapses can influence their size and function.

The critical importance of tightly controlled autophagy in the nervous system (whose major aspects are described in part I) is underlined by the evidence that in neurons this process can be regulated in a different manner than non-neural cells (Mizushima *et al.*, 2008). For example, LC3-positive autophagosomes are hardly detected in healthy neurons, due to a highly efficient elimination of newly formed autophagosomes, thereby avoiding a build-up of autophagic intermediates even when the process is strongly induced, whereas massive

accumulation of autophagic vacuoles is observed under pathological conditions (Boland *et al.*, 2008).

The importance of maintaining a basal level of autophagy in neurons is also confirmed by some studies carried out on mice with targeted inactivation of *Atg5* or *Atg7* genes in the nervous system (Hara *et al.*, 2006; Komatsu *et al.*, 2006). In *Atg5*^{-/-} and *Atg7*^{-/-} mice autophagy cannot be activated, leading to growth retardation, progressive motor deficits and neurodegeneration, thus indicating a crucial role for autophagy in neuronal homeostasis.

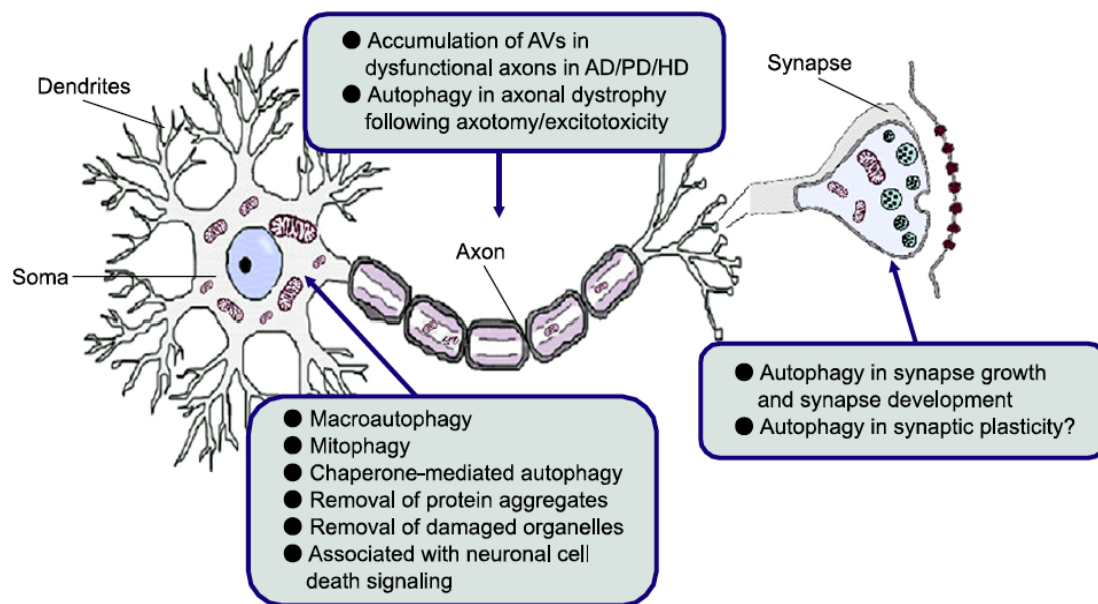


Figure 2. The physiologic and pathogenic roles of autophagy in neurons. Neurons have highly specialized structures for intracellular communication. In the soma, basal levels of autophagy occur to maintain normal cellular homeostasis. In the axon, organelles and proteins are transferred over significant distances by axoplasmic transport. Axotomy and excitotoxic insults trigger the accumulation of autophagosomes resulting in dystrophic axonal swellings. Autophagic vacuoles (AV) have also been observed within dysfunctional axons in Alzheimer's Disease (AD), Parkinson's Disease (PD) and Huntington's Disease (HD). Synapses are region of high energy demand and protein turnover, and they contain abundant mitochondria and polyribosomes. Autophagy is known to play an important role in the development and maintenance of synapses (Son *et al.*, 2012).

In particular, autophagy impairment causes the accumulation of ubiquitin-positive protein aggregates in neurons as well as neuronal loss in the cerebral cortex, hippocampus and cerebellum. The finding that *Atg5*^{-/-} and *Atg7*^{-/-} mice display an accumulation of polyubiquitinated proteins opened new perspectives about the mechanisms regulating protein degradation in neurons. The ubiquitin-proteasome system (UPS) is another essential mechanism that allows an effective protein quality control in neurons, together with the endo-lysosomal system, which can degrade membrane proteins and receptors (Lee, 2009). The

above studies in mice suggested that a strong correlation exists between autophagy and UPS, since the impairment of one of them is able to compromise the activity of the other one, by triggering a self-feeding loop (Fig. 3) (Komatsu *et al.*, 2006). Indeed, growing evidence indicate that p62 is a receptor for ubiquitinated proteins, necessary for their degradation in lysosomes through the binding to LC3, thus resulting in a modulation of the autophagy/UPS crosstalk. Besides its function as a receptor for ubiquitinated proteins, p62 is involved in several signal transduction pathways through its ability of self-oligomerization. p62 is also a scaffold protein for cell survival and death signaling pathways, such as the NF- κ B pathway, the Wnt pathway and apoptosis, and it is plausible that excessive accumulation of p62 leads to dysregulated activation of these signaling pathways (Ichimura and Komatsu, 2011).

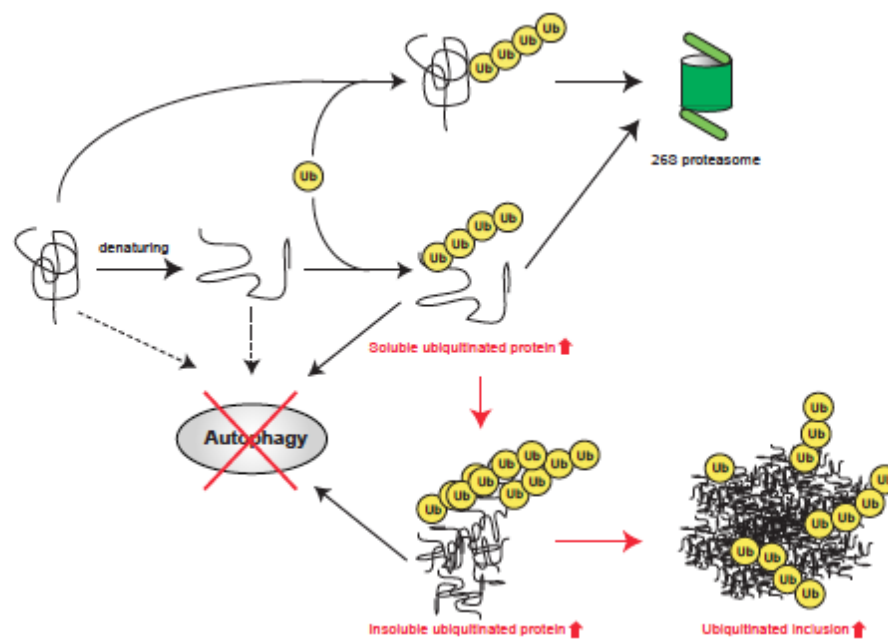


Figure 3. Unfolded/misfolded proteins generated by environmental stresses or genetic mutations are degraded by the UPS after polyubiquitination. Polyubiquitinated protein aggregates can be degraded selectively by the autophagic pathway via the polyubiquitin-binding protein p62/SQSTM1. Therefore, autophagy might degrade polyubiquitinated proteins (straight line) as well as non-ubiquitinated proteins (dotted lines). Defective autophagy causes the accumulation of highly ubiquitinated proteins, a process that is also observed during aging. The red symbols highlight the consequences caused by a defective activity of the autophagic process. Ub, ubiquitin (Komatsu *et al.*, 2006).

The relationship between autophagy and UPS is increasingly detectable in aging, when both systems undergo striking changes decreasing their efficiency. Aging cells display also notable changes in lysosomes, which appear increased in volume, less stable and defective in hydrolases activity, leading to intra-lysosomal accumulation of indigestible material called lipofuscin. These changes correlate with a decrease in total capacity for degradation of long-lived proteins in many tissues of aged animals, also accounting for the occurrence of increased protein aggregates inside cells. A diminished turnover of intracellular

components and a reduced ability of cells to adapt to changes in the extracellular environment are the major consequences of age-related autophagy decline. The impaired clearance of old and damaged mitochondria likely contributes to the increase in oxidative damage in aging cells (Mc Cray and Taylor, 2008).

These findings led to think that enhancing autophagy might allow to prevent neurons from the occurrence of neurodegeneration. On the other side, a growing body of evidence shows many neurological disorders can be associated with the accumulation of autophagosomes in brain. Therefore, like two sides of the same coin, autophagy seems to be protective at a basal level, and detrimental to neuronal survival if excessively induced (Lee, 2009). Indeed in Alzheimer's disease, Parkinson disease, and Huntington disease, the pathological accumulation of autophagosomes and abnormalities in the endosomal-lysosomal pathway were documented by electron microscopy both in patients and model mice tissues (Jaeger and Wyss-Coray, 2009). Beclin-1 protein levels were found decreased in the cortex of patients affected by Alzheimer's disease, despite an increase in the number of autophagosomes and in the levels of LC3-I/LC3-II (Son *et al.*, 2012). A possible explanation for this apparent contradiction is that the autophagosomal flux is altered, impairing in turn endosomal-lysosomal degradation, leading to a build-up of intracellular vesicular compartments over time. Parkinson disease and Huntington disease are mainly caused by mutations in specific proteins, making neurons more prone to accumulate protein aggregates, and in both cases the pharmacological induction of autophagy seems able to enhance the clearance of aggregates, thus supporting a neuroprotective role for autophagy (Jaeger and Wyss-Coray, 2009; Cheung and Ip, 2011). Some other neurodegenerative diseases were linked to autophagy deregulation, such as fronto-temporal dementia and amyotrophic lateral sclerosis. Deregulation of autophagy was also found in different brain insults, such as hypoxia/ischemia, brain trauma, pharmacological injury models and trophic factor deprivation, in which again experimental observations revealed increased levels of autophagy proteins and/or autophagosomes number (Luo *et al.*, 2011). Growing evidence show that although a basal level of autophagy is required for neuronal survival, activation of certain pathways associated to "pathological" autophagy may push the level of autophagy to the extreme, leading to cell death (Cheung and Ip, 2011).

1.4 *In vitro* models to study neural processes

Given the complexity of CNS morphology, architecture and processes, many studies are performed on cell culture models, in order to elucidate specific signalling pathways, to

dissect molecular components or to understand physiological processes such as synaptic plasticity, all aspects that would be almost impossible to highlight if studied in the whole tissue. The same is true for highly regulated processes like the ones involved in neurodegeneration. Cellular models are far from being able to reproduce the complexity of neurodegenerative processes, but they can provide valuable insights for validation in animal models or in human specimens. Generally *in vitro* models (established cell lines, primary cultures or stem cells) offer the advantage of a controlled environment, but may lack the cellular microenvironment critical to disease development (Alberio et al., 2012).

Different types of cellular models were employed to investigate pathways involved in neurodegeneration. One example is represented by neuroblastoma cell lines, which are transformed neural crest-derived cells capable of unlimited proliferation *in vitro*. These cells are able to differentiate into neuronal cell types according to different treatments in culture. The ability of neuroblastoma cells to proliferate as well as to differentiate make them an excellent *in vitro* system for various studies. Both murine and human neuroblastoma cell lines are largely used for several applications, such as for studying the protective role of autophagy, for creating disease models by transfecting cells with mutant pathogenic proteins, and for testing drugs or treatments able to arrest and rescue neurodegeneration (Shastry *et al.*, 2001; Zeng and Zhou, 2008; Yamamoto *et al.*, 2006; Krüger *et al.*, 2011).

The immortalized and clonally uniform murine neuroblastoma 3 spinal cord (NSC) hybrid cell lines, developed as a model for the study of motor neuron biology, are largely used to investigate spinal bulbar muscular atrophy (Piccioni *et al.*, 2001). NSC hybrids were produced through somatic fusion between neuroblastoma cells and motor neuron-enriched embryonic spinal cord cells. One of these clones, NSC-34, expresses many of the morphological and physiological properties of motor neurons, including extension of processes, formation of contacts with cultured myotubes, synthesis and storage of acetylcholine, support of action potentials, induction of myotube twitching, and expression of neurofilament proteins (Matusica *et al.*, 2008). But the most used cell models in neurobiology are constituted by neuronal primary cultures from rats or mice. With such a tool it is possible to analyze properties related to cellular trafficking, cellular structure and individual protein localization using a variety of biochemical techniques. However, some difficulties may arise due to the possible occurrence of minimum contaminations by other brain cell types (Seibenhener *et al.*, 2012).

Primary neural cultures are commonly derived from embryonic or postnatal stages, while cultures from adult animals are not so frequently used due to limitations in handling

mature neurons *in vitro*. However, cultures from embryos or pups result less homogeneous than adult ones, since they are derived from a pool of siblings (Ray *et al.*, 2009). These cultures can be considered as mixed cultures, consisting of variable proportions of different cell types, and can be enriched in a particular cell type by using specific purification protocols or differentiating media. Some features of primary neural cultures, such as their survival capabilities, the cellular composition and their sensitivity to different insults, can be affected by many intrinsic and extrinsic factors including the originating brain region, the developmental stage, the animal gender and genetic background, the permanence in culture and the culture conditions. The most appropriate *in vitro* model should be chosen, based on the specific aspects that are going to be investigated. Therefore, it is fundamental to characterize the culture in use. Neuronal cultures are considered one of the essential models to perform advance research in different neurodegenerative diseases (Chen and Herrup, 2008).

In my thesis work I also started by establishing an *in vitro* culture model, derived by cortices and hippocampi of neonatal pups, resulting in mixed neural cultures. This allowed me to investigate critical cellular pathways related to the presence of collagen VI, before moving to the *in vivo* context.

2. Methods

2.1 Mice

2-day, 7-month, 12-month- and 23 month-old wild-type C57BL/6 and *Col6a1*^{-/-} (Bonaldo *et al.*, 1998) mice were used to perform the studies described in this thesis. As far as CNS analysis is concerned, animals were sacrificed by cervical dislocation, brains were dissected and rapidly frozen in liquid nitrogen for protein extracts and histological analysis. For PNS analysis, animals were deeply anesthetized by i.p. injection with Avertin (150 mg/kg body weight) and transcardially perfused with saline solution supplemented with heparin, followed by 4% paraformaldehyde in PBS. One part of the dissected sciatic nerves was postfixed overnight in 4% buffered paraformaldehyde and, after cryoprotection with 30% sucrose, frozen in liquid nitrogen. Another part of the dissected nerves was embedded in OCT and rapidly frozen in nitrogen, and finally a third part was postfixed in glutaraldehyde and embedded in epoxid resin.

2.2 Behavioural tests

Rotarod. Motor performance was measured on a rotating bar using the Rotarod device. 7- and 23-month-old animals were trained for 2 days, in order to get used to the rotating bar, and then tested on three consecutive days. Each day, three runs were conducted with each animal. Mice were placed on the Rotarod at a fixed speed (30 round per minutes). In the last day, the time each mouse stood on the rotating rod was measured and recorded.

Footprint analysis. The analysis was performed using a 1 m long and 6 cm wide walking track, laid out with paper strips. 7-month-old mice were trained one or two times before the first measurement. Forepaws and hindpaws of mice were dipped in atoxic black paint or green paint, respectively. Based on the footprints, stride length, base width, footprint overlap and foot angle to walk direction were measured. The stride variability was calculated by subtracting the shortest stride from the longest stride. The angles between footsteps and walking direction were measured with the support of ImageJ software.

Ledged beam test. The analysis was performed on 7- and 23-month-old mice using a suspended runway 80 cm long and 6 cm wide at the starting point, which gradually narrowed down to 0,5 cm. The distance from the starting point to the point where the first foot fault occurred was measured. The number of total hind foot faults and the time spent to cross the

runway were recorded. Mice were tested at different ages.

Hot plate test. 3-month, 7-month and 12-month-old mice were placed on temperature-controlled plate heated to 55°C and the time was measured until animals displayed one the following responses: lick of forepaws, jumping, or climbing the plate walls. Once the response was elicited, the mouse was immediately taken off the plate and placed back in its original cage.

2.3 CNS analysis

2.3.1 Brain and spinal cord sections

Right and left hemispheres of dissected brains were separated, rapidly frozen by liquid nitrogen immersion and used to obtain cryo-sagittal sections of 7 µm. Slices were in part collected onto glass slides and in part used for preparing protein extracts, in order to perform comparable analysis. 7-µm spinal cord sections were cut and used for immunofluorescence analysis.

Immunofluorescence on sections. Cryosections of brains and spinal cord were fixed, permeabilized for 10 minutes in cold 100% methanol at -20 °C and then dried. After three washing in PBS, samples were incubated for 2 hours with 4% BSA IgG-Free (BBBSA, Jackson) in PBS solution, washed in PBS buffer and treated for 30 minutes with a blocking solution containing 0.05 mg/ml, anti-mouse IgG Fab fragment (Jackson Immunoresearch). Slides were washed three time in PBS and incubated at 4°C over night with primary antibodies diluted in BBBSA solution. The following primary antibodies were used: rabbit anti-collagen VI AS72 (kindly supplied by Prof. A. Colombatti, CRO, Aviano); rabbit and guinea-pig anti-alpha3 collagen VI (kindly supplied by Prof. R. Wagener, Colonia); mouse anti-GFAP (Millipore); mouse anti β3-tubulin (Sigma-Aldrich); rabbit anti-p62 (Sigma-Aldrich). Slides were then washed three times in PBS before incubation for 1 hour with secondary antibodies at room temperature. The following secondary antibodies were used: anti-mouse CY2 (115-226-062, Jackson Immunoresearch); anti-rabbit CY2 (111-225-144, Jackson Immunoresearch); anti-rabbit CY3 (111-165-144, Jackson Immunoresearch); anti-rabbit IRIS5 (5WS-08, Cyanine Technologies); anti-guinea-pig CY2 (706-545-148, Jackson Immunoresearch). Nuclei were stained by incubation with Hoechst 33258 (Sigma). After washing slides three times in PBS, slides were mounted in 80% glycerol-PBS and analyzed by fluorescence microscope.

TUNEL analysis on brain sections. TUNEL (TdT-mediated dUTP Nick-End Labeling) assay was performed with the Dead End Fluorometric *in situ* apoptosis detection system (Promega). The system is able to detect 3'-OH ends in fragmented DNA molecules of apoptotic cells, by incorporating fluorescein-12-dUTP, using the recombinant Terminal Deoxynucleotidyl Transferase enzyme (rTdT). Brain cryosections were permeabilized for 10 minutes at -20°C in cold 100% methanol. Slides were dried, washed in PBS, treated for 5 minutes with proteinase K at room temperature, washed again in PBS and incubated with equilibration buffer for 10 minutes. Samples were then incubated for 1 hour at 37 °C with a buffer containing fluorescent nucleotides, rTdT enzyme and Hoechst. SSC solution was used to block the activity of rTdT enzyme, before washing and preparing slides for microscopy analysis.

Western blotting. Brain cryo-sections were lysed in a lysis solution (Tris 50 mM, pH 7.5, NaCl 150 mM, MgCl₂ 10 mM, DTT 0.5 mM, EDTA 1 mM, glycerol 10%, SDS 2%, Triton X-100 1%) in the presence of phosphatase inhibitors (Cocktail II, Sigma) and protease inhibitors (Complete EDTA free, Roche), and proteins quantified with the BCA Protein Assay kit (Pierce). 20 µg of protein lysates were separated by SDS-PAGE on 12% or 4-12% polyacrylamide gels (Invitrogen) and blotted onto PDVF membrane (Millipore). Membranes were incubated overnight at +4°C with the primary antibodies, in a 0.1% Tween-TBS (TTBS) solution supplemented with 5% BSA (Sigma). Membranes were then washed three times with TTBS and incubated for 1 hour at room temperature with HRP-conjugated secondary antibodies (Amersham Bioscience) in TTBS supplemented with 5% milk. Detection was by chemiluminescence (Pierce). When needed, membranes were stripped using a stripping buffer (25 mM glycine, 1% SDS, pH 2.0) and re-probed. The following primary antibodies were used: rabbit polyclonal anti-Bcl-1 (Cell Signalling Technologies); guinea pig polyclonal anti-p62 (Progen); rabbit polyclonal anti-LC3B rabbit (Sigma-Aldrich); mouse monoclonal anti-Bcl2 (BD Transduction Laboratories); mouse monoclonal anti-β-actin (Chemicon International). Western blots were performed in at least three independent experiments. When indicated, densitometry was carried out using the ImageJ software.

DHE staining. When oxidized by ROS, DHE forms ethidium bromide, emitting red fluorescence and intercalating DNA. 7-µm brain cryosections were immersed in a PBS solution containing 5 µM DHE (Sigma) and kept at 37°C for 30 min in dark environment. Slides were then washed twice with PBS and prepared for microscopy analysis. Fluorescence intensity was measured by Photoshop software.

2.3.2 Primary neural cultures

Preparation of primary neural cultures. Cortexes and hippocampi from P0-P1 mice were dissociated in trypsin (0.8 mg/ml, Sigma) for 10 min at 37 °C. Digestion was blocked by a solution containing trypsin inhibitor (6.3 µg/ml, Sigma) and DNase I (40 µg/ml, Invitrogen). Dissociated cells were plated at a density of 5×10^5 cells on glass coverslips coated with either poly-L-lysine (100 µg/ml), collagen I (Sigma), or murine native collagen VI (Irwin et al., 2003). The culture medium consisted of MEM (GIBCO) containing glucose (20 mM), L-glutamine (0.5 mM), N2 supplement (1%), B27 supplement (0.5%), biotin (0.875 mg/l), pyruvic acid (1 mM), penicillin (25 µg/ml) streptomycin (25 µg/ml), fungizone (50 µg/ml) and horse serum (10%, GIBCO). Cytosine-β-d-arabinofuranoside (3 µM) was added 24 h after plating. Cultures were grown for 7 days, and the last day cells were subjected to different treatment conditions for 4.5 hours. The following treatments were used: DMEM (GIBCO) without serum (“no serum” condition); DMEM without serum, in the presence of 3-methyladenine (10 mM, Sigma); DMEM without serum, in the presence of cloroquine (50 µM, Sigma); DMEM without serum, in the presence of rapamycin (100 nM, LC-Laboratories).

Immunofluorescence on cells. Primary cultures on slides were washed in PBS, permeabilized for 3 minutes at room temperature with PBS in the presence of 0.1% Triton X-100, washed three times in PBS, and incubated for one hour with a blocking solution containing 10% goat serum (Sigma) in PBS. Cells were incubated for 2 hours at room temperature or over night at 4° C with primary antibodies diluted in 5% goat serum in PBS. The following antibodies were used: anti-collagen VI AS72 (kindly supplied by Prof. A. Colombatti, CRO, Aviano); rabbit and guinea-pig anti-alpha3 collagen VI (kindly supplied by Prof. R. Wagener, Colonia); mouse anti-GFAP (Millipore); mouse anti β3-tubulin (Sigma-Aldrich); rabbit anti-NG2 (kindly provided by Prof. R. Perris, CRO, Aviano); rabbit anti-vimentin (Santa Cruz Biotech); rabbit anti-p62 (Sigma-Aldrich). After three washing in PBS, slides were incubated for one hour with the appropriate secondary antibody diluted in 5% goat serum in PBS solution. The following secondary antibodies were used: anti-mouse CY2 (115-226-062, Jackson Immunoresearch); anti-rabbit CY2 (111-225-144, Jackson Immunoresearch); anti-rabbit CY3 (111-165-144, Jackson Immunoresearch); anti-rabbit IRIS5 (5WS-08, Cyanine Technologies); anti-guinea-pig CY2 (706-545-148, Jackson Immunoresearch). Nuclei were stained by incubation with Hoechst 33258 (Sigma). After washing three times in PBS, slides were mounted in 80% glycerol-PBS and analyzed by fluorescence microscope.

Cells transfection. On the sixth day of culture, plasmids of interest at 1 $\mu\text{g}/\mu\text{l}$ concentration were used to transfect primary cells using the Transfectin Lipid Reagent (Bio-Rad), according to manufacturer's guidelines. The pMito-red (kindly provided by Prof. L. Scorrano, Padova) and pEYFP-hLC3 (Clontech) plasmids were used in this study.

DNA laddering analysis. Cells plated at 1.5×10^6 per well in a 6-well-plate (Falcon) were washed in PBS after medium removal and lysed in a solution containing Tris-HCl 10 mM, pH 8, sodium acetate 0.3 M, EDTA 1 mM, pH 8, SDS 1% and proteinase K 200 $\mu\text{g}/\mu\text{l}$. Extracts were incubated for 6 hours at 37° C and for 3 hours at 56° C and finally frozen for 10 minutes at -80° C. After centrifuging the frozen samples at 4° C to remove SDS, the aqueous phase was recovered and DNA was extracted by two incubations in one volume phenol-chloroform (1:1 v/v), followed by one incubation in one volume chloroform, and precipitated by one volume of isopropanol and 1/30 volume of sodium acetate 3 M. After centrifugation, DNA pellet was washed in 70% ethanol, dried and resuspended in TE buffer (Tris-HCl 10 mM, EDTA 0.1 mM, pH 8). DNA was quantified by Nanodrop and analyzed by electrophoresis on a 1% agarose gel containing Gel Red.

TUNEL assay on cells. TUNEL analysis was performed with the Dead End Fluorometric *in situ* apoptosis detection system (Promega), as described above. Cells were first stained for immunofluorescence and then, once washed the secondary antibody, directly incubated with equilibration buffer for 10 minutes. Cells were further incubated for 1 hour at 37 °C with a buffer containing fluorescent nucleotides, rTdT enzyme and Hoechst. SSC solution was used to block the activity of rTdT enzyme, then slides were washed and prepared for microscopy analysis.

Western Blotting. Primary neural cells, cultured in 6-well-plates (1.5×10^6 cells per well), were washed in PBS, scraped in a lysis buffer containing Tris-HCl 50 mM, pH 7.5 NaCl 150 mM; EDTA 20 mM and NP40 0.5%, in the presence of phosphatase inhibitors (Cocktail II, Sigma) and proteases inhibitors (Complete EDTA free, Roche). Proteins were quantified with the BCA Protein Assay kit (Pierce). 20 μg of protein lysates were separated by SDS-PAGE on 12% or 4-12% polyacrylamide gels (Invitrogen) and blotted onto PDVF membrane (Millipore). Membranes were incubated overnight at +4° C with primary antibodies in TTBS solution supplemented with 5% BSA (Sigma). Membranes were then washed three times with TTBS, and incubated for 1 hour at room temperature with HRP-conjugated secondary antibodies (Amersham Bioscience) in TTBS supplemented with 5% milk. Detection was by chemiluminescence (Pierce). When needed, membranes were stripped using a stripping buffer

(25 mM glycine, 1% SDS, pH 2.0) and re-probed. The following primary antibodies from Cell Signalling Technologies were used: rabbit polyclonal anti-AMPK; rabbit polyclonal anti-phospho-AMPK (Thr172); rabbit monoclonal anti-Bcl_{X_L} (clone 54H6). Guinea pig polyclonal anti-p62 was from Progen. Rabbit polyclonal anti-LC3B rabbit were from Sigma. Rabbit polyclonal anti-Bax (N-20) was from Santa Cruz. Mouse monoclonal anti-Bcl2 was from BD Transduction Laboratories. Mouse monoclonal anti-β-actin was from Chemicon International. Western blots were performed in at least three independent experiments. Densitometric analysis was carried out using the ImageJ software.

ROS measurements. Cells were seeded on slides at 1.5×10^6 per well in 6-well plates. ROS production was evaluated with the reduced Mitotracker Red probe (MTR, Molecular Probes), by measuring the increase in fluorescence intensity that occurs when MTR is oxidized. Cells were incubated for 15 minutes at 37°C with 25 nM MTR in DMEM. Cells were then washed twice with fresh DMEM and monitored using the Metamorph (Universal Imaging) imaging software, applied to an inverted microscope (Olympus IMT-2) equipped with a xenon lamp as a fluorescence light (75W), a 12 bit CCD camera provided with a cooling system (Miromax Princeton Instruments). Regions of interest were defined as regions rich in mitochondria and belonging to cells showing clear neuronal morphology. Fluorescence in these regions was monitored for the whole length of the experiment, and kinetics were then obtained.

2.4 PNS analysis

2.4.1 Sciatic nerve sections

Morphometry. Morphological observations were performed by light microscopy on semithin sections stained with blue toluidine, prepared as described above (paragraph 2.1). Fields were randomly chosen at 1000X magnification, where each field covered 0.016 mm^2 of the nerve. Morphometric analysis of sciatic nerves was performed manually through the ImageJ software. At least 500 myelinated fibers (MF) per nerve were evaluated. Data from fibers with evident degeneration signs, or sectioned in a longitudinal way, were not collected. For each MF, the axon perimeter was traced, obtaining axonal cross sectional area. Fiber and axon diameters were traced and the g ratio (axon diameter vs. fiber diameter) was calculated.

Electron microscopy. Sciatic nerve ultrathin sections were stained with uranyl acetate and lead citrate, and observed in a FEI Tecnai 12 transmission electron microscope (Electron Microscopy Service, Biology Department, University of Padova).

Immunofluorescence on sciatic nerve sections. Sections on slides were fixed and permeabilized for 10 minutes in cold 100% methanol at -20 °C, then slides were dried and washed three times in PBS. Subsequently immunofluorescence was performed as described above (paragraph 2.3.1). The following primary and secondary antibodies were used: anti-collagen VI AS72 (kindly supplied by Prof. A. Colombatti, CRO, Aviano); guinea-pig anti-alpha3 collagen VI (kindly supplied by Prof. A. Wagener, Colonia); rat anti-p75 (Chemicon); anti-rabbit IRIS5 (5WS-08, Cyanine Technologies); anti-rat CY3 (715-225-153, Jackson ImmunoResearch); anti-guinea-pig CY2 (706-545-148, Jackson ImmunoResearch). Nuclei were stained by incubation with Hoechst 33258 (Sigma-Aldrich).

2.4.2 Analysis on teased fibers

Immunofluorescence on teased fibers. Single fibers from sciatic nerves were teased apart after removal of the perineurium using fine stainless-steel needles, dried overnight, and stored at -20°C. For immunostaining, fibers were permeabilized in cold methanol for 10 min at -20°C. After blocking for 1 hour in PBS supplemented with 10% goat serum and 0.1% Triton X-100, samples were incubated overnight at 4°C with primary antibodies. The primary antibodies used were rabbit anti-Caspr (Ori Peles); rabbit anti-Kv1.1 (Alomone Labs); rabbit anti-Nav1.6 (Abcam); rat anti-MBP (Abcam); and rabbit anti-NrCAM (Abcam). After washing in PBS, fibers were incubated for 1 hour with secondary antibodies and DAPI (Roche). The secondary antibodies used were anti-rabbit CY2 (111-225-144, Jackson ImmunoResearch), anti-rabbit CY3 (111-165-144, Jackson ImmunoResearch) and anti-rat CY3 (715-225-153, Jackson ImmunoResearch).

2.5 Microscopy analysis

Unless differently specified, all images were acquired by optical and epifluorescence microscopy (Leica DC500 ZEISS Axioplan), using the IM2000 software, or confocal microscopy (Leica SP5), supporting LAS software.

2.6 Statistical analysis

Data are expressed as means \pm s.e.m. Statistical significance was determined by unequal variance Student's t test. A *P* value of less than 0.05 was considered statistically significant.

3. Results

3.1 Collagen VI detection in the nervous system

To investigate the presence of collagen VI in the nervous system, I performed immunofluorescence analysis in sections from central nervous system (CNS) and peripheral nervous system (PNS) of wild-type and *Col6a1*^{-/-} mice. Concerning CNS, brain and spinal cord were analyzed. As expected, collagen VI was detected in CNS sections from wild-type animals but was not found in knockout samples (Fig. 1A, *a* and *b*). Collagen VI labeling was present along meninges and in the inner cortical region (figure 1A, *a*). In particular, the protein was found in close contact with GFAP-positive cells, which correspond to glial cells, reaching meninges with their extensions (Fig. 1A, *b*). In mouse adult spinal cord sections, Collagen VI was found again along meninges (Fig. 1B, *a*) and in the inner regions. Also in this tissue the protein was found close to GFAP-positive cells and in some cases the protein colocalized with β III-tubulin, a neuronal marker (Fig. 1B, *b* and *c*).

To analyze the distribution of collagen VI in the PNS, I performed immunofluorescence on sciatic nerve sections and dorsal root ganglia from wild-type and *Col6a1*^{-/-} mice (Fig. 2A and B). In wild-type animals, staining for collagen VI was higher and more regularly localized around cell bodies in DRG and around each nerve fiber in the sciatic nerve. The protein was particularly abundant in the perineurium and in the endoneurium.

3.2 Analysis of the role of collagen VI in the CNS

3.2.1 Establishment and characterization of primary neural cell cultures from wild-type and *Col6a1*^{-/-} mice.

I established primary neural cell cultures from hippocampi and cortices of wild-type and collagen VI null newborn (P0 to P1) mice, in order to set up an *in vitro* model for studying some critical pathways, such as apoptosis and autophagy, which we found to be altered in collagen VI null skeletal muscles (see part I). First, I characterized the neural cultures I obtained from wild-type and *Col6a1*^{-/-} mice, by using different cell type markers, such as β III-tubulin (marker for neurons), GFAP (glial cells), vimentin (immature glial cells), and NG2 (oligodendrocytes precursors) (Fig. 3A). The percentage of cells stained by the different markers was then quantified. In cultures from both genotypes, the major component corresponded to neurons (i.e., β III-tubulin-positive cells), whose proportion in the different

culture preparations was in the range of 48% to 65% of the total cells. Notably, wild-type cultures displayed a significantly higher proportion of neurons when compared to collagen VI null cultures (Fig. 3B). Concerning the other markers, the GFAP-positive population was significantly less represented in collagen VI null cultures, whereas vimentin and NG2 did not display any significant difference between cultures derived from the two genotypes (Fig. 3B).

3.2.2 Production of collagen VI by neural cell cultures.

To confirm that this *in vitro* model was suitable for the studies I aimed to perform, I analyzed the production of collagen VI by primary neural cultures using immunofluorescence and confocal microscopy. Collagen VI labelling was detected in wild-type cultures, but as expected the protein was completely absent in *Col6a1*^{-/-} cultures (Fig. 4A). In wild-type cultures, collagen VI was detected in the proximity of the plasma membrane of cells displaying both glial and neuronal morphology. At higher magnifications, and taking advantage of confocal z-stacks three-dimensional reconstruction, it was possible to appreciate how collagen VI labelling of neuronal cells reproduced the waving surface of the cells, which was easily recognizable in the corresponding phase-contrast microscopy images (Fig. 4B). No labelling for collagen VI was detectable in the surroundings of cells, thus suggesting that if the protein is secreted, it must be in close contact with the surface of cells.

Double immunofluorescence for β III-tubulin showed that collagen VI labelling was present either in β III-tubulin-positive and in β III-tubulin-negative cells, suggesting that both neurons and glial cells are able to produce collagen VI (Fig. 4C).

3.2.3 Lack of collagen VI affects the neuronal fraction and causes increased apoptosis in neural cell cultures.

I next focused on the phenotype of neurons, also taking into account previous work where it was reported that neurons are able to over-express α 1(VI) chain following A β -peptides treatment (Cheng *et al.*, 2009). The data I obtained with primary neural cell cultures, showing that neurons are present in larger amount in wild-type cultures than collagen VI null cultures, suggested that collagen VI may be beneficial for neuronal proliferation and/or survival in culture. To further assess this, I investigated the effect of growing wild-type and *Col6a1*^{-/-} neural cells in the presence of purified native collagen VI, provided as a substrate. This set of experiments demonstrated that the neuronal fraction was increased when the cells were seeded on collagen VI. Indeed the incidence of neurons, in terms of percentage of β III-

tubulin-positive cells, was significantly higher in cultures of both genotypes grown onto purified collagen VI, when compared to the corresponding cultures grown in the absence of purified collagen VI (Fig. 5A).

Previous studies showed that collagen VI exerts a cytoprotective role in skeletal muscle, an aspect that is strengthened by the fact that collagen VI deficiency leads to increased spontaneous apoptosis of muscle fibers (Irwin *et al.*, 2003). Starting from this concept, and based on the data I obtained above with neural cultures, I therefore investigated whether lack of collagen VI may affect apoptosis in this *in vitro* primary neural culture model. TUNEL analysis showed that *Col6a1*^{-/-} neural cultures display a significantly higher incidence of spontaneous apoptosis than the corresponding wild-type cultures (Fig. 5, B and C). Remarkably, the incidence of TUNEL-positive nuclei was lowered in cultures of both genotypes when cells were seeded onto collagen VI, but not when they were seeded onto collagen I (Fig. 5C), thus indicating that collagen VI elicited an anti-apoptotic response that was not mimicked by another abundant ECM component.

DNA fragmentation analysis by gel electrophoresis is another qualitative method used, also in neuronal cultures, to assess apoptosis by directly accounting the effects on DNA, which usually breaks into multiples of ~200 base pair size fragments, thus giving rise to a sort of regular laddering in gels (Tan *et al.*, 1998; Ioannou and Chen, 2006). Analysis of genomic DNA extracted from wild-type and *Col6a1*^{-/-} primary neural cultures (Fig. 5D) showed that the DNA laddering was more intense in *Col6a1*^{-/-} cultures. Moreover, the laddering intensity appeared slightly reduced when *Col6a1*^{-/-} cultures were grown onto collagen VI, but not when they were grown on collagen I (Fig. 5D). Western blot analysis for some pro- and anti-apoptotic factors in total protein extracts from wild-type and *Col6a1*^{-/-} neural cultures revealed increased levels of Bax in *Col6a1*^{-/-} samples (Fig. 5E). The higher abundance of this pro-apoptotic factor further supports the concept that the apoptotic pathway is affected in the absence of collagen VI. Conversely, the anti-apoptotic factor BCL-X_L displayed apparently similar levels in cultures of both genotypes, whereas BCL-2 was noticeably increased in *Col6a1*^{-/-} samples (Fig. 5E).

3.2.4 Lack of collagen VI causes alterations of the mitochondrial network in neural cell cultures.

Collagen VI deficiency in the skeletal muscle was found to lead to mitochondrial dysfunction, with mitochondrial swelling and abnormal cristae (Irwin *et al.*, 2003). To investigate whether any structural modification of the mitochondrial network could be

detected in *Col6a1*^{-/-} primary neural cultures, I transfected cells with a plasmid coding for a red fluorescent protein targeted to mitochondria. Transfected cells were carefully analyzed at the fluorescent microscope and divided into two categories, according to the fact they displayed elongated or fragmented mitochondria (Fig. 6A). Interestingly, most *Col6a1*^{-/-} cells displayed fragmented mitochondria, whereas the major part of wild-type cells displayed elongated mitochondria. Indeed, the fraction of *Col6a1*^{-/-} neural cultures characterized by the presence of fragmented mitochondria (72.2%) was statistically higher than the respective fraction (43.2%) of wild-type neural cultures (Fig. 6B).

3.2.5 The autophagic flux is impaired in *Col6a1*^{-/-} neural cell cultures.

We recently demonstrated that skeletal muscles from collagen VI null mice display compromised autophagy (Grumati *et al.*, 2010). Considering the importance of autophagy for the homeostasis of CNS, I investigated the autophagic pathway in *Col6a1*^{-/-} neural cell cultures. One well-established marker for autophagy is LC3 (microtubule-associated light chain 3), the mammalian homologue of yeast Atg8, which is conjugated to phosphatidylethanol-amine to be recruited to autophagosomes, an essential step in the autophagic pathway. LC3 lipidation can be easily monitored by western blot analysis thanks to the molecular weight shift of the protein, which allows to distinguish between the soluble LC3-I form and the lipid-conjugated LC3-II form (Klionsky *et al.*, 2008). Notably, LC3 lipidation appeared markedly decreased in *Col6a1*^{-/-} neural cell cultures when compared to the corresponding wild-type cultures, in standard culture conditions (Fig. 7A). At the same time, *Col6a1*^{-/-} neural cultures displayed a higher level of p62, a protein usually monitored to study the autophagic flux, which inversely correlates with autophagic activity (Fig. 7A). It is well established that p62 is degraded through the autophagic pathway, whereas this protein is found increased when the autophagic flux is impaired, forming aggregates which can be readily detected by immunofluorescence (Ichimura *et al.*, 2008). Accordingly, the increased p62 levels, revealed by western blot in *Col6a1*^{-/-} cultures extracts, were matched by the presence of increased p62 aggregates inside the cells (Fig. 7B).

The above findings pointed at the presence of a defective activation of autophagy in *Col6a1*^{-/-} neural cell cultures. In order to investigate this aspect in further detail, I evaluated the ability of wild-type and *Col6a1*^{-/-} neural cultures to activate autophagy following different stimuli. Towards this aim, I maintained the cells in serum-free culture medium and treated them with specific drugs, namely rapamycin, a well-known autophagy-inducer, and chloroquine, a lysosomal inhibitor that blocks the fusion and degradation of autophagosomes,

thus stressing an autophagic response. Wild-type neural cultures responded as expected, by inducing LC3 lipidation when either rapamycin or chloroquine was added to serum-free medium. Conversely, neither rapamycin nor chloroquine was able to elicit any significant increase in the LC3II/LC3I ratio in *Col6a1*^{-/-} neural cultures (Fig. 7, C and D), thus confirming a defective regulation of autophagy in collagen VI deficient neural cells.

To better monitor the autophagic flux, I derived primary neural cell cultures from wild-type and *Col6a1*^{-/-} mice that were previously crossed with the GFP-LC3 transgenic animals, which ubiquitously express GFP-tagged LC3 (Mizushima *et al.*, 2004). In the cells of these mice the conversion of LC3I to LC3II can be monitored in terms of changes in the subcellular localization of the fluorescent protein, from a diffuse cytosolic distribution to a punctuate appearance, once associated with autophagic vesicles. Primary neural cells derived from GFP-LC3;*Col6a1*^{+/+} mice and grown in serum-free medium for 4.5 hours displayed a slightly punctuate LC3 fluorescence, consistent with autophagosome formation (Fig. 8, A and B). When the same experiment was performed in the presence of chloroquine, GFP-LC3;*Col6a1*^{+/+} cells displayed a dramatic increase of fluorescent dots inside the cells as expected, whereas 3-methyladenine, a class III PI3-kinase inhibitor that inhibits the lipid kinase complex required for the initial formation of the autophagosome isolation membrane, led to a markedly decreased fluorescence in GFP-LC3;*Col6a1*^{+/+} cells (Fig. 8, A and B). Conversely, although in GFP-LC3;*Col6a1*^{-/-} cells a distinctly punctuate fluorescence was detected after culture in serum-free medium for 4.5 hours, treatment with chloroquine did not achieve any overt increase in the amount of fluorescent autophagosomes, thus suggesting that in these cells the autophagic flux triggered by serum withdrawal was taken to a sort of exhaustion reproducing the condition in which autophagosomes are no longer degraded (Fig. 8, A and B). A clear response to 3-methyladenine was instead detected in GFP-LC3;*Col6a1*^{-/-} cells, with a marked decrease of fluorescent dots, thus indicating that they were able to modulate autophagosome formation and that the observed altered response involved the later stages but not the earlier stages. To understand whether the presence of collagen VI could directly affect the autophagic response, I performed the same treatments on cells grown onto purified collagen VI and collagen I as substrates. When grown on collagen VI, wild-type cells displayed a significant increase in fluorescent autophagosomes compared to basal serum-free condition, suggesting that the presence of the protein can somehow render them more sensitive to serum deprivation, thus to autophagy induction. As expected then, upon chloroquine treatment, the number of cells presenting autophagosomes significantly increases. Differently *Col6a1*^{-/-} cultures grown on collagen VI showed a reduced number of

autophagosomes in general, but remarkably, upon the addition of chloroquine to the no serum condition, the presence of autophagosomes significantly increased, suggesting they can better clear autophagosomes if grown on collagen VI (figure 8, A and B). On collagen I *Col6a1*^{-/-} cultures display the same responses to treatments as without specific substrate. In the case of wild-type cells the response to chloroquine treatment appears a little lowered, losing significance. These results strongly sustain that the absence of collagen VI leads to an impaired autophagic flux likely due to problems in the late stages of autophagosomes degradation

3.2.6 *Col6a1*^{-/-} neural cell cultures are more vulnerable to oxidative damage.

In initial experiments aimed at analyzing autophagy on wild-type and *Col6a1*^{-/-} cells, I performed transfection of primary neural cell cultures with a plasmid coding for LC3 fused to GFP. The low level of transfection and expression of the plasmid did not allow me to detect the characteristic autophagic dots that should be expected, and therefore, as described above, I derived cultures from GFP-LC3 transgenic mice bred with wild-type and *Col6a1*^{-/-} animals. Even so, these transfected cultures were useful since the low efficiency of transfection allowed me to detect in detail the morphology of isolated cells. Strikingly, *Col6a1*^{-/-} cells displayed a high number of swollen buttons along their processes, whereas these features were much more infrequent in wild-type cells (Fig. 9A). To assess whether these alterations could be due to transfection itself, I analyzed non-transfected neural cells by cresyl violet staining. This analysis underlined that the presence of the above alterations persisted and that again they were much higher in *Col6a1*^{-/-} cells when compared to the corresponding wild-type cells (Fig. 9, B and C).

Next, I aimed at investigating the cause of the abundant swollen buttons observed in the processes of *Col6a1*^{-/-} primary neural cells. Similar alterations were reported in literature for other conditions, where they were found to be related to the presence of oxidative damage within cells, giving rise to the so-called beaded axons (Roediger and Armati, 2003). Based on this, I performed some experiments aimed at exacerbating oxidative stress by treating wild-type and *Col6a1*^{-/-} primary neural cells with different concentrations of hydrogen peroxide. High dose treatments, such as 40 mM H₂O₂ for 90 minutes, induced a remarkable loss of cells in *Col6a1*^{-/-} cultures, at a much higher extent to that observed in wild-type cells (Fig. 10A). A milder hydrogen peroxide treatment (10 mM H₂O₂ for 90 minutes) was then applied to measure apoptotic cell death by TUNEL assay and to evaluate the effect of plating onto purified collagen VI. Upon 10 mM H₂O₂ treatment, apoptosis was increased in both wild-type

and *Col6a1*^{-/-} cells, whereas plating onto collagen VI had a remarkably protective effect in both cultures from the damage triggered by hydrogen peroxide treatment (Fig. 10B).

In order to highlight differences in sensitivity to oxidative damage between the two genotypes, I exposed neural cell cultures to micromolar concentrations of hydrogen peroxide. Interestingly, at both 50 μM H_2O_2 and 100 μM H_2O_2 *Col6a1*^{-/-} cells showed several signs of degeneration, such as loss of neuronal network and dendrite shrinkage, whereas wild-type cells appeared much healthier at both H_2O_2 concentrations (Fig. 10C). Further results showed that ROS production is increased in *Col6a1*^{-/-} cells. In this set of experiments, I assessed ROS production by using reduced MitoTracker Red as a probe. This probe loads into mitochondria, thanks to the presence of a chloromethyl group. Following an increase in ROS production, MitoTracker Red is oxidized causing an increase in the emitted fluorescence, which is directly proportional to the increase of oxidative stress (Degli Esposti, 2002). In the absence of hydrogen peroxide treatment, wild-type and *Col6a1*^{-/-} neural cell cultures showed similar fluorescence intensities after loading with MitoTracker Red. Conversely, following treatment with 200 μM H_2O_2 , *Col6a1*^{-/-} cells displayed a marked increase of fluorescence, whereas wild-type cells maintained similar fluorescence intensities to untreated cells (Fig. 10D).

Altogether, these data indicate that in the absence of collagen VI neural cells develop a higher sensitivity to oxidative stress.

3.2.7 Neurodegeneration hallmarks in aged *Col6a1*^{-/-} mice.

To assess whether the alterations I detected in *Col6a1*^{-/-} neural cells were mirrored by phenotypical defects *in vivo*, and in order to understand the *in vivo* significance of the cytoprotective role displayed by collagen VI in primary neural cell cultures, I carried out different studies in brain sections from wild-type and *Col6a1*^{-/-} mice.

I first investigated the incidence of apoptosis in brain sections of mice at different ages. Towards this aim, I carried out TUNEL analysis on sagittal brain sections from newborn (2-day-old), adult (7-month-old), and old (23-month-old) mice of both genotypes (Fig. 1 A) and counted the number of apoptotic nuclei per section and per area unit. While brain sections of 7-month-old mice of the two genotypes did not display any significant difference in the incidence of apoptosis, the analysis of TUNEL-positive nuclei per area in brain sections from newborn mice revealed a significantly increased incidence in *Col6a1*^{-/-} samples when compared to the corresponding wild-type samples (Fig. 1 B). Notably, the incidence of TUNEL-positive nuclei was remarkably higher in brain sections from 23-month-old *Col6a1*^{-/-} mice (Fig. 11B). These data indicate that lack of collagen VI leads to an abnormal increase of

spontaneous apoptosis, which is particularly evident at later ages during life, thus suggesting a protective role of collagen VI in the CNS during aging. Given the remarkable apoptotic phenotype displayed by older *Col6a1*^{-/-} mice, for the subsequent *in vivo* studies I mostly focused on aged animals.

Western blot analysis of protein extracts from brain of 23-month-old mice revealed only slightly higher levels of BAX, but BCL-2 is increased in *Col6a1*^{-/-} samples (Fig. 11C), as well as displayed by the *in vitro* data obtained with neural cultures. Since collagen VI null cultures showed higher sensitivity to oxidative stress, I evaluated the presence of ROS in the brain of wild-type and *Col6a1*^{-/-} mice by dihydroethidium (DHE) staining (Fig. 11D). DHE is used to determine ROS production in tissues, since it becomes oxidized in the presence of ROS, thus generating ethidium bromide, a molecule which is able to intercalate with DNA and emit red fluorescence. Quantification of DHE fluorescence showed that ROS production was significantly higher in the brain of 23-month-old *Col6a1*^{-/-} mice, compared to age-matched wild-type samples, while analysis on 7-month-old mouse brains did not reveal any difference between the two genotypes (Fig. 11E). These findings further support a protective role of collagen VI against age-induced oxidative damage.

Aging is a process tightly related to the decreased efficiency of the autophagic pathway, particularly in post-mitotic tissues such as CNS. Because of this, and given the altered autophagic response I detected in *Col6a1*^{-/-} neural cultures, I analyzed the protein levels of some autophagic markers in brain extracts 23-month-old wild-type and *Col6a1*^{-/-} mice. Brain extracts from *Col6a1*^{-/-} mice displayed increased levels of Beclin1, a key regulator of autophagosome formation, thus suggesting induction of autophagy. Interestingly, p62 levels and LC3-II/actin ratio were also significantly increased in *Col6a1*^{-/-} extracts, suggesting a block in the autophagic flux with defective autophagosome degradation (Fig. 12, A and B). Moreover, immunofluorescence analysis of brain sections from 23-month-old wild-type and *Col6a1*^{-/-} mice confirmed that p62 was present at higher levels in *Col6a1*^{-/-} sections and showed the presence of p62 aggregates (Fig. 12C). These findings indicated that the autophagic pathway is altered in aged *Col6a1*^{-/-} mouse brain.

Finally, to assess whether aged mice lacking collagen VI displayed behavioral alterations, I tested the motor coordination of adult (7-month-old) and old (23-month-old) wild type and *Col6a1*^{-/-} using the rotarod test. Differently from 7-month-old mice, which had the same rotarod performance as age-matched wild-type animals, 23-month-old *Col6a1*^{-/-} mice displayed reduced performance when compared to the corresponding age-matched wild-

type animals (Fig. 13). The rotarod analysis suggested lower coordination and balance in *Col6a1*^{-/-} mice, for which deficits in CNS can be accountable.

Altogether, these studies revealed the presence of increased apoptosis, abnormal autophagic flux and higher levels of protein aggregates in the CNS of aged *Col6a1*^{-/-} mice, accompanied by altered motor coordination. All these aspects are considered hallmarks of neurodegeneration, strongly suggesting that collagen VI exerts a distinct role in protecting CNS from aging.

3.3 Analysis of the role of collagen VI in the PNS

3.3.1 Lack of collagen VI leads to hypermyelination and alterations in Remak bundles.

As discussed in detail above (section 3.1), immunofluorescence analysis of sciatic nerves showed that collagen VI is present in the PNS, even at higher levels than in the CNS (see Fig. 2A). In particular, collagen VI was abundantly found in the endoneurium of sciatic nerve and partially colocalized with nerve growth factor p75 receptor (Fig. 14A), thus suggesting that collagen VI is produced by Schwann cells, the main cell type accountable for myelin formation in the PNS.

To assess whether collagen VI is involved in the proper formation of myelin sheath and in the maintenance of sciatic nerve structure, toluidine blue staining and morphometric analysis were performed on semithin sections of sciatic nerves from wild-type and *Col6a1*^{-/-} mice. Light microscopy analysis of toluidine blue stained sections suggested that the global tissue organization of sciatic nerves was similar between the two genotypes, although several fibers showed abnormal shapes in *Col6a1*^{-/-} samples (Fig. 14B). Morphometric analysis indicated that the total mean number of axons per field was unaltered in *Col6a1*^{-/-} mice, but the distribution of fibers according to axon diameter showed a trend in which smaller fibers increased and larger one decreased, although this difference did not reach statistical significance (Fig. 14, C and D). To evaluate the possible effect of collagen VI lack on myelin formation, I measured for each nerve fiber the g-ratio, which corresponds to the ratio between axon diameter and entire fiber diameter (axon plus myelin sheath). Remarkably, *Col6a1*^{-/-} fibers displayed thicker myelin sheaths when compared to wild-type, resulting in significantly decreased g-ratio (Fig. 14E). More interestingly, a significantly lower g-ratio was maintained in all classes of fibers when grouped according to their axonal diameter (Fig. 14E). Hypermyelination was also supported by ultrastructural analysis of sciatic nerves by

transmission electron microscopy, which revealed that myelin was thicker in *Col6a1*^{-/-} nerves than in wild-type nerves, when comparing fibers of similar diameter (Fig. 14F).

Ultrastructural analysis also revealed that *Col6a1*^{-/-} nerves display altered organization of C-fibers, which are surrounded by non-myelinated Schwann cells in Remak bundles. *Col6a1*^{-/-} Remak bundles showed more loosely packed fibers, when compared to the tightly and regularly organized fibers of wild-type ones. In collagen VI null Remak bundles, fibers were often filled with vesicles of unknown origin, and the Schwann cell cytoplasm was less electron-dense (Fig. 15A). Moreover, *Col6a1*^{-/-} nerves showed partial fusion between the basal lamina of adjacent myelinating Schwann cells (Fig. 15B), suggesting that lack of collagen VI leads to defects in endoneurial basement membrane.

Since the alterations detected in *Col6a1*^{-/-} nerves primarily affect Schwann cells, the structure of Ranvier nodes was also analyzed, in collaboration with Laura Feltri (DIBIT - San Raffaele, Milan). Immunofluorescence analyses for different voltage-gated channels were performed on sciatic nerve teased fibers from 10-week-old wild-type and *Col6a1*^{-/-} mice, in order to evaluate the organization of node, paranode and juxtaparanode regions. No differences were found in the distribution of Nav1.6, the predominant voltage-gated sodium channel at the node of Ranvier, of Caspr, a paranodal marker, and of Kv1.1, a marker for juxtaparanode regions (Fig. 16), thus indicating no major alterations of these domains of myelinated axons.

3.3.2 *Col6a1*^{-/-} mice display abnormalities in motor and sensory functions.

To assess the functional consequences of the structural alterations detected in *Col6a1*^{-/-} sciatic nerves, we performed some functional tests aimed at evaluating both motor function, since hypermyelination could affect it, and sensory function, since Remak bundles, mainly constituted by sensory C-fibers, were found altered.

We used different tests to evaluate motor function affected by PNS alterations. Footprint analysis was performed on 7-month-old wild-type and *Col6a1*^{-/-} mice, by marking their hind- and forepaws with different colours, observing the walking tracks and measuring different parameters (Fig. 17A). Base width was significantly lower in *Col6a1*^{-/-} mice compared to wild-type, suggesting they adopt a different posture (Fig. 17B). One parameter used to evaluate damages affecting sciatic nerve is provided by the angles between foot steps and walking direction, that were wider in *Col6a1*^{-/-} animals than in wild-type ones (Fig. 17C). No significant difference was detectable in stride width between the two genotypes, but stride

length variability was increased in *Col6a1*^{-/-} mice (figure 17, D and E), suggesting increased gait instability.

We next performed the ledged beam walking test, which is able to assess control of balance and coordination, by training mice to traverse a beam which gets narrower at its end. We assessed both 7-month-old and 23-month-old mice, and the time and incidence of hindfoot faults occurrence were registered. Analysis of 7-month-old mice showed that the distance of the first foot fault from the starting point of the beam was significantly lower in *Col6a1*^{-/-} mice compared to wild type ones, meaning that their initial faults already take place where the beam is wider (Fig. 18A). Moreover, the total number of hindfoot slips was significantly increased in *Col6a1*^{-/-} mice, suggesting that motor coordination and balance are impaired (Fig. 18A). These differences in beam walking test performances were also confirmed in 23-month-old mice. Also at this age, nerve function appeared compromised in the absence of collagen VI. First foot fault occurred significantly earlier in *Col6a1*^{-/-} mice and the total number of faults was higher in aged wild-type than in younger mice (Fig. 18B). Conversely, no differences were detected at both ages between the two genotypes in the total time needed to reach the end of the beam (Fig. 18, A and B). Altogether, this set of data supports an impairment of motor balance and coordination in *Col6a1*^{-/-} mice.

Finally, we assessed sensory function, in terms of response to acute pain, by performing a hot plate test in young (3-month-old), adult (7-month-old) and aged (12-month-old) wild-type and *Col6a1*^{-/-} mice. Significant differences between genotypes were detected only at 7 months of age. Indeed the hot plate test showed significantly increased response latency to the thermal stimulus in *Col6a1*^{-/-} mice compared to wild-type (Fig. 18C), indicating a delay in nociception.

In conclusion, these studies carried out in the PNS, where collagen VI expression is higher compared to CNS, revealed structural and functional defects in *Col6a1*^{-/-} mice and suggest that this ECM protein exerts a critical function in maintaining proper nerve morphology and structure, preserving motor and sensory functions.

4. Discussion

Collagen VI is an ECM protein whose studies spread in the past years among a wide range of tissues, such as skin, cartilage, adipose tissue, heart and tendons, but mainly in skeletal muscle (Keene et al., 1988; Quarto et al., 1993; Braghetta et al., 1996; Kuo et al., 1997; Khan et al., 2009). Collagen VI was described as exerting a cytoprotective role, by counteracting apoptosis and oxidative damage both *in vitro* and in physiological studies (Rühl et al., 1999; Irwin et al., 2003; Menazza et al., 2010). *Col6a1*^{-/-} mice largely helped to unveil this role *in vivo*, showing that the absence of this peculiar ECM component leads to alterations in processes such as cell differentiation, apoptosis, autophagy, responses to different types of injury and tumor growth and vascularization (Irwin et al., 2003; Iyengar et al., 2005; Grumati et al., 2010; Christensen et al., 2012; Luther et al., 2012; You et al., 2012). These findings threw new light on the relevance of this protein by itself, but also of the ECM in regulating different intracellular pathways.

The tissue in which collagen VI was mostly studied is skeletal muscle. The generation of a mouse model lacking collagen VI, by means of targeted inactivation of the *Col6a1* gene, provided a peerless tool to investigate the physiological role of collagen VI in skeletal muscle and other tissues. Moreover, this *Col6a1* null mouse model helped elucidating, in parallel to studies on human patients, the pathophysiology of UCMD and Bethlem myopathy, starting from the discovery of the genetic defect causing these muscular diseases, then highlighting the biological relevance of collagen VI in skeletal muscle, and finally achieving valuable information on the underlying pathomolecular mechanisms and on the muscle physiological processes in which the protein takes part and that are altered when the protein is mutated (Bonaldo et al., 1998; Irwin et al., 2003; Lampe and Bushby, 2005; Grumati et al., 2010).

The initial characterization of *Col6a1*^{-/-} mice demonstrated a myopathic phenotype affecting diaphragm and other skeletal muscles, with degeneration and regeneration of myofibers and reduced muscular strength (Bonaldo et al., 1998). Further ultrastructural analyses of *Col6a1*^{-/-} muscles by electron microscopy revealed marked alterations of sarcoplasmic reticulum and mitochondria, which was paralleled by a latent mitochondrial dysfunction and spontaneous apoptosis of muscle fibers (Irwin et al., 2003). Based on the pathophysiological defects detected in collagen VI deficient mice, studies were carried out in muscle biopsies and cultured myoblasts derived by UCMD and Bethlem patients, which allowed to reveal similar alterations to those found in *Col6a1*^{-/-} muscles (Angelin et al., 2007).

More recent studies, to which I collaborated during my PhD, allowed to elucidate the mechanism causing accumulation of altered organelles in *Col6a1*^{-/-} muscles. In particular, we

demonstrated that lack of collagen VI determines a failure of the autophagic machinery in skeletal muscle, thus causing retention of dysfunctional organelles, particularly mitochondria, and ultimately leading to apoptosis, ROS production and myofiber degeneration (Grumati *et al.*, 2010). Interestingly, these findings unveiled a novel and unexpected role for the ECM in the regulation of autophagy, an intracellular process playing a key role in cell homeostasis, organelle recycling and energy production, which is essential for the proper functioning of muscle. In the absence of collagen VI, abnormal phosphorylation of Akt kinase causes a defective regulation of the protein levels for Beclin1 and Bnip3, two key mediators involved in autophagy induction (Grumati *et al.*, 2010). In agreement with this, rescue of Beclin 1 protein levels by *in vivo* electroporation of *Col6a1*^{-/-} tibialis anterior muscle with a *Beclin1* cDNA construct is sufficient to reactivate a proper autophagic flux in muscle fibers, with a corresponding decreased incidence of apoptosis in the transfected fibers. Restoration of autophagy in skeletal muscles of *Col6a1*^{-/-} mice can be also obtained by nutritional means, such as prolonged starvation for 30 hours or feeding mice with a low protein diet for 15 days, as well as by pharmacological means, such as treating mice with rapamycin. Notably, these *in vivo* treatments allowed us to establish that the autophagic defect plays a key pathogenic role in the onset of the myopathic phenotype in collagen VI deficient mice, since reactivation of a proper autophagic flux enables *Col6a1*^{-/-} muscles to promptly remove damaged organelles, with a corresponding recovery of the myopathic features and a significant increase of muscle strength (Grumati *et al.*, 2010). Similar defects in Beclin1 and Bnip3 proteins were found in muscle biopsies from patients affected by UCMD or Bethlem myopathy (Grumati *et al.*, 2010), thus opening new perspectives on potential therapeutic approaches, which so far were mainly based on the desensitization of mitochondrial PTP by cyclosporin A (Merlini *et al.*, 2008a).

The studies mentioned above allowed to obtain a detailed understanding of the role of collagen VI in skeletal muscle. Even so, other studies suggested that collagen VI exerts a cytoprotective role also in other tissues. Although collagen VI has a broad distribution in several tissues, with a complex and dynamic pattern of regulation of gene expression during both embryonic and postnatal life (Braghetta *et al.* 1996; Marvulli *et al.*, 1996), it was never found in certain tissues, such as blood and CNS. However, recent studies revealed that collagen VI can be expressed even by certain cell types that are not usually considered as producing an ECM, such as neurons. The study of collagen VI expression in the nervous system was mostly focused on the PNS compartment, since during mouse embryogenesis and postnatal development no overt presence of collagen VI transcripts and protein was ever

detected in CNS, whereas in the PNS abundant collagen VI expression was evident, mostly in nerves as a sheath around axon bundles (Marvulli *et al.*, 1996). In the last three years, a couple of works pointed at collagen VI as being expressed in the CNS, peculiarly by neurons, where it was found to exert a protective role against cell death induced by specific injuries (Cheng *et al.*, 2009; Cheng *et al.*, 2011). This is of great interest, since the presence of an ECM in the CNS has been a source of controversy and almost completely neglected until 1970s, although this was increasingly recognized in most recent times (Rutka *et al.*, 1988). The finding of collagen VI as an ECM protein which can be expressed by neurons was even more unexpected, since collagens are among the major components of the ECM but they are absolutely uncommon in the mature nervous system, except for very few examples expressed by neurons, such as collagen types XIII, XXV, XVI and XVII (Hubert *et al.*, 2008).

The first cited work, from Mucke and colleagues, suggested a neuroprotective role for collagen VI against the toxicity of A β -peptides, a critical step in the pathogenesis of Alzheimer's disease. These peptides can modulate TGF- β signaling in neurons, thus up-regulating collagen VI expression. A neuroprotective role for collagen VI was found both *in vitro* and *in vivo*, since the authors found increased collagen VI mRNA and protein in samples from both Alzheimer's patients and transgenic hAPP mice, an animal model for Alzheimer's disease. Moreover, these authors demonstrated that A β -peptides treatment triggered collagen VI expression in neuronal cell cultures, and that A β -peptide-induced cell death is higher in cultures derived from *Col6a1*^{-/-} mice (Cheng *et al.*, 2009). The second work mentioned above demonstrated increased levels of *Col6a1*, *Col6a2* and *Col6a3* transcripts and of collagen VI protein in UV-irradiated primary hippocampal neurons. Furthermore, this study demonstrated that soluble collagen VI is able to prevent UV irradiation-induced cell death, mitochondrial dysfunction and neurite shrinkage, by acting through the Akt and JNK pathways (Cheng *et al.*, 2011).

The primary interest of my PhD thesis work on collagen VI function in CNS rose from the new venues opened by the two papers mentioned above. The *Col6a1*^{-/-} mouse was generated in our laboratory, our main interest was focused on skeletal muscle, but we had a more general interest in understanding the biological function of collagen VI and for the first time we became aware of the presence of the protein in the CNS. At the beginning of my PhD, I was mainly involved in the study of collagen VI role in regulating the autophagic flux in skeletal muscle. Considering the growing evidence underlining the importance of an efficient autophagic clearance for the homeostasis of the CNS, and its implication in neurodegenerative diseases (Son *et al.*, 2012), I was convinced by the fact that if collagen VI

was present in that tissue, then it was conceivable that its protective role could be exerted by influencing some key intracellular pathways as it does in skeletal myofibers. Initially, I established primary neural cell cultures from wild-type and *Col6a1*^{-/-} mice, to assess the *in vitro* function of collagen VI. In particular, I investigated whether lack of collagen VI in neural cells has any impact on some key processes, such as autophagy, and affects apoptosis and oxidative damage, as we established in skeletal myofibers. In these studies, I decided to use combined cortices and hippocampi deprived of meninges, dissected from neonatal (P0-P1) wild-type and *Col6a1*^{-/-} mice, in order to derive mixed neuronal/glial cultures (hereafter defined neural cell cultures) where cell proliferation was inhibited. By characterizing these cultures for different cell markers, I found that the major component in cultures from both genotypes was provided by neurons, but wild-type cultures had a significantly and consistently higher proportion of neurons than *Col6a1*^{-/-} ones. This aspect, accompanied by the finding that culture of freshly dissected neural cells onto purified collagen VI leads to a significant increase of the neuronal fraction, suggests that collagen VI promotes neuronal survival in culture.

In order to understand the basis for the decreased number of neurons in *Col6a1*^{-/-} cells and investigate the role of collagen VI in cell survival, I investigated apoptosis in cultures of both genotypes. The studies I carried out showed higher incidence of spontaneous apoptosis in *Col6a1*^{-/-} neural cells. Furthermore, both wild-type and *Col6a1*^{-/-} neural cultures displayed a significant decrease of apoptosis when cells were grown on collagen VI as a substrate, but not when they were grown on another ECM substrate, such as collagen I. The significant difference in the incidence of spontaneous apoptosis between wild-type and *Col6a1*^{-/-} neural cells is an important aspect that was not assessed in the two studies cited above, which focused instead on the increase of collagen VI expression after different types of neuronal damages, and represents the first evidence of a phenotypic alteration in CNS cells of *Col6a1*^{-/-} mice. Indeed, none of the two cited works mentions any difference in apoptosis under basal condition. The work published by Mucke and colleagues in 2009 showed only a significantly different response to A β -peptides-induced cell death (Cheng *et al.*, 2009). A basal difference between wild-type and *Col6a1*^{-/-} cells was not detected, but actually the cultures used in that study were mostly neuronal, while the ones I produced are mixed glial/neuronal cultures. Furthermore, in the cited work cell death was analyzed by Trypan blue staining, a method which allows to measure global cell death but that is not specific for apoptosis. The use of TUNEL assay allowed me to achieve a more precise estimation on the influence of collagen VI in the protection from apoptosis. On the other side, the work published by Chao and

colleagues in 2011 did not even investigate the expression and function of endogenous collagen VI, but focused on the demonstration that anti-collagen VI antibodies can neutralize the cytoprotective role of the endogenous protein (Cheng et al., 2011).

The work by Mucke and colleagues clearly showed that collagen VI is expressed by neurons, but the production and localization of the protein was not addressed in detail. Therefore, I investigated the presence of collagen VI in the primary neural cultures by immunofluorescence. As expected, reactivity for collagen VI was present in wild-type cells but not in *Col6a1*^{-/-} ones, thus confirming the specificity of the antibody in these cells and indicating that in the absence of the $\alpha 1(\text{VI})$ chain no collagen VI can be produced by neurons and glial cells, as previously also demonstrated for fibroblasts and other cell types (Bonaldo et al., 1998). In wild-type neural cultures, collagen VI was detected close to the cell surface of both neuronal and glial cell types, but it remains difficult to ascertain whether it was secreted or not. Since collagen VI is an ECM component, it may be expected that the protein should be secreted. However, some studies indicate that certain cell types retain collagen VI on their cell surface, as recently shown for macrophages (Gualandi et al., 2011). Further investigations are needed to address this point, for example by immunogold electron microscopy. In addition, based on the recent finding of three novel and genetically distinct chains that are differentially expressed in other tissues and can form specific collagen VI isoforms (Gara et al., 2008; Gara et al., 2011), it will be interesting to investigate the biochemical and supermolecular composition of collagen VI produced by neural cells.

In vivo analyses, where I performed immunofluorescence on brain sections from wild-type and *Col6a1*^{-/-} mice, revealed that collagen VI is expressed in the CNS not only after injuries, but also in basal conditions. As expected, the most abundant labelling for collagen VI was found along meninges, which are made of connective tissue. Previous studies indicated that the distribution of collagens in the CNS is mostly limited to three locations, the CNS-associated connective tissues, the basement membranes between the nervous system and other tissues (such as the endothelial microvascular tissue) and the sensory end organs (Hubert et al., 2008). Notably, immunofluorescence of brain sections allowed me to establish that collagen VI is also present in the inner cortical regions and in association with GFAP-positive cells. Although the significance of this *in vivo* localization remains to be characterized in further details, it witnesses that the presence of collagen VI is not only limited to the connective tissues but also extends to proper neural tissues. As previously mentioned, only few examples of collagens are expressed by neurons and they were suggested to fulfil functional, rather than merely structural roles. In particular, collagen XVII was detected in

neurons of human brains and it was suggested to be involved in neuronal migration and synaptic plasticity (Seppänen *et al.*, 2006). Collagen XVI is expressed *in vitro* by both neuronal and non-neuronal cells and *in vivo* by DRG neurons, and it was shown to be regulated by nerve injury (Hubert *et al.*, 2007). Collagen XIII is a transmembrane protein expressed in the CNS and PNS during development, enhancing neurite outgrowth (Sund *et al.* 2001). Also gliomedin is a transmembrane collagen, which is expressed at the Ranvier nodes regulating Na⁺-channel clustering (Maertens *et al.*, 2007). Finally, collagen XXV, another member of the same family, is cleaved from neuronal membranes and can bind fibrilized A β , implicating this protein in β -amyloidogenesis (Hashimoto *et al.*, 2002). These examples illustrate the potential functional role that some specific types of collagens can exert both in CNS and PNS, thus pointing at collagen VI as a protein fulfilling a functional role in the CNS.

One specialized ECM structure of the CNS, which is attached to neuronal cell surfaces, is provided by the so-called perineuronal net. Perineuronal nets are lattice-like structures enwrapping cell soma and proximal neurites, whose alterations can affect specific intracellular pathways, since they can attract and trap neurotrophic factors, and influence synaptic activity and even the transmission of electrochemical signals (Karetko and Skangiel-Kramsa, 2009). The components of these nets are varied, and alterations in their composition can induce several effects. It is known that the absence of specific ECM proteins, like aggrecans, can impair the formation of perineuronal nets (Giamanco *et al.*, 2010). In addition, loss of certain ECM components, such as tenascin-R, cause reduced reactivity for brevican, reduced expression of hyaluronan and neurocan, and no detection of phosphacan (Giamanco *et al.*, 2010). Therefore, reciprocal reductions in the levels of other ECM molecules in the CNS of *Col6a1*^{-/-} mice merit to be investigated, to evaluate the relevance of collagen VI in the organization of brain ECM as well as in the formation of perineuronal nets.

As described above, my *in vitro* studies highlighted a higher incidence of spontaneous apoptosis in primary neural cells from *Col6a1*^{-/-} mice, thus indicating that lack of collagen VI impacts on the survival of neural cells. Further analysis of the apoptotic process showed a higher level of the pro-apoptotic Bax protein, nonetheless Bcl-2, which is an anti-apoptotic factor, is also increased. The increase of Bcl-2 protein was quite unexpected, considering the increased apoptosis of *Col6a1*^{-/-} cultures. In this respect it should be noted that increased levels of Bcl-2 are not only connected to its anti-apoptotic role, but also to its inhibiting effects on autophagy (Eisenberg-Lerner *et al.*, 2009). Bax is a well-known factor able to accelerate cell death when overexpressed, and it also binds Bcl-X_L-Bcl-2 heterodimers, thus

inhibiting their anti-apoptotic role (Xu *et al.*, 2007). Therefore, Bax can counteract the increased level of Bcl-2, driving the delicate balance between these factors toward an apoptotic ending. The observed increase of Bax levels could be accountable also for the higher frequency of fragmented mitochondria found in *Col6a1*^{-/-} cultures in basal condition. In fact Bax is known to translocate to mitochondria, localizing to Mfn2 and Drp1 protein clusters, which subsequently become sites for mitochondrial fragmentation (Karbowski *et al.*, 2002). Moreover a correlation between mitochondrial fission and the induction of apoptotic signaling is largely reported in literature (Scorrano, 2005). This supports that the mitochondrial fragmentation detected in *Col6a1*^{-/-} cells is able to render them more prone to apoptosis. According to this, an interesting point is the association between alterations of mitochondrial dynamics and the occurrence of neurodegenerative disease. Perturbations in mitochondrial dynamics are involved in several human neurodegenerative diseases, even if the mechanisms involved remain undefined. It is becoming increasingly clear that several factors likely contribute to the changes in mitochondrial shape, thus influencing various aspects of mitochondria activity, including fusion, fission, transport and mitophagy, and thereby cellular homeostasis (Chen and Chan, 2009).

Another aspect I investigated in my *in vitro* studies with primary neural cultures concerns the involvement of collagen VI in the regulation of the autophagic process, since we previously found that autophagy is deregulated in skeletal muscle when collagen VI is lacking. Towards this aim, I analyzed protein extracts from wild-type and *Col6a1*^{-/-} neural cell cultures to assess the capability of these cells to induce autophagy. Under basal conditions, LC3 lipidation was lower in *Col6a1*^{-/-} cultures, thus suggesting either impaired autophagosome formation or excessive autophagosome degradation. Previous literature work on the reporter LC3-GFP mouse indicated that autophagosomes are rarely detectable in the CNS, due to remarkably rapid autophagosome degradation (Mizushima *et al.*, 2004). This would seem to infer that the lower LC3 lipidation detected in *Col6a1*^{-/-} cultures could be due to excessive autophagic flux, rather than impaired autophagosome formation. However, the presence of a high level of p62 in *Col6a1*^{-/-} cultures was indicating that autophagic clearance is defective in collagen VI deficient cells. Therefore, I assessed whether the observed changes were due to an on-rate defect, meaning that autophagy induction was impaired, considering also the lower LC3-II to LC3-I ratio. Towards this aim, I used some treatments under serum-free conditions for analyzing the autophagic flux, such as rapamycin, a widely used autophagy inducer, and chloroquine, a lysosomal inhibitor able to block the degradation of autophagosomes (Rubinsztein *et al.*, 2007; Mizushima *et al.*, 2010). Notably, the sole serum

withdrawal led to an increase of LC3 lipidation in *Col6a1*^{-/-} cultures, to an extent not significantly different from the response to rapamycin or chloroquine. This underlines the presence of a regulatory defect in collagen VI deficient cells, when compared to the responses attained in wild-type cells.

To investigate further the autophagic flux, I derived primary neural cell cultures from GFP-LC3;*Col6a1*^{+/+} and GFP-LC3;*Col6a1*^{-/-} mice, which allow to monitor the subcellular distribution of LC3 in the two genotypes by following GFP fluorescence, and analyzed the cells by confocal microscopy after the different treatments. In these experiments, I measured for each condition the percentage of cells displaying more than five GFP-LC3 dots, a well-accepted procedure for evaluating the incidence of autophagy (Young *et al.*, 2009). These analyses, carried out on three independent preparations, confirmed that in wild-type cells a significant increase in autophagy induction is seen only following the addition of chloroquine to serum-free condition, whereas in *Col6a1*^{-/-} cells the serum-free condition itself is able to induce a significant increase in the incidence of autophagic dots, which is comparable to the response obtained after chloroquine treatment. These data suggest that serum depletion stresses so much *Col6a1*^{-/-} neural cells that they maximally induce autophagy, reaching a condition of exhaustion, without being able to complete the clearance of autophagosomes, as chloroquine normally induces. Similar findings were reported in the literature for other *in vitro* and *in vivo* models, showing that defective autophagosomal clearance is accountable for increased evidence of autophagosomes even in the absence of lysosomal inhibitors or autophagy inducers (Yu *et al.*, 2005; Sanchez-Danes *et al.*, 2012). This is remarkable when we consider that plating freshly derived neural cells onto native collagen VI as a substrate decreases the levels of detectable LC3 dots in the serum-free condition and retrieves significant differences between serum-free and chloroquine-supplemented serum free conditions. Moreover, wild-type cells plated on collagen VI display a significant increase of autophagy induction upon serum-free condition, as if the presence of collagen VI was able to render cells more sensitive to serum deprivation. In a literature work, Young and co-workers studied the response of autophagy to serum deprivation in primary neural cell cultures similar to ones I used in my study, and by analyzing the different components of medium supplements they demonstrated that it is due specifically to insulin withdrawal (Young *et al.*, 2009). In detail, they demonstrated that insulin withdrawal is able to induce the increase in the number of cells presenting autophagic dots, from 15% to 35%. Differently, the wild-type cultures I analyzed showed almost 35% of cells presenting LC3 dots both in basal and in serum-free conditions. This different response to basal (complete medium) conditions can be

explained by the fact that different basal conditions were applied in the study by Young and co-workers and in this thesis work. In particular, in the study by Young and co-workers the authors changed the medium after three days, therefore adding new fresh serum and additives to cell cultures, while in my case the basal condition maintained the same medium already present in the culture, and analyses were performed at seven days. If, as argued by the work of Young et al., the autophagic response attained by serum deprivation in neural cultures is only due to insulin withdrawal, then this sustains the fact that in my study cells in complete medium are already under stress, and then serum deprivation leads *Col6a1*^{-/-} cells to exhaustion of the autophagic flux. Given the suggested relationship between insulin withdrawal and autophagy activation, it will be interesting to understand whether collagen VI may influence insulin receptor expression or signaling in neural cultures. The results I obtained underline a possible role for collagen VI in wild-type cultures as an ECM inducer of autophagy under serum deprivation, while its lack somehow alters the correct regulation of the process.

Autophagy regulation in neurons is also related with ROS, and recent studies even pointed at an essential role for ROS in starvation-induced autophagy (Huang *et al.*, 2011). Conversely, several studies demonstrated that compromised autophagy or defective lysosomal activity can increase the presence of ROS in cultures as well as in mouse models for neurodegenerative diseases (Terman *et al.*, 2006). Indeed, the axonal alterations I detected more frequently in *Col6a1*^{-/-} cultures were reported in other systems to be related to oxidative damage (Roediger and Armati, 2003). Notably, treatment with micromolar concentrations of hydrogen peroxide causes remarkable degenerative features in *Col6a1*^{-/-} neural cultures, indicating that in both basal and stress conditions *Col6a1*^{-/-} cells are more vulnerable to oxidative damage. Preliminary experiments on ROS measurements sustain that in the absence of collagen VI more ROS are generated, thus suggesting a possible link between the presence of oxidative stress and the defect in autophagy regulation in *Col6a1*^{-/-} cultures. Moreover, plating onto collagen VI protects *Col6a1*^{-/-} cultures from the increased incidence of apoptosis after hydrogen peroxide, underlining a cytoprotective role for the protein also relatively to oxidative damage.

As far as signalling is concerned, it was reported that signals conveyed by integrins can lead to increased ROS production upon ligand binding (Svineng *et al.*, 2008). In particular, Taddei and co-workers showed that fibroblasts adhesion to fibronectin through integrins resulted in mitochondrial release of ROS, with a characteristic timing and according to the subsequent cell spreading (Taddei *et al.*, 2007). This means that if collagen VI contacts

integrin receptors, it is also possible that upon its lack the alteration of integrin binding activity may induce an abnormal release of ROS. Indeed, lack of collagen VI is known to alter the deposition of fibronectin by cultured fibroblasts (Sabatelli *et al.*, 2001), therefore alterations in the surrounding ECM and in the signals transduced by integrins can be expected, depending on which kind of ECM is present in the CNS.

The data I obtained with brain-derived cultures revealed that lack of collagen VI affects the homeostasis of neural cells *in vitro*, however a major aspect was also to verify the relevance of the protein in the CNS *in vivo*. Towards this aim, I investigated in brain section from wild-type and *Col6a1*^{-/-} mice the processes that I found altered in the *in vitro* model and again I found them specifically altered in *Col6a1*^{-/-} tissues. Quantification of spontaneous apoptosis in brain sections from wild-type and *Col6a1*^{-/-} mice showed that it is increased in collagen VI deficient mice at different ages. In particular, apoptosis is significantly increased in newborn (2-day-old) mice and in aged (23-month-old) mice, while young adult (7-month-old) mice do not show any significant difference in the incidence of spontaneous apoptosis between the two genotypes. Analysis of ROS, evaluated by DHE staining of brain sections, revealed a major increase in cortices from aged (23-month-old) *Col6a1*^{-/-} mice when compared to the corresponding wild-type animals, while again no significant differences were detectable in 7-month-old mice. These results parallel what I observed *in vitro* and indicate that collagen VI displays a cytoprotective role also *in vivo* against cell death and preserving the nervous tissue from oxidative damage, which is known to increase during aging (Terman *et al.*, 2006).

Given the remarkable apoptotic phenotype and ROS increase I detected in the CNS of aged collagen VI deficient mice, and based on our demonstration that lack of collagen VI affects autophagy in skeletal myofibers (Grumati *et al.*, 2010), I analysed autophagic markers in brain sections of 23-month-old mice of both genotypes. Interestingly, this analysis revealed that aged *Col6a1*^{-/-} mice also display a marked increase of p62, which localized in intracellular and extracellular aggregates. The presence of p62 aggregates or clusters was previously reported in connection with aging, and p62 was reported as a common component of neuronal cytoplasmic inclusions found so often in patients affected by motor neuron diseases (Soontornniyomkij *et al.*, 2012; Seppänen *et al.*, 2009). Moreover, Beclin1 protein levels and LC3-II/actin ratio were increased in brain sections of aged *Col6a1*^{-/-} mice when compared to age-matched wild-type samples, thus suggesting that lack of collagen VI in the CNS cause a dysregulation of the autophagic flux during aging.

An increasing number of studies on aging models showing alterations in the

autophagic pathway were reported in the literature. One of such mouse models for aging is provided for instance by the senescence-accelerated prone mouse (SAMP), displaying a shortened life span and early manifestations of senescence (Takeda *et al.*, 1997). SAMP8 is a non-genetically modified mouse strain that is widely considered an excellent model of aging and senile dementia, used to study age-related cognitive dysfunction and neurodegeneration. SAMP8 mice display symptoms similar to human aging, such as shorter lifespan, lordosis, reduced physical activity and hair loss but also neurodegenerative features, such as early onset deficits of learning and memory, altered emotions, abnormal circadian rhythm, neuronal cell loss and decreased release of neurotransmitters in the brain (Ma *et al.*, 2011; Caballero and Cot-Montes, 2012). Moreover, the SAMP mouse model display alterations of autophagy related to aging. Indeed, studies in the brain of SAMP mice showed increased LC3-II/actin ratio and a peculiar trend for Beclin1 increase at 7 months of age, as I found in 23-month-old *Col6a1*^{-/-} mice, and Beclin1 decline at 12 months of age (Ma *et al.*, 2011). The opposite changes of autophagy reported for SAMP mice at different ages are not surprising, since a number of studies in different tissues in both physiological and pathological conditions indicate that autophagy is a tightly regulated process whose correct activity is essential for cell and tissue homeostasis, so that both inefficient activation or excessive activation of autophagy are both detrimental (Shintani and Klionsky, 2004; Mizushima and Komatsu, 2011). For instance, it was previously reported that Beclin1 is reduced in the brain of Alzheimer's disease patients, and this reduction was indicated as promoting neurodegeneration (Pickford *et al.*, 2008). On the other side, Beclin1 was found to be increased in some neurodegenerative disorders, and this was interpreted as a sign of autophagy upregulation related to pathogenic proteins or injury (Erlich *et al.*, 2006). In the studies on SAMP mouse, as discussed above, Ma and co-workers reported that Beclin1 levels increase in 7-month-old and decline in 12-month-old mice, and the authors suggested that autophagic activity may increase at the beginning of Alzheimer's disease while the pathological features of aged SAMP mice are similar to the late-onset Alzheimer's disease, with a decline of autophagy activity (Ma *et al.*, 2011). Based on the findings I obtained in *Col6a1*^{-/-} mice, I can suppose that a similar effect of increased autophagic response can be elicited by the increase of p62 aggregates, resulting in increased levels of Beclin1 as a protective response, while the downstream efficiency of autophagy is already defective since both LC3-II/actin ratio and p62 levels are augmented.

The complex net of effects involving autophagy in aging is also illustrated by the *Zmpste24* deficient mouse, which is considered a good model for human Hutchinson-Gilford

progeria, a type of accelerated aging in which autophagy was found involved. The lacking protein is a metalloproteinase involved in the maturation of lamin A, causing abnormalities in the nuclear envelope (Marino and Lopez-Otin, 2012). Researchers reported that these prematurely aged mice exhibit autophagy induction, rather than reduction, and put these alterations in connection with metabolic changes, such as lower insulin and glucose levels in blood, similar to effects occurring under caloric restriction, thus rising a novel paradoxical role for autophagy during pathological aging processes (Mariño *et al.*, 2008; Mariño *et al.*, 2010). Thus, different influences can affect autophagy in the CNS during aging.

A part of my PhD thesis work was focused on the PNS, and in particular on the study of the consequences caused by collagen VI deficiency in peripheral nerves. In wild-type mice, I found that collagen VI is abundant in the endoneurium and perineurium of the sciatic nerve, where the protein is partially colocalized with nerve growth factor p75 receptor, a marker for Schwann cells. These data are in full agreement with previous studies from our laboratory, which demonstrated that collagen VI is expressed by Schwann cells. In particular, those studies revealed that Schwann cell precursors start expressing collagen VI when they begin to differentiate and that the expression decreases as soon as the cells acquire the features of myelinating mature cells (Vitale *et al.*, 2001). Considering the primary role of Schwann cells in producing myelin sheaths surrounding axons in the PNS, I first focused on morphometric analyses of sciatic nerves from wild-type and *Col6a1*^{-/-} mice by light and electron microscopy. These studies unveiled a marked increase of myelin thickness in *Col6a1*^{-/-} sciatic nerve fibers when compared to the corresponding wild-type samples. Moreover, the ultrastructural analyses at electron microscopy revealed further alterations in *Col6a1*^{-/-} sciatic nerve fibers, with an altered packaging of sensory function-deputed Remak bundles, and a partial fusion of the basement membrane of adjacent Schwann cells. These alterations suggest that lack of collagen VI in peripheral nerves causes not only a defective regulation in myelin production, but also a deregulation of cell differentiation, with defects in both myelinating and on non-myelinating Schwann cells.

In order to assess the functional consequences of the defects detected in peripheral nerve fibers of collagen VI deficient mice, we carried out some behavioural studies that allowed to reveal that the structural alterations affect motor function and sensory perception of *Col6a1*^{-/-} mice. Literature studies, carried out in different pathogenic conditions and models, reported about motor function impairment due to hypermyelination, in correlation to slower nerve conduction (Pujol *et al.*, 2002; Ahmad *et al.*, 2012). Our findings of decreased motor function and defective pain perception in collagen VI null mice is also sustained by

previous work on mice lacking WARP, a recently identified ECM molecule expressed in several tissues including peripheral nerves, where the authors found similar sensory and motor deficits (Allen *et al.*, 2009). Interestingly, ablation of WARP also leads to a marked decrease of collagen VI in the endoneurium of WARP null mice (Allen *et al.*, 2009), thus suggesting a possible functional link between these two molecules in the ECM of peripheral nerves.

Similar findings on enhanced myelination in connection with extracellular environmental changes were found in mice with lentivirus-mediated knockdown of TACE in motor neurons. TACE (also known as ADAM17) is a zinc-dependent membrane-anchored metalloproteinase of the ADAM family. ADAMs are known to regulate myogenesis, neurogenesis, fertilization and myelination (Yang *et al.*, 2006). La Marca and co-workers demonstrated that knockdown of ADAM17/TACE in motor neurons leads to hypermyelination and to alterations in Remak bundles, which contain less regular and loosely packed sensory fibers (La Marca *et al.*, 2011). Moreover, the authors demonstrated that these effects are due to increased signaling downstream neuregulin-1 type III, a soluble molecule that is modulated by ADAM17/TACE cleavage (La Marca *et al.*, 2011). This nicely underlines the importance of growth factor modulation in correct myelination, opening a potential role for collagen VI in participating to these processes. For instance, it is known that metalloproteinase activity, in terms of their upregulation, inhibition and localization, can be regulated by integrins (Yue *et al.*, 2012). Thus, the presence of collagen VI in the ECM may influence integrin-mediated outside-in signaling, whereas when collagen VI is absent, rearrangements in the ECM three-dimensional organization may occur and subsequently lead to changes of integrin-mediated signaling.

Previous studies from our laboratory accounted axonal neuregulin as responsible for triggering *Col6a1* expression in neural crest cells, when starting differentiating (Vitale *et al.*, 2001). However, in the following processes of Schwann cells differentiation, *Col6a1* expression becomes independent from the same signals and at last ceases when Schwann cells acquire their mature phenotype (Vitale *et al.*, 2001). This suggests that mature Schwann cells may be able to ‘perceive’ the presence of secreted collagen VI, so that in *Col6a1*^{-/-} nerves the lack of collagen VI deposition may alter signals involved in the regulation of Schwann cells differentiation, leading to the defects we found in *Col6a1*^{-/-} nerves, such as hypermyelination and abnormal organization of sensory fibers. Regardless the underlying mechanisms involved in the observed abnormalities, the finding of structural and functional defects caused by collagen VI deficiency in peripheral nerves strongly suggest that this ECM protein fulfils a

specific role in the PNS. Future studies, aimed at investigating in further detail the PNS phenotype of *Col6a1*^{-/-} mice, will allow elucidating the role of collagen VI in this tissue and the mechanisms involved in the patho-physiological defects caused by its absence.

In conclusion, the data obtained in this PhD thesis work highlighted a role for collagen VI in both the central and peripheral nervous tissues. The localization of the protein, as also sustained by previous literature studies, points at different sources for collagen VI expression, mostly neuronal for CNS and Schwann cells for PNS. Also the functional consequences caused by ablation of the protein in these tissues appear different, but nonetheless remarkable in both, with a major involvement of autophagy deregulation. These differences suggest that, intriguingly, the peculiarity must stand in the specific receptors present in these different types of cells able to bind collagen VI and to transduce differential signals from the ECM. This becomes even more interesting when we consider that some pathomolecular alterations found in skeletal muscles of collagen VI deficient mice are also paralleled in the CNS of the same animals. In this context, it is worthy to consider that several muscular diseases have implications or correlations with CNS defects. The most known and studied example is provided by Duchenne muscular dystrophy. CNS abnormalities were found in the dystrophin deficient *mdx* mouse, such as decreased number of neurons and neuronal shrinkage in regions of the cerebral cortex and brainstem. A certain degree of cognitive impairment and lower IQ, accompanied by disordered CNS architecture, was found in Duchenne patients (Anderson *et al.*, 2002). Myotonic dystrophy is another muscle genetic disease with CNS implications. It is actually considered as multisystemic, since it displays muscular, endocrine, ocular, cardiac and cognitive impairment, and also in this case the cognitive impairment was related to the genetic cause of the disease but not directly dependent on the muscular disorder (Perini *et al.*, 1999). Although no cognitive impairment was reported for patients affected by skeletal muscle diseases linked to collagen VI deficiency, such as UCMD and Bethlem myopathy (Lampe and Bushby, 2005), the evidence obtained for *Col6a1*^{-/-} mice in this PhD thesis work supports the interest in deepening the studies on the occurrence of CNS-related defects in UCMD and Bethlem myopathy patients. PNS-related deficits in UCMD and Bethlem myopathy patients are even more plausible, given the peripheral nerve defects and the motor-sensory defects displayed by *Col6a1*^{-/-} mice. In more general terms, the data obtained with this PhD study indicate that it will be interesting to unravel whether the nervous compartment may indeed contribute to the pathology of collagen VI diseases in humans, thus allowing a better understanding of the range of clinical symptoms and becoming a new potential target for therapy.

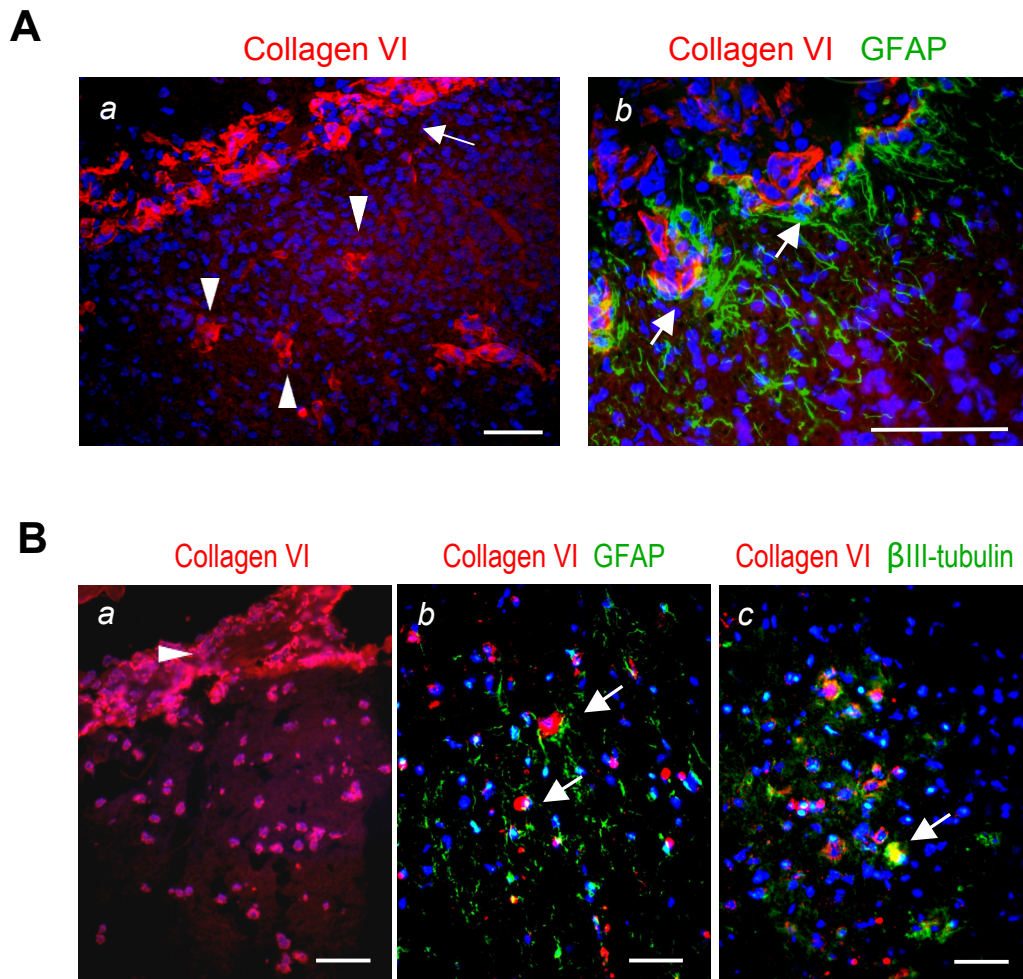


Figure 1. Collagen VI localization in the central nervous system.

A. Detection of collagen VI in mouse neonatal neocortex sections by immunofluorescence. Collagen VI (red) is present along meninges (*a*, arrow) and in the inner cortical region (*a*, arrowhead). The protein is found close to GFAP-positive (green) cells, as indicated by arrows in *b*. Nuclei were stained with Hoechst (blue). Scale bar, 50 μ m.

B. Detection of collagen VI in mouse adult spinal cord sections by immunofluorescence. Collagen VI (red) is present along meninges (*a*, arrowhead) and in the inner regions. Also in this tissue the protein is found close to GFAP-positive (green, *b*) cells, as indicated by arrows in *b*. In some cases collagen VI was found to colocalize with β III-tubulin-positive cells (green, *c*), as indicated by arrows in *c*. Nuclei were stained with Hoechst (blue). Scale bar, 50 μ m.

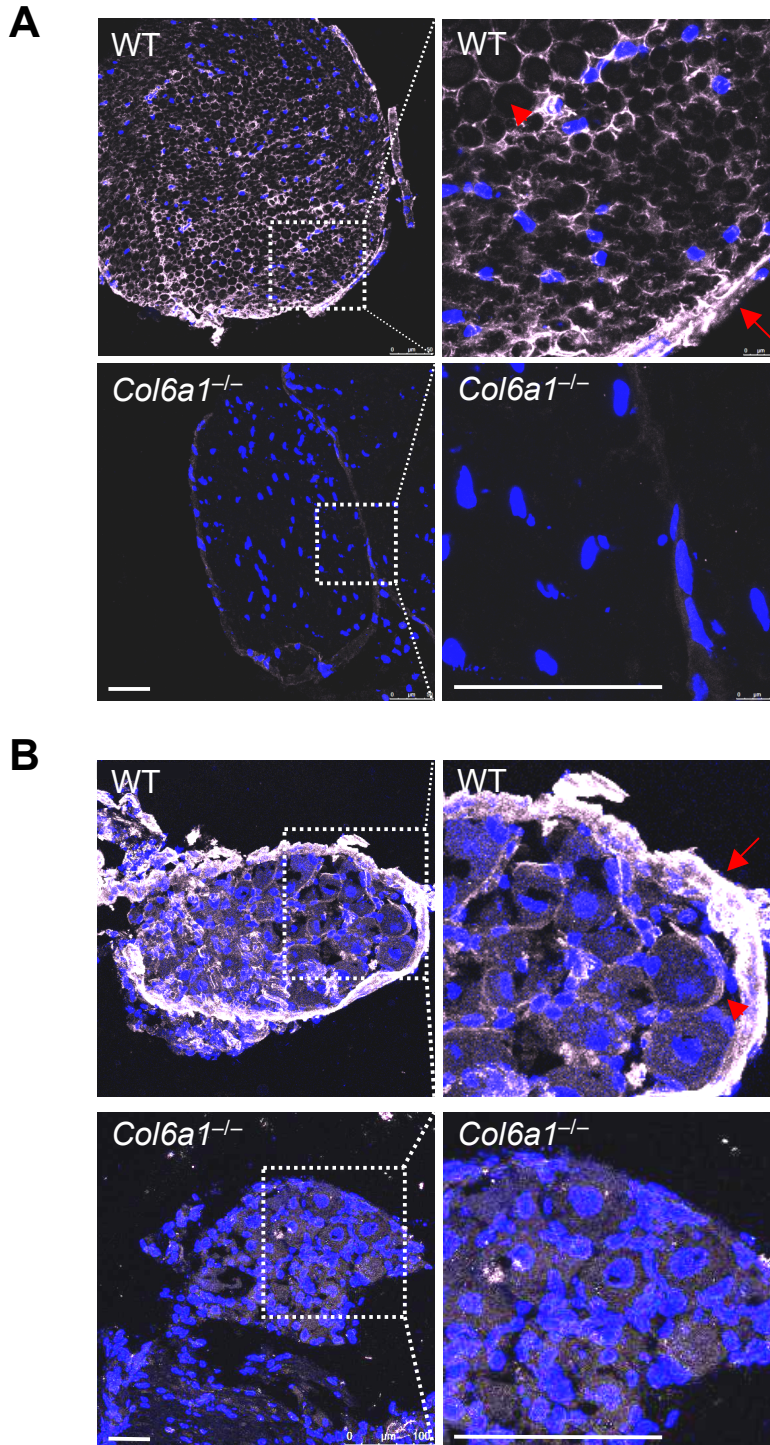


Figure 2. Collagen VI localization in the peripheral nervous system.

Detection of collagen VI by immunofluorescence in sciatic nerve (A) and in DRG (B) from adult wild-type and *Col6a1*^{-/-} mice. Collagen VI (white) was found in the perineurium (arrow) and in the endoneurium (arrowhead). The right panels show an higher magnification of the boxed area of the respective left panels. Nuclei were stained with Hoechst (blue). Scale bar, 50 μm. WT, wild-type.

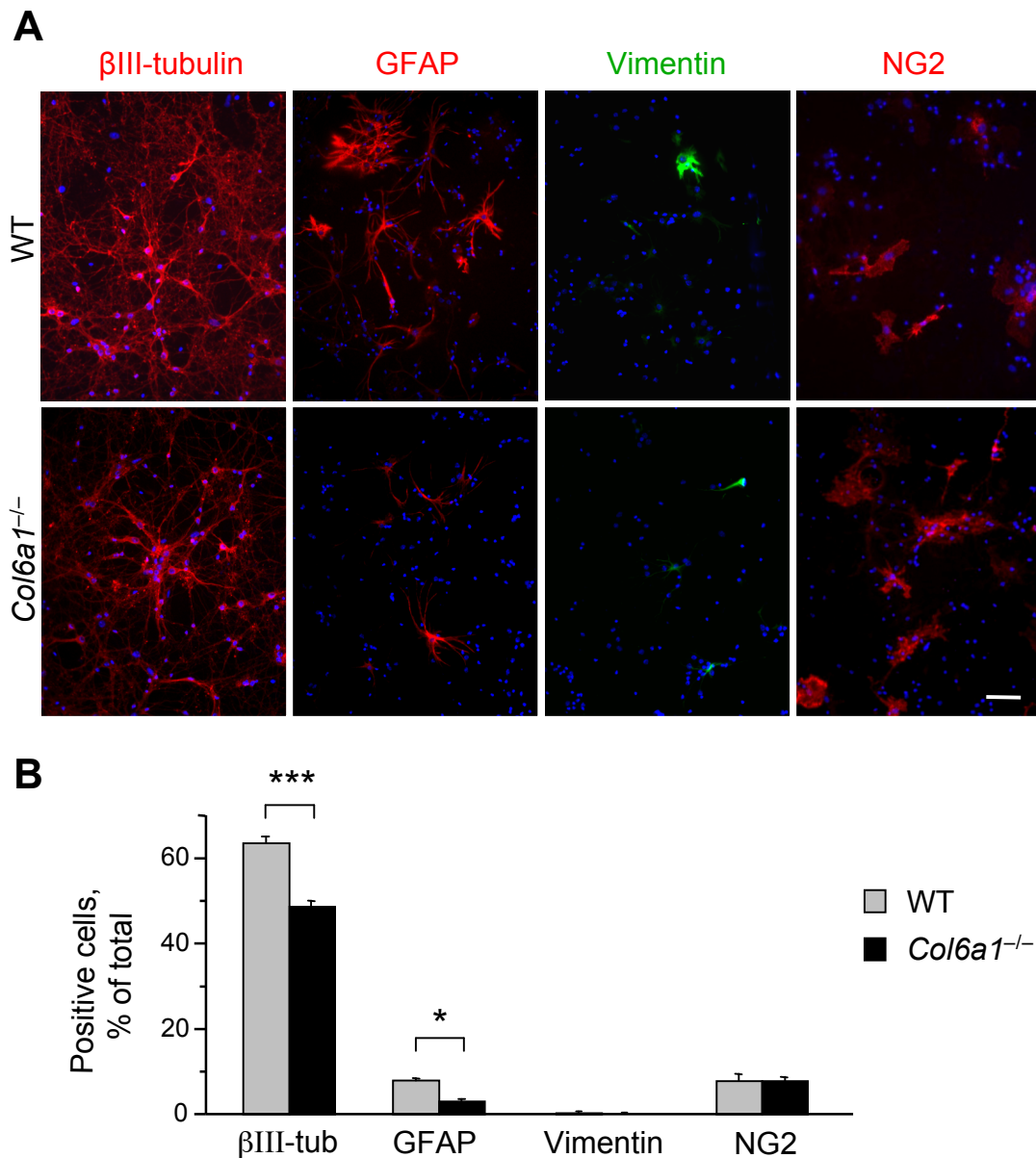


Figure 3. Characterization of primary neural cultures derived from cortex and hippocampus of newborn wild-type and *Col6a1*^{-/-} mice.

A. Immunofluorescence analysis of primary neural cell cultures from wild-type and *Col6a1*^{-/-} mice, using the indicated specific cell markers: βIII-tubulin (neurons), GFAP (glia-astrocytes), vimentin (glial and neuronal precursors), NG2 (oligodendrocyte precursors). Scale bar, 100 μm. WT, wild-type.

B. Percentage of cells in culture positive for each marker. The percentage of neurons is significantly lower in *Col6a1*^{-/-} cultures compared to wild-type cultures. Also the percentage of GFAP-positive cells is significantly decreased in *Col6a1*^{-/-} cultures (***, $P < 0.001$; *, $P < 0.05$; $n = 3$).

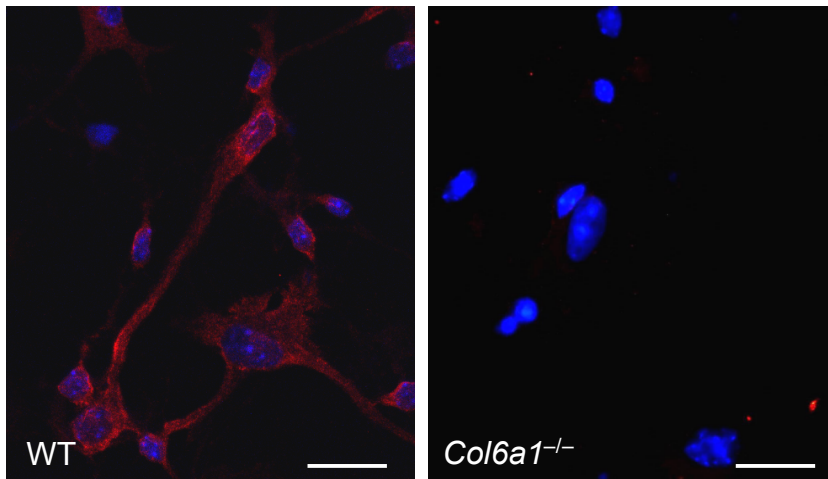
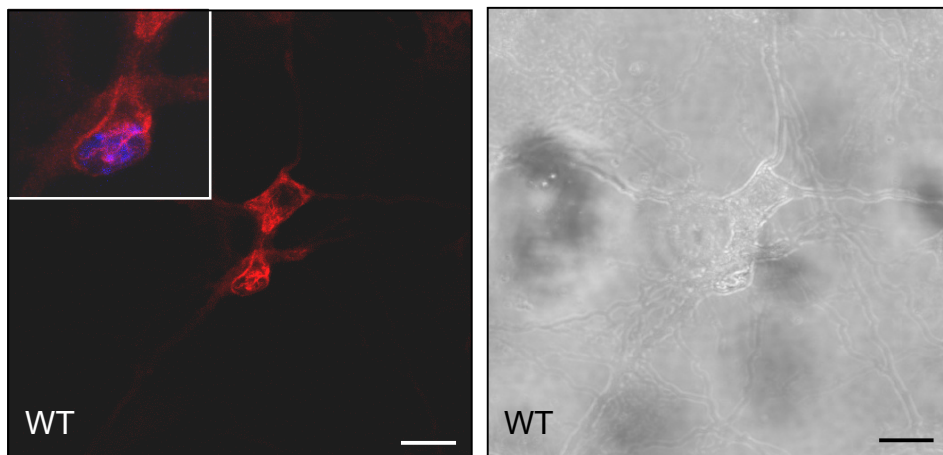
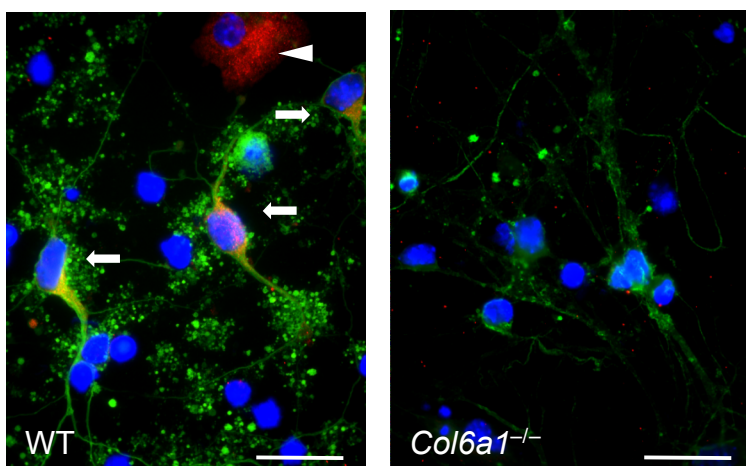
A**B****C**

Figure 4. Collagen VI detection in primary neural cell cultures.

A. Confocal microscopy analysis of immunofluorescence for collagen VI in primary neural cell cultures. Collagen VI (red) is detected in wild-type cultures but not in *Col6a1*^{-/-} cultures. Nuclei were stained with Hoechst (blue). Scale bar, 100 μm . WT, wild-type.

B. Immunofluorescence for collagen VI (red) on wild-type cultures (left panel) and relative phase contrast image (right panel). An intense labelling for collagen VI is present along the plasma membrane (inset, left panel), as also confirmed by the phase contrast image. Scale bar, 50 μm . WT, wild-type.

C. Immunofluorescence for collagen VI (red) and β III-tubulin (green). In wild-type cultures, collagen VI labelling is detected in both neuronal (arrows) and glial (arrowhead) cells. Nuclei were stained with Hoechst (blue). Scale bar, 100 μm . WT, wild-type.

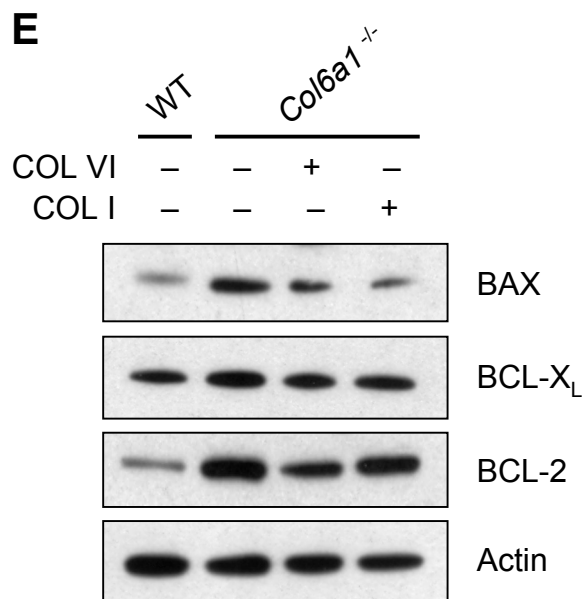
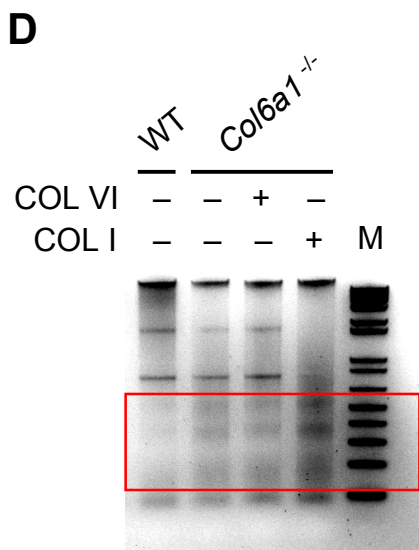
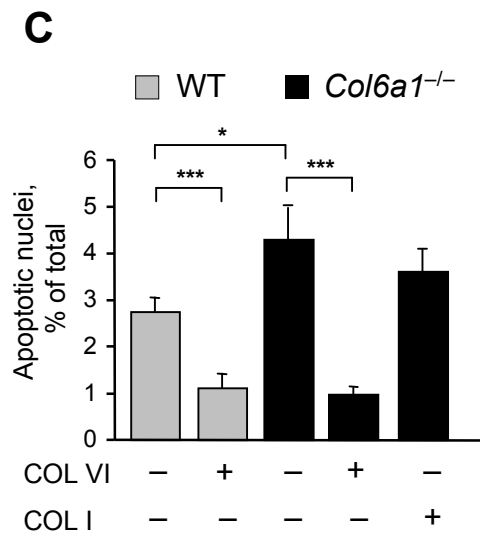
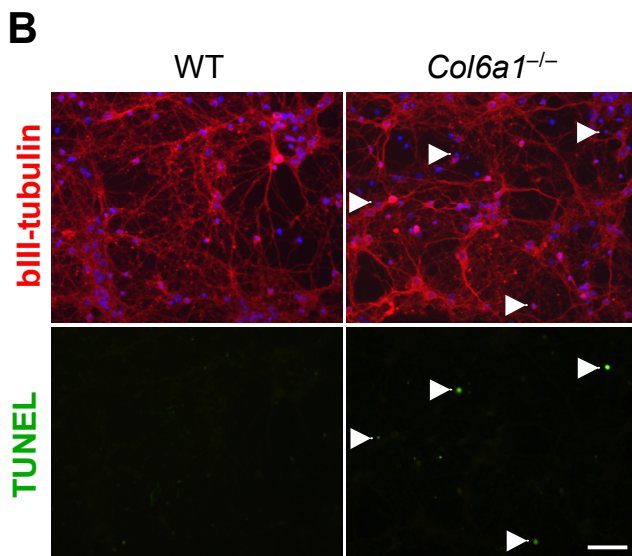
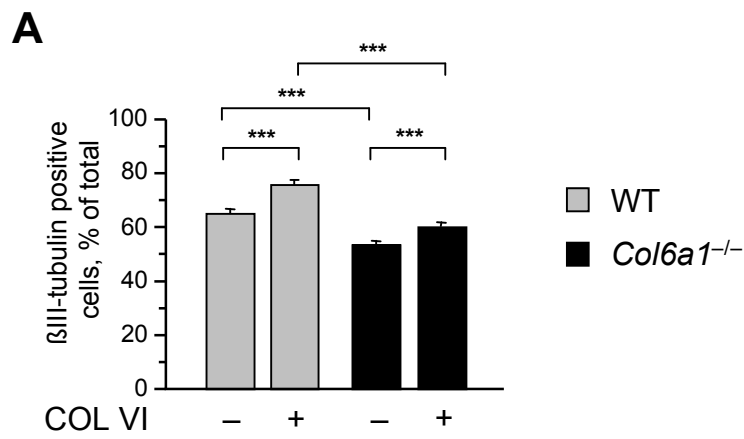


Figure 5. Collagen VI lack affects the neuronal fraction and induces increased apoptosis *in vitro*.

A. Quantification of the percentage of β III-tubulin positive cells in primary neural cell cultures derived from WT and *Col6a1*^{-/-} mice, grown in the absence (-) or in the presence (+) of purified collagen VI as a substrate (***, $P < 0.001$; $n = 6$). COL VI, purified collagen VI; WT, wild-type.

B. Representative images of TUNEL assay in primary neural cell cultures derived from WT and *Col6a1*^{-/-} mice. Neurons were stained by immunofluorescence for β III-tubulin (red, upper panels), nuclei were stained with Hoechst (blue upper panels). TUNEL-positive nuclei (green, lower panels) were identified by the Dead End Fluorometric *in situ* apoptosis detection system. Scale bar, 50 μ m. WT, wild-type.

C. Quantification of TUNEL-positive nuclei in primary neural cell cultures derived from wild-type and *Col6a1*^{-/-} mice, grown in the absence (-) or in the presence (+) of purified collagen VI or collagen I as substrates (*, $P < 0.05$; ***, $P < 0.001$; $n = 3$). COL I, purified collagen I; COL VI, purified collagen VI; WT, wild-type.

D. DNA fragmentation analysis by gel-electrophoresis of DNA extracted from WT and *Col6a1*^{-/-} primary neural cell cultures. DNA laddering highlighted in red is typical of apoptosis. COL I, purified collagen I; COL VI, purified collagen VI; WT, wild-type.

E. Western blot analysis of pro- and anti-apoptotic factors in total protein extracts derived from wild-type and *Col6a1*^{-/-} primary neural cell cultures. Actin was assessed as a loading control. COL I, purified collagen I; COL VI, purified collagen VI; WT, wild-type.

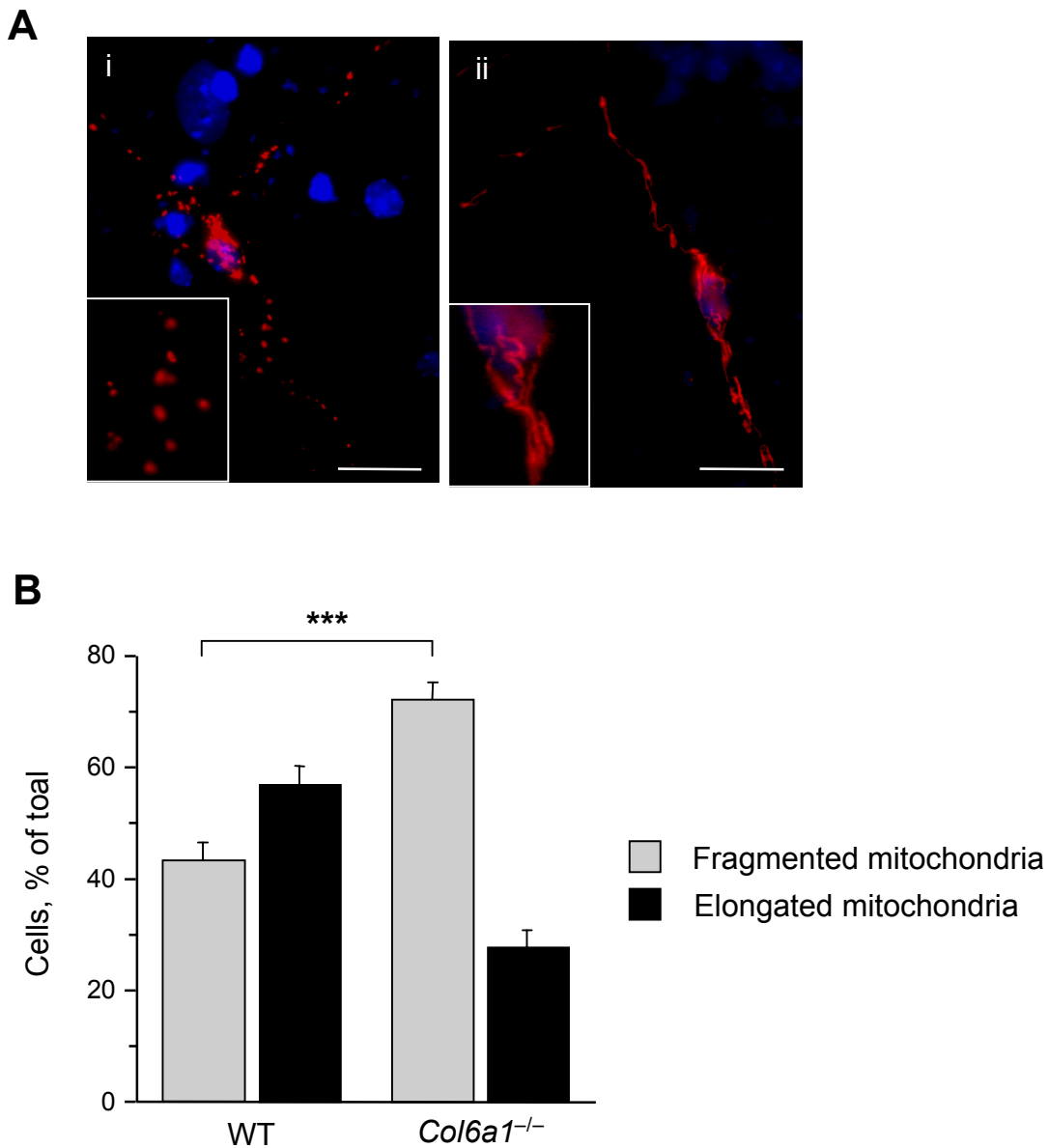


Figure 6. Analysis of mitochondrial morphology in neural cultures.

A. Representative fluorescence microscope images of neural cultures displaying either fragmented mitochondria (i) or elongated mitochondria (ii), following transfection with a plasmid expressing a red fluorescent tagged protein targeted to mitochondria. Nuclei were stained with Hoechst (blue). Scale bar, 50 μ m.

B. Quantification of transfected wild-type and *Col6a1*^{-/-} cells displaying fragmented mitochondria or elongated mitochondria (***) $P < 0.001$; $n = 3$).

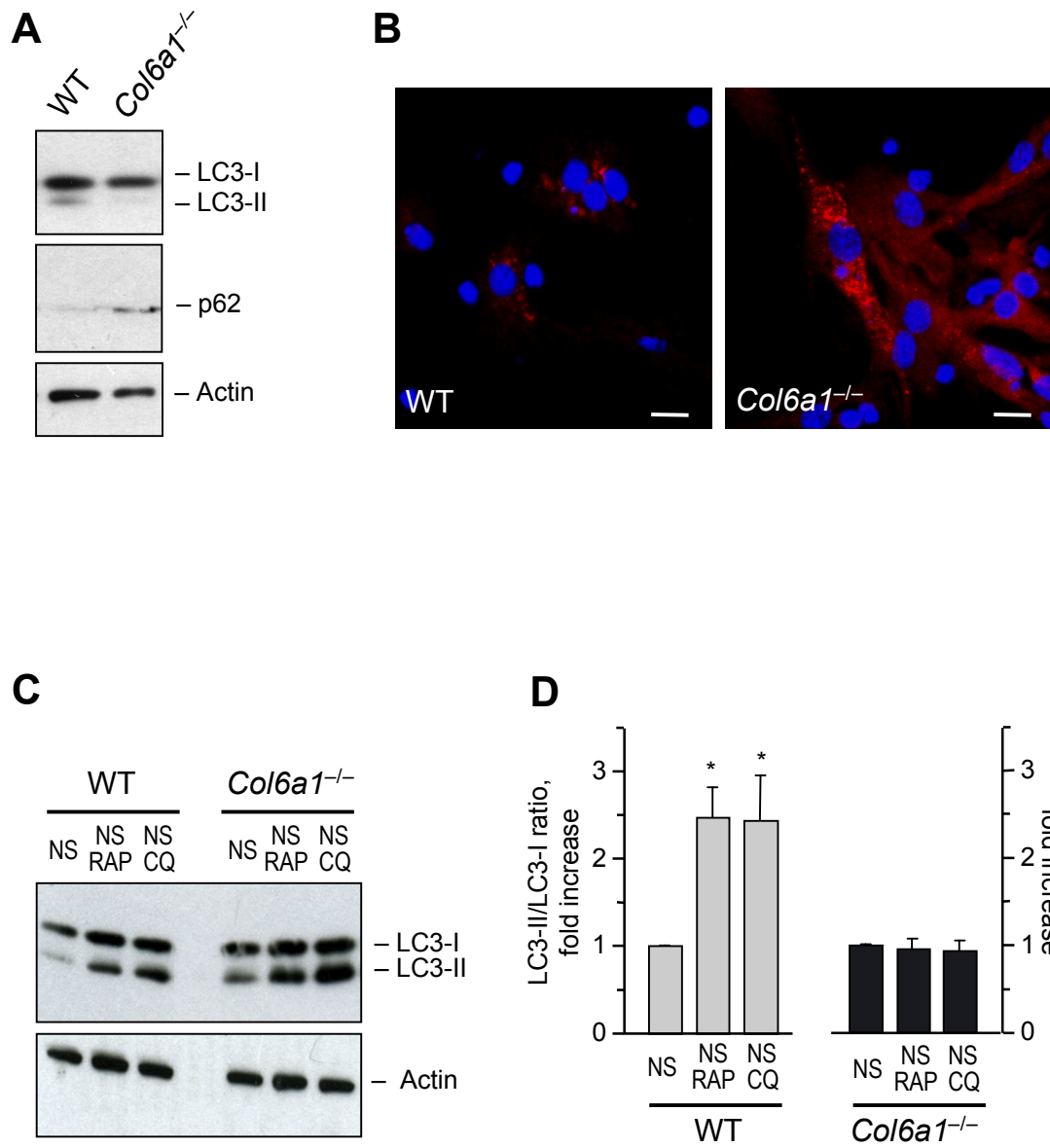


Figure 7. *Col6a1*^{-/-} neural cultures display impaired response to autophagy induction.

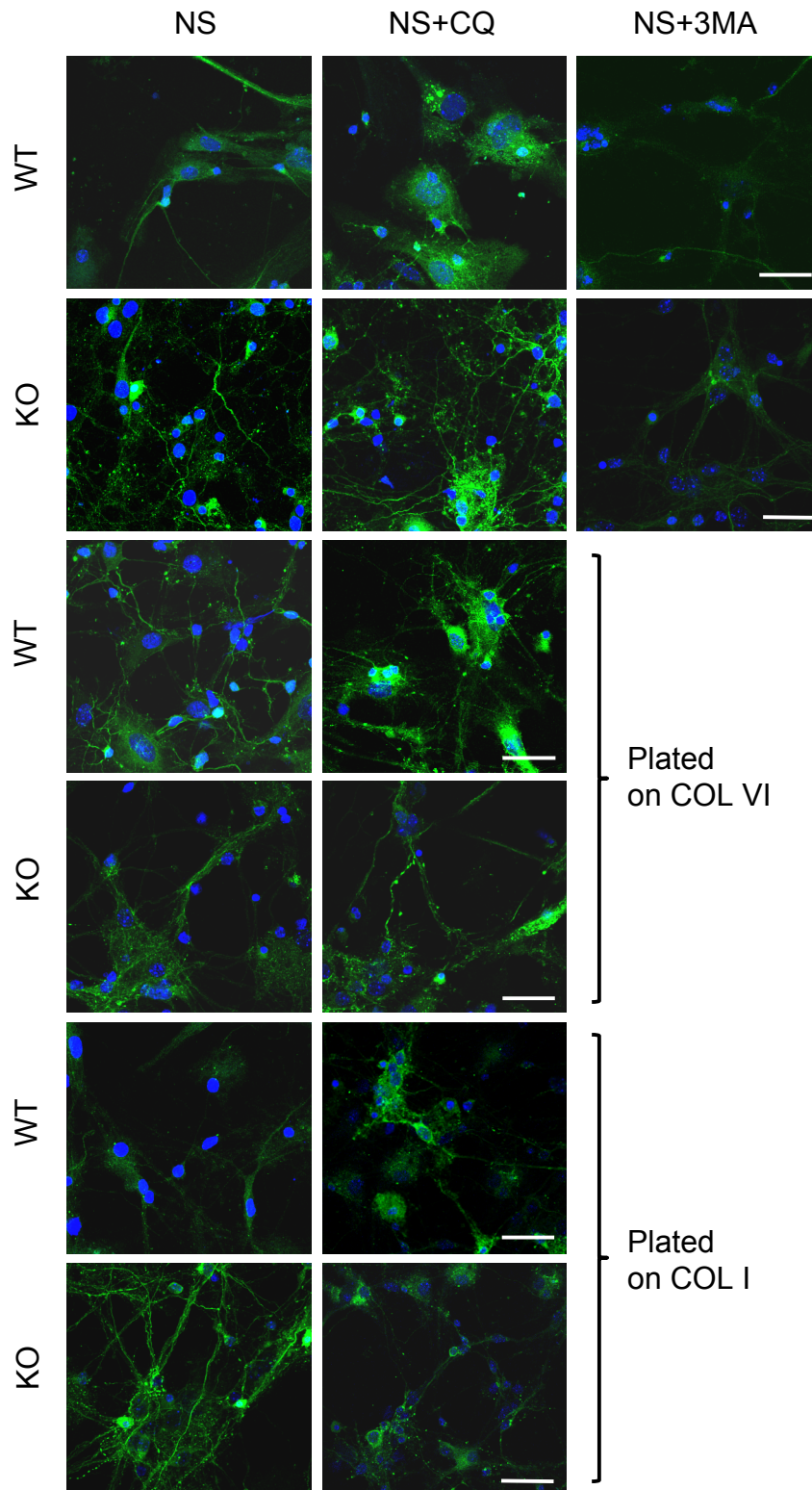
A. Western blot analysis of LC3 and p62 in protein lysates from wild-type and *Col6a1*^{-/-} primary neural cell cultures. Actin was assessed as a loading control. WT, wild-type.

B. Immunofluorescence for p62 (red) in wild-type and *Col6a1*^{-/-} primary neural cultures, showing accumulation of p62 aggregates in *Col6a1*^{-/-} cells. Nuclei were stained with Hoechst (blue). Scale bar, 100 μ m.

C. Western blot analysis for LC3 in protein lysates from wild-type and *Col6a1*^{-/-} primary neural cultures maintained for 4.5 hours under different conditions: serum-free medium (NS), serum-free medium with 100 nM rapamycin (NS RAP), serum-free medium with 50 μ M chloroquine (NS CQ). Actin was assessed as a loading control. WT, wild-type.

D. Densitometric quantification of the LC3-II/LC3-I ratio as determined by western blot from three independent primary neural cultures from wild-type and *Col6a1*^{-/-} mice. The LC3-II/LC3-I ratio is expressed as fold-change relative to the serum-free condition (*, $P < 0.05$; $n = 3$). NS, no serum; NS CQ, no serum plus chloroquine; NS RAP, no serum plus rapamycin. WT, wild-type.

A



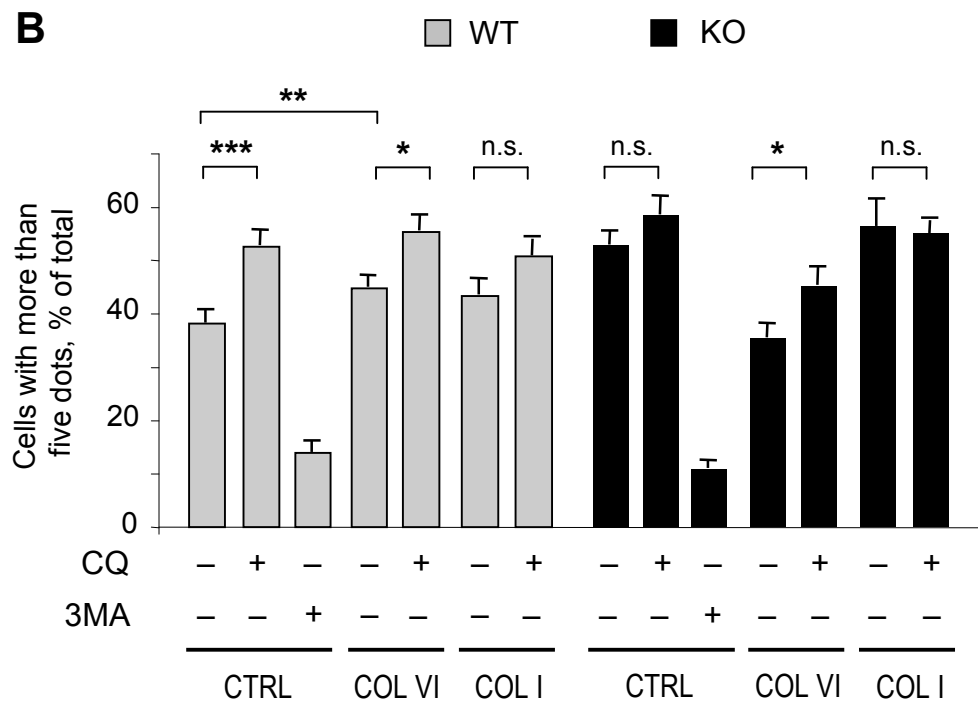


Figure 8. Collagen VI enhances autophagy induction in wild-type cultures and recovers the defective autophagy of *Col6a1*^{-/-} cultures.

A. Fluorescence microscope analysis of GFP-LC3 distribution in neural cell cultures derived from GFP-LC3;*Col6a1*^{+/+} and GFP-LC3;*Col6a1*^{-/-} mice and maintained for 4.5 hours in serum-free medium in the absence (NS) or in the presence of 50 μ M chloroquine (NS+CQ) or of 10 mM 3-methyladenine (NS+3MA). Where indicated, before the experiment cells were seeded onto purified collagen VI (COL VI) or collagen I (COL I) as substrates. Nuclei were stained with Hoechst (blue). Scale bar, 50 μ m. KO, GFP-LC3;*Col6a1*^{-/-}; WT, GFP-LC3;*Col6a1*^{+/+}.

B. Quantification of GFP-LC3 dots in neural cell cultures derived from GFP-LC3;*Col6a1*^{+/+} and GFP-LC3;*Col6a1*^{-/-} mice and maintained in the different conditions described above. The histogram shows the percentage of cells with more than five fluorescent dots for each condition (***, $P < 0.001$; *, $P < 0.05$; n.s., not significant; $n = 3$). 3MA, 3-methyl-adenine; COL I, adhesion onto collagen I; COL VI, adhesion onto collagen VI; CQ, chloroquine; KO, GFP-LC3;*Col6a1*^{-/-}; WT, GFP-LC3;*Col6a1*^{+/+}.

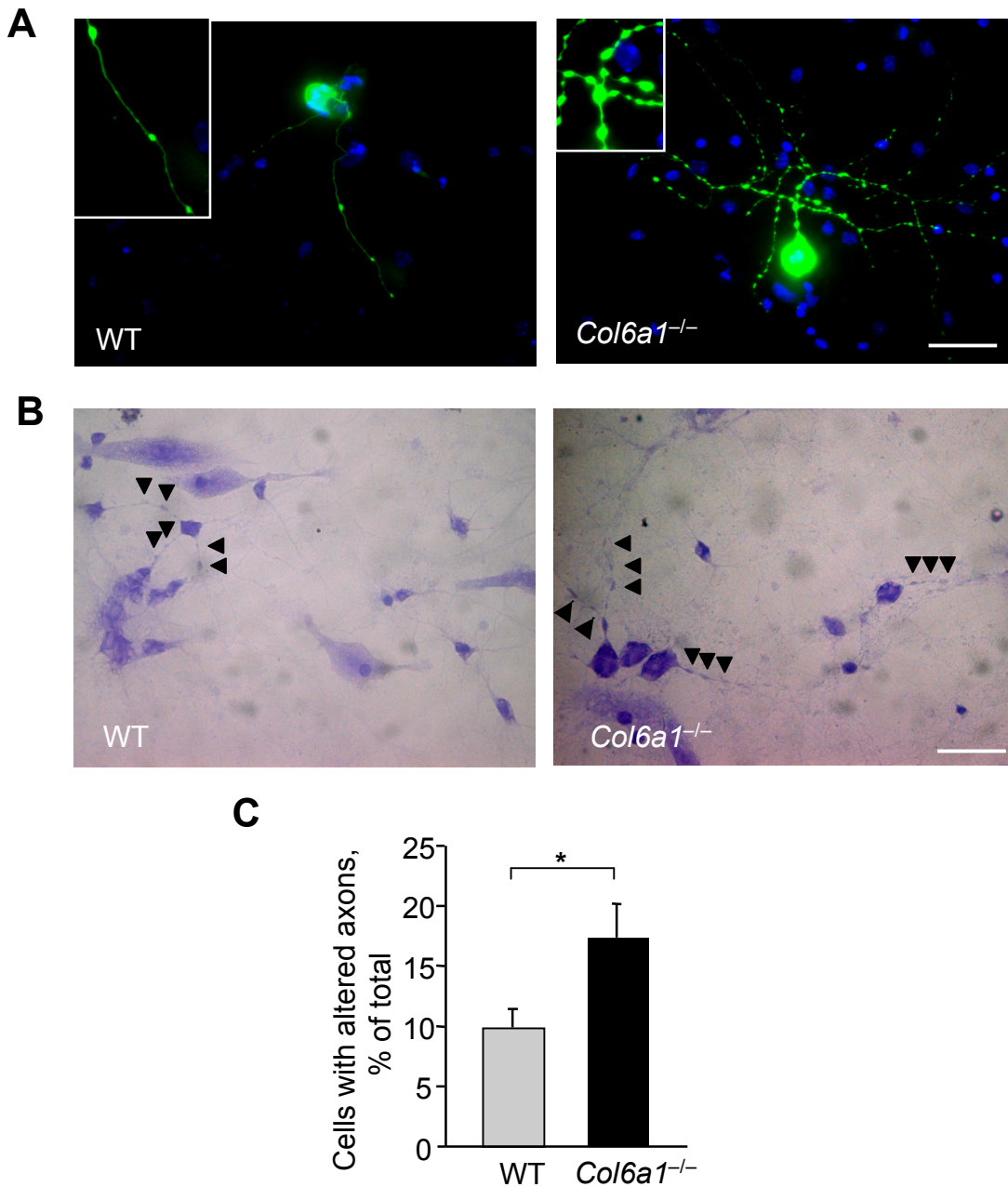
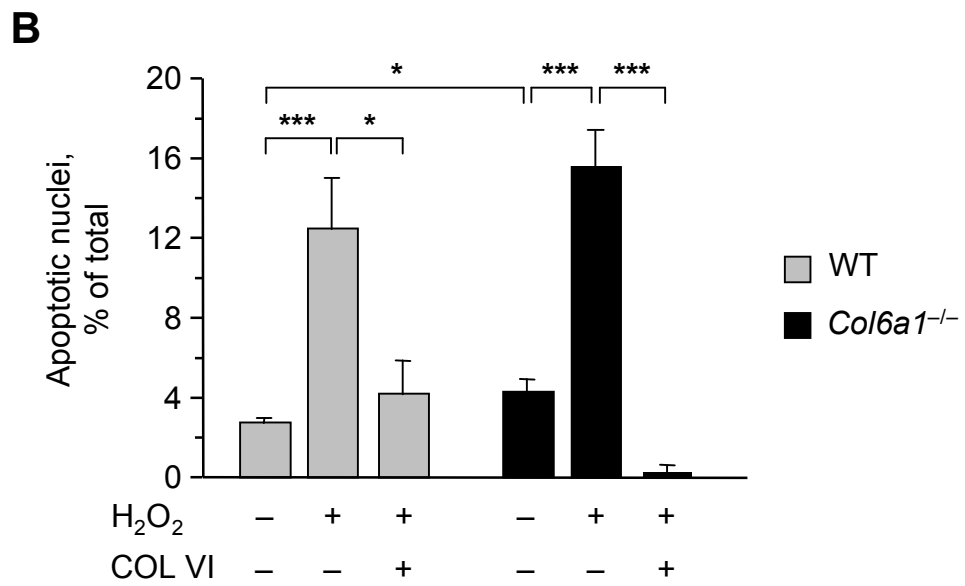
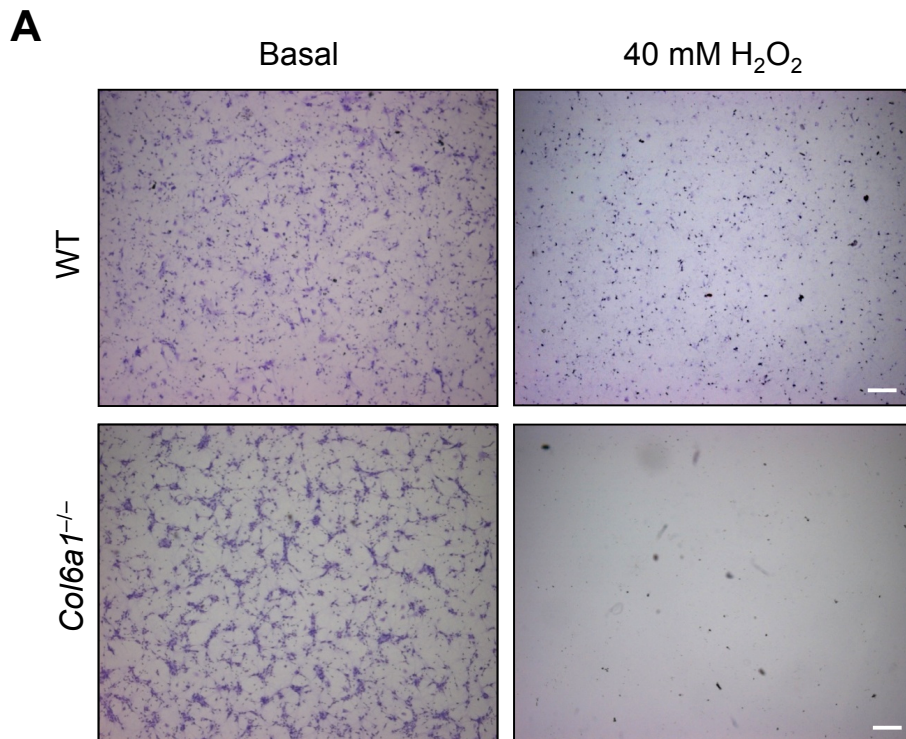


Figure 9. Axonal alterations in *Col6a1*^{-/-} neural cultures.

A. Fluorescence microscopy of transfected wild-type and *Col6a1*^{-/-} neural cells expressing an EYFP tagged protein. Transfected *Col6a1*^{-/-} cells display marked axonal alterations. The insets show a higher magnification detail. Nuclei were stained with Hoechst (blue). Scale bar, 100 μ m. WT, wild-type.

B. Light microscopy analysis of non-transfected wild-type and *Col6a1*^{-/-} neural cells stained with cresyl violet, showing abundant axonal alterations (arrowheads) in *Col6a1*^{-/-} axons. C. Quantification of cells with altered axons, following staining with cresyl violet. (*, $P < 0.05$; $n = 3$). WT, wild-type.



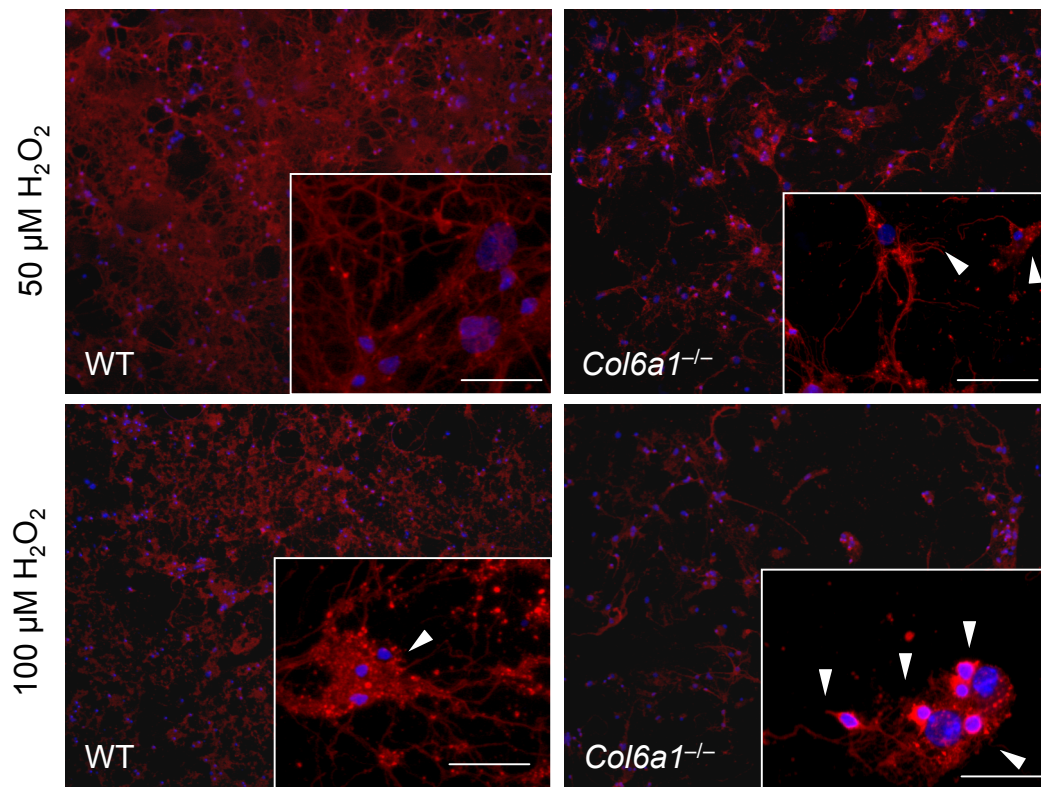
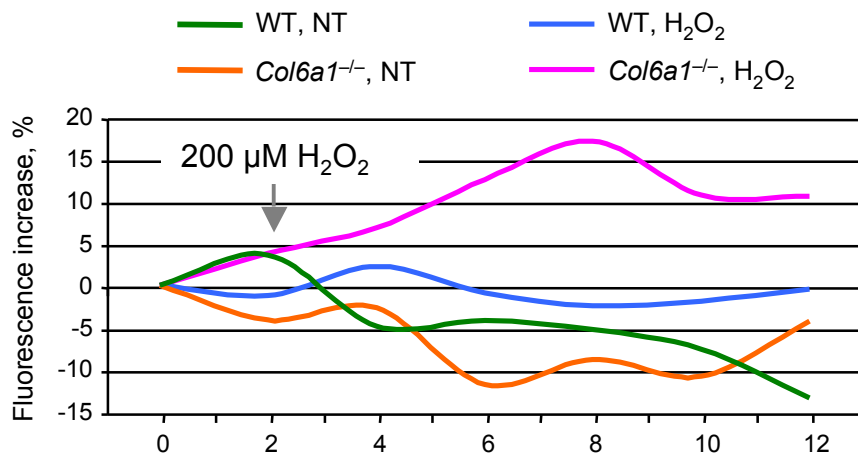
C**D**

Figure 10. *Col6a1*^{-/-} neural cultures are more sensitive to oxidative damage.

A. Light microscopy analysis of wild-type and *Col6a1*^{-/-} neural cells maintained in standard condition and after treatment for 90 minutes with 40 mM H₂O₂. Cells were fixed and stained with cresyl violet. Scale bar, 100 μm. WT, wild-type.

B. Quantification of apoptotic nuclei by TUNEL in wild-type and *Col6a1*^{-/-} neural cell cultures maintained in standard condition or after treatment for 90 minutes with 10 mM H₂O₂. Where indicated, cells were grown onto purified collagen VI before treatment with 10 mM H₂O₂ (***, $P < 0.001$; $n = 3$). COL VI, adhesion onto collagen VI. WT, wild-type.

C. Immunofluorescence for βIII-tubulin in wild-type and *Col6a1*^{-/-} neural cell cultures after treatment for 90 minutes with 50 μM H₂O₂ (top panels) or 100 μM H₂O₂ (bottom panels). Even at lower doses of hydrogen peroxide, *Col6a1*^{-/-} cultures display a less dense neuronal network, with higher incidence of dendrite shrinkage (arrowheads in insets). The insets show higher magnification details of each panel. Nuclei were stained with Hoechst (blue). Scale bar, 50 μm. WT, wild-type.

D. ROS measurements in wild-type and *Col6a1*^{-/-} neural cells by monitoring the increased fluorescence due to the oxidation of reduced MitoTracker Red probe. Where indicated (arrow), 200 μM H₂O₂ was added. NT, not treated. WT, wild-type.

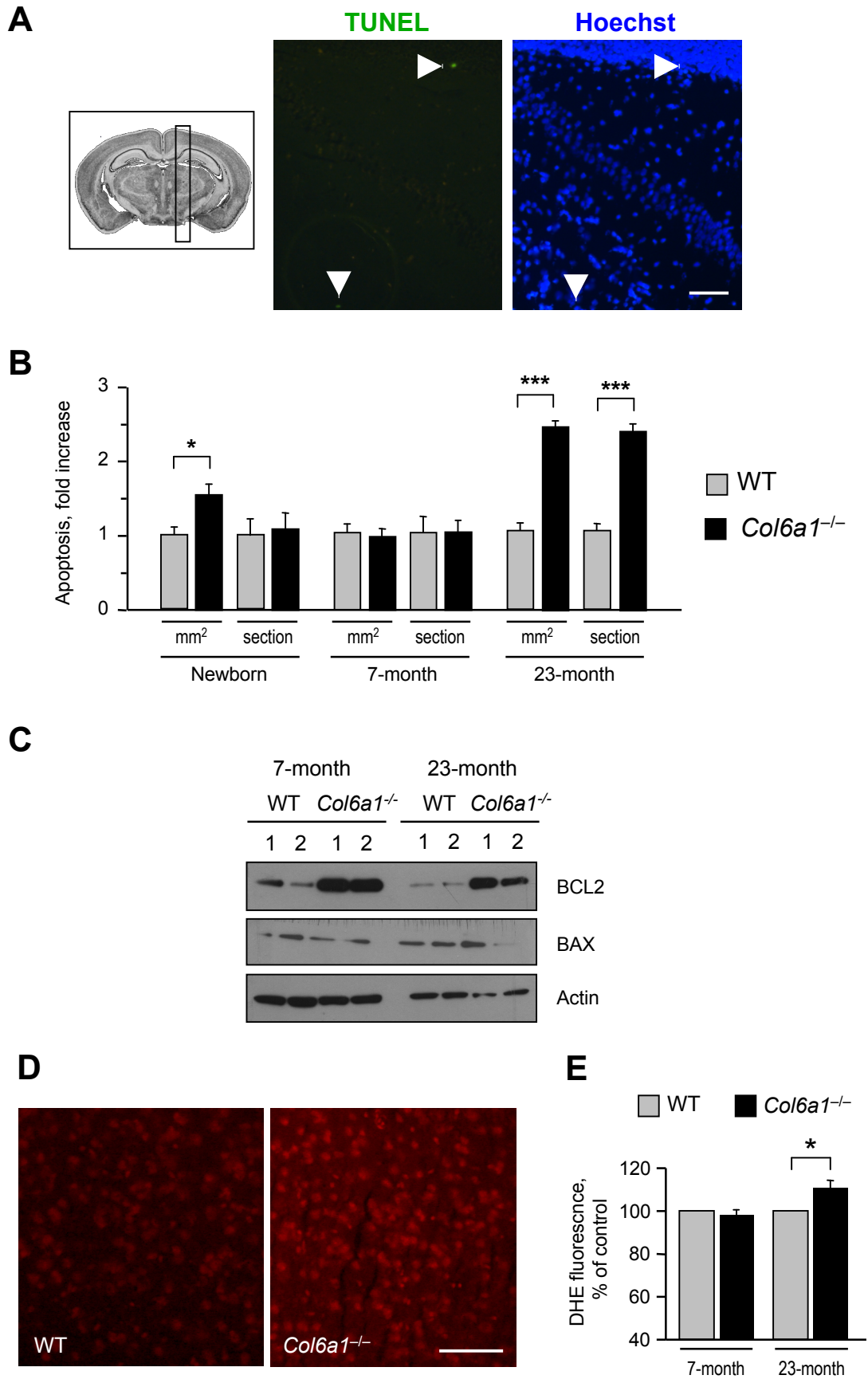


Figure 11. Apoptosis is increased in newborn and aged *Col6a1*^{-/-} mice.

A. Representative images of TUNEL assay in adult brain sections derived from the region showed in the inset on the left. TUNEL-positive nuclei (green, middle panel) were identified by the Dead End Fluorometric *in situ* apoptosis detection system. Nuclei were stained with Hoechst (blue, right panel). Scale bar, 50 μ m.

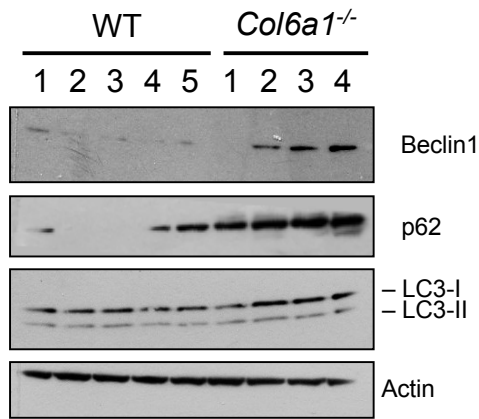
B. Quantification of TUNEL-positive nuclei in sagittal sections of brains of newborn, 7-month-old ($n = 3$) and 23-month-old ($n = 7$) wild-type and *Col6a1*^{-/-} mice. TUNEL-positive cells were counted per area (mm^2) and per section. substrates (*, $P < 0.05$; ***, $P < 0.01$). WT, wild-type.

C. Western blot analysis for BCL-2 and BAX in total protein extracts derived from the brain of wild-type and *Col6a1*^{-/-} mice. Actin was assessed as a loading control. WT, wild-type.

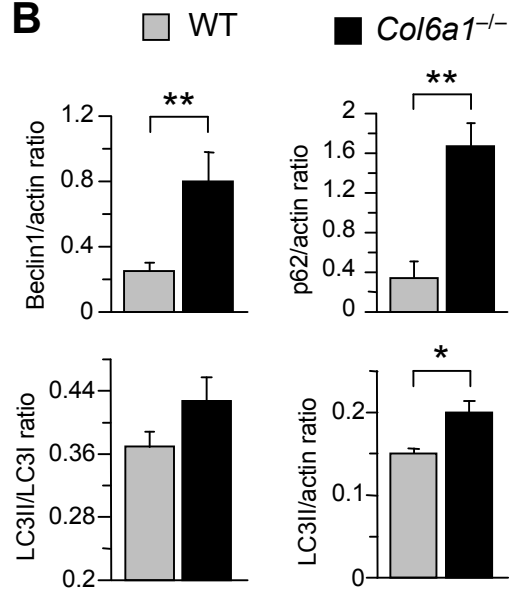
D. Representative images of DHE staining in brain sections of 23-month-old wild-type and *Col6a1*^{-/-} mice. Scale bar, 100 μ m. WT, wild-type.

E. Quantification of DHE fluorescence in brain sections of 7-month-old ($n = 3$) and 23-month-old ($n = 7$) wild-type and *Col6a1*^{-/-} mice. ROS accumulation is significantly higher in aged *Col6a1*^{-/-} mice. (*, $P < 0.05$). WT, wild-type.

A



B



C

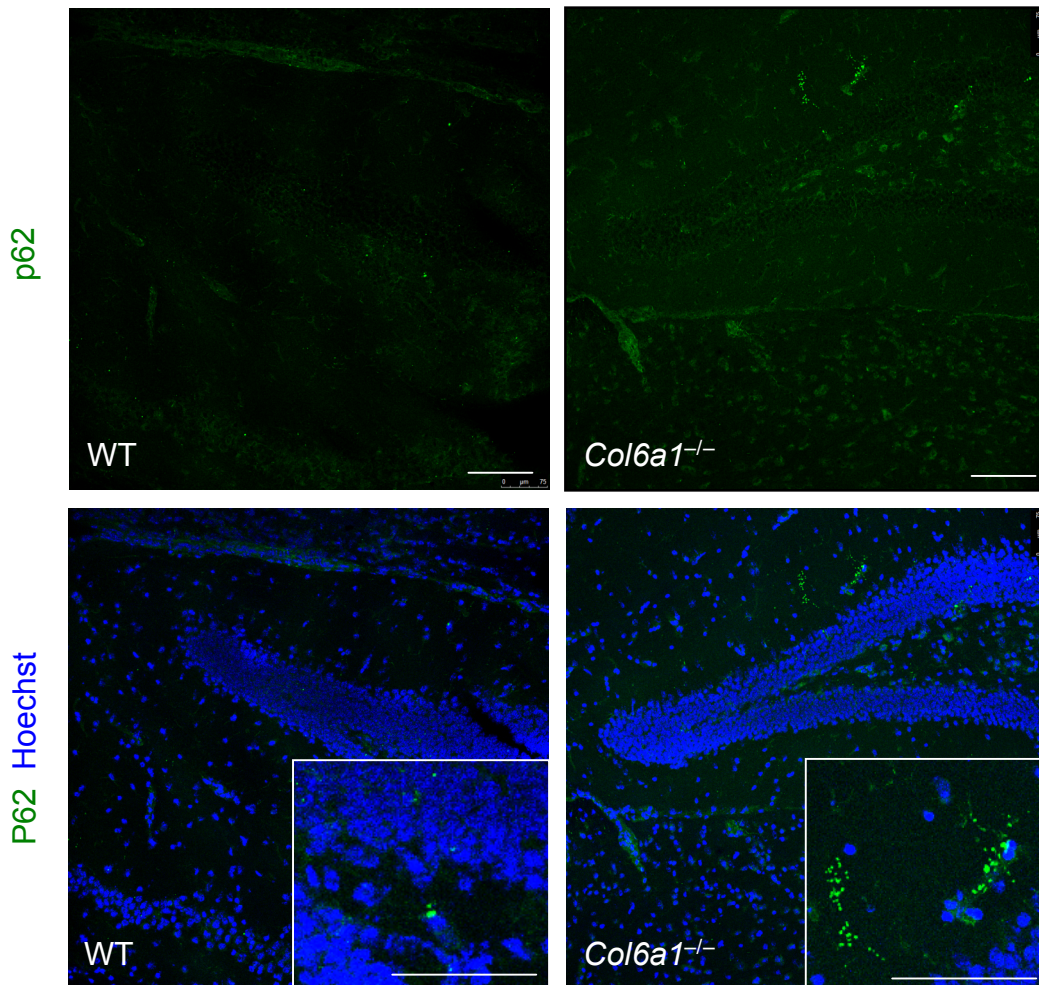


Figure 12. Autophagy is altered in aged *Col6a1*^{-/-} mice.

A. Western blot analysis of the autophagic markers Beclin1, p62 and LC3 in total protein extracts from brain of 23-month-old wild-type and *Col6a1*^{-/-} mice. Actin was used as a loading control. WT, wild-type

B. Densitometric quantification of Beclin-1/actin ratio, p62/actin ratio, LC3-II/LC3-I ratio and LC3-I/actin ratio, as determined by three independent western blot experiments of brain extracts from 23-month-old wild-type and *Col6a1*^{-/-} mice. (*, $P < 0.05$; **, $P < 0.01$; $n = 3$). WT, wild-type.

C. Immunofluorescence for p62 in brain sections from 23-month-old wild-type and *Col6a1*^{-/-} mice, revealing increased p62 labeling in *Col6a1*^{-/-} samples. Insets show p62 aggregates at higher magnification. Scale bar, 100 μm . WT, wild-type.

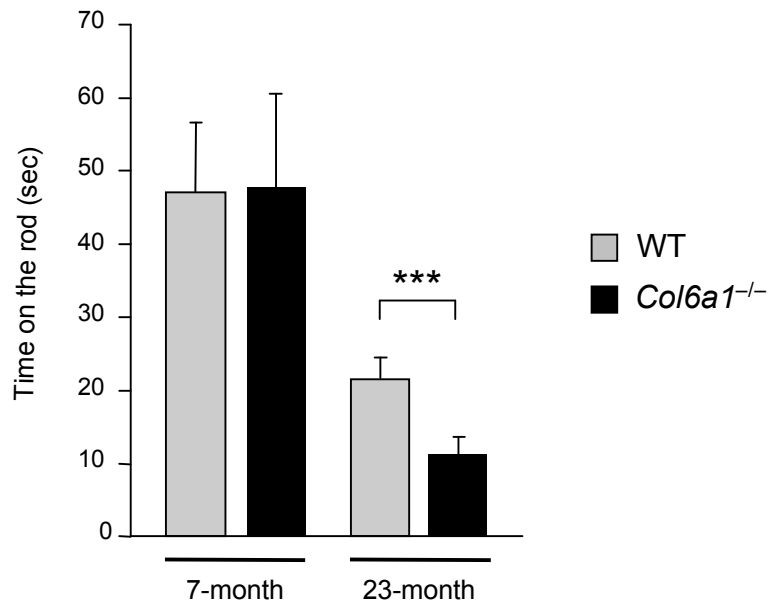


Figure 13. Altered motor coordination in *Col6a1*^{-/-} aged mice.

Rotarod test on 7-month-old and 23-month-old wild-type and *Col6a1*^{-/-} mice. Time on the rod (in seconds) is reported in the graph. 23-month-old *Col6a1*^{-/-} mice show reduced time to fall on rotarod compared to controls (***, $P < 0,001$; $n = 4$).

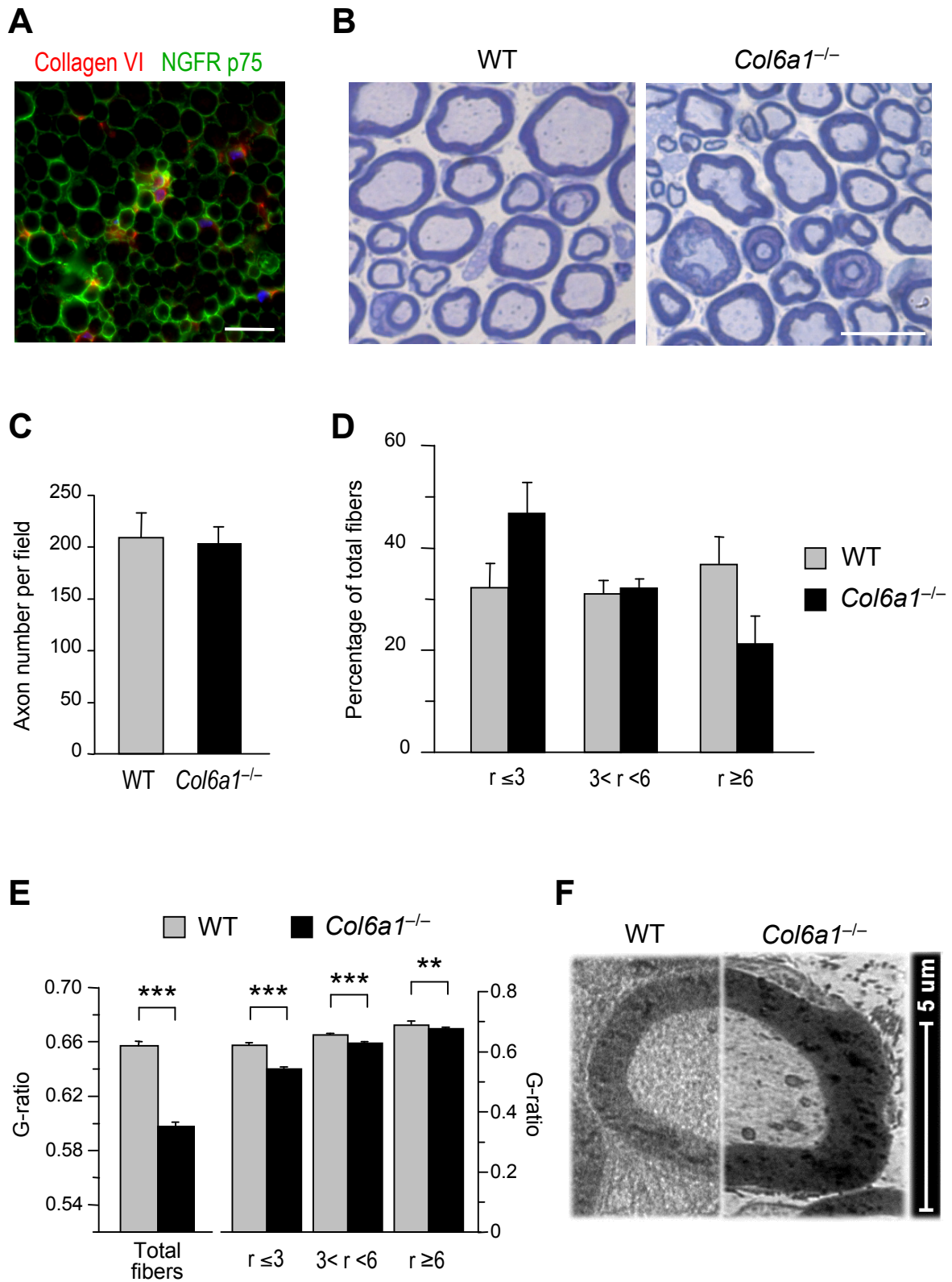


Figure 14. Morphometric analysis of sciatic nerves in wild-type and *Col6a1*^{-/-} mice.

A. Immunofluorescence analysis for low affinity nerve growth factor receptor (NGFR p75, green) and collagen VI (red) in transverse section of wild-type sciatic nerve. Scale bar, 25 μm .

B. Light microscope images of semithin transverse sections of sciatic nerves from wild-type and *Col6a1*^{-/-} mice, following staining with toluidine blue. Scale bar, 50 μm . WT, wild-type.

C. Quantification of the total number of axons in transverse sections of wild-type and *Col6a1*^{-/-} sciatic nerves. Mean total number of axons per field does not show any significant difference between the two genotypes ($n = 4$). WT, wild-type.

D. Quantification of fibers displaying different axon diameters in transverse sections of wild-type and *Col6a1*^{-/-} sciatic nerves. The histogram provides the percentage of fibers in the two genotypes, where fibers were grouped into three classes according to axon radius ($r \leq 3 \mu\text{m}$; $3 < r < 6 \mu\text{m}$; $r \geq 6 \mu\text{m}$) (not significant; $n = 4$). WT, wild-type.

E. Quantification of g-ratio (ratio of the axon diameter divided by the diameter of the axon and its myelin sheath) in sciatic nerves from wild-type and *Col6a1*^{-/-} mice. The g-ratio was calculated for total fibers (left panel) and for fibers with different diameters, grouped in three classes as above (right panel). *Col6a1*^{-/-} sciatic nerves display significantly increased g-ratio for all fiber classes (**, $P < 0.01$; ***, $P < 0.001$; $n = 4$).

F. Transmission electron micrographs of transverse sections of sciatic nerve from wild-type (left panel) and *Col6a1*^{-/-} (right panel) mice. *Col6a1*^{-/-} sciatic nerves display increased thickness of the myelin sheath. WT, wild-type.

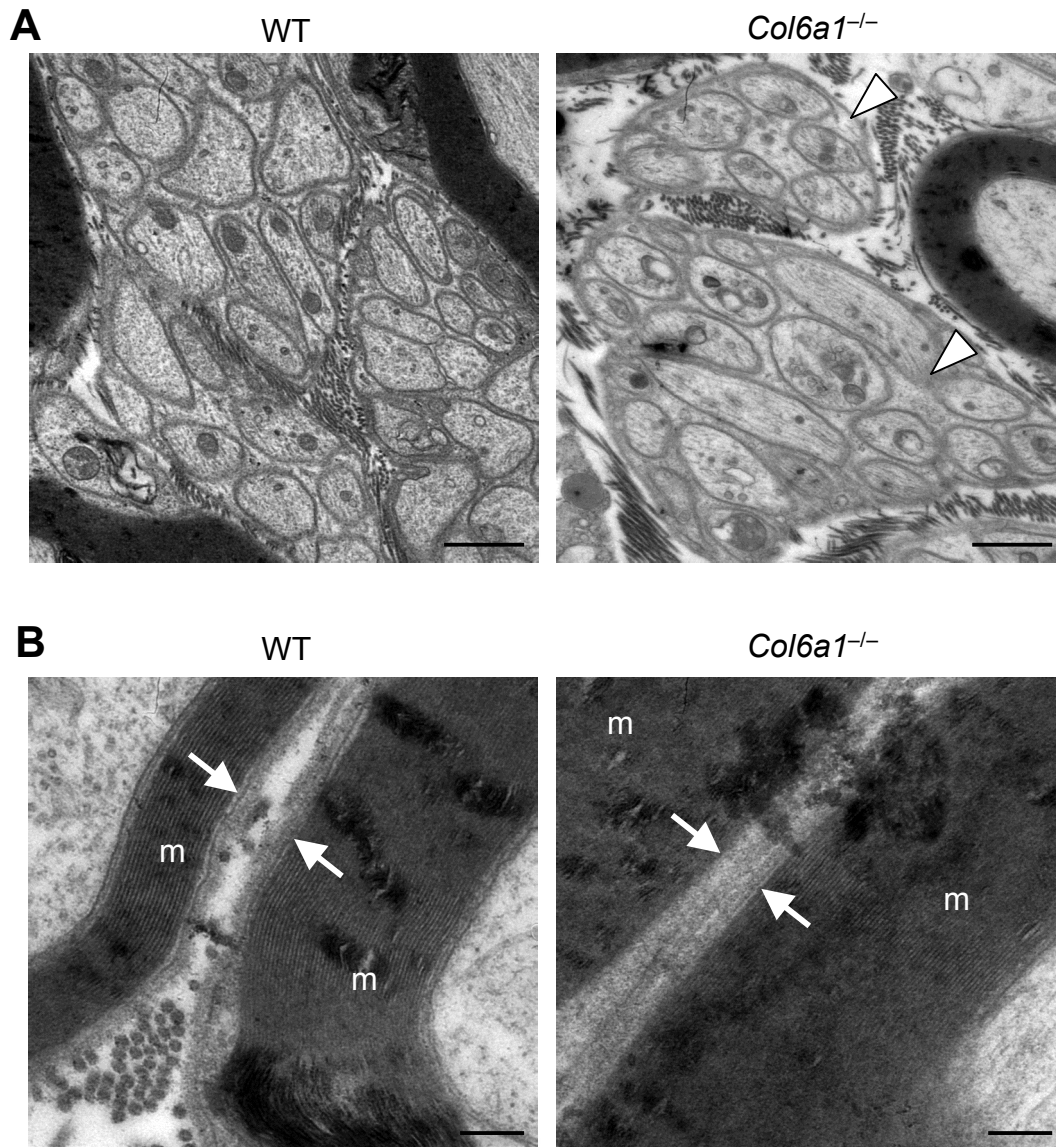


Figure 15. Transmission electron microscopy of sciatic nerve sections from wild-type and *Col6a1*^{-/-} mice.

A. Low-power magnification, showing Remak bundles in wild-type and *Col6a1*^{-/-} sciatic nerve. *Col6a1*^{-/-} nerves display more irregular and loosely packed fibers (arrowheads) in Remak bundles. Scale bar, 1 μ m.

B. High-power magnification, showing basal lamina of adjacent Schwann cells in wild-type and *Col6a1*^{-/-} sciatic nerve. *Col6a1*^{-/-} nerves display a partial fusion between the basal laminae (arrows). The increased thickness of myelin sheath (m) in *Col6a1*^{-/-} nerves is also evident. Scale bar, 200 nm.

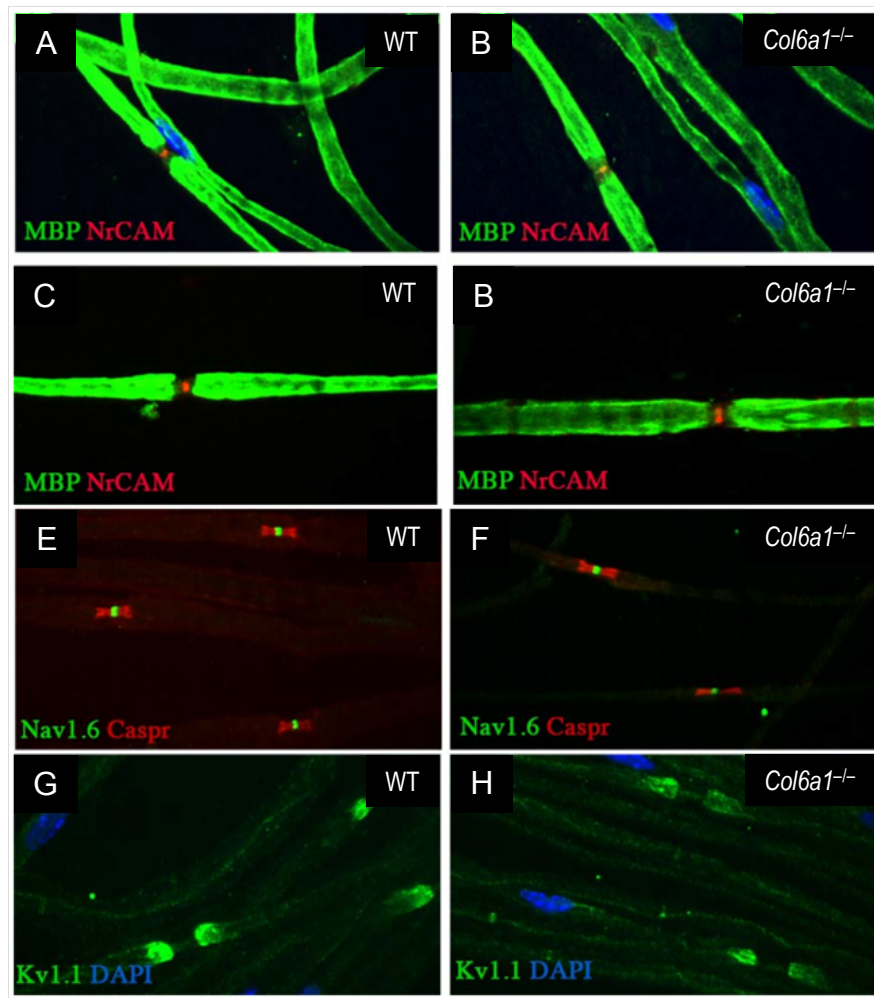


Figure 16. Immunofluorescence of teased fibers from wild-type and *Col6a1*^{-/-} sciatic nerves.

A-D. Immunofluorescence for myelin basic protein (MBP, green) and NrCAM (red), marking Ranvier nodes in myelinated axons.

E-F. Immunofluorescence for Nav1.6 (green), the predominant voltage-gated sodium channel at the Ranvier nodes, and for Caspr, which marks paranodes (red).

G-H. Immunofluorescence for Kv1.1 (green), a voltage-gated potassium channel labeling the juxtaparanode region. Nuclei were stained with DAPI.

Scale bar, 5 μ m. WT, wild-type.

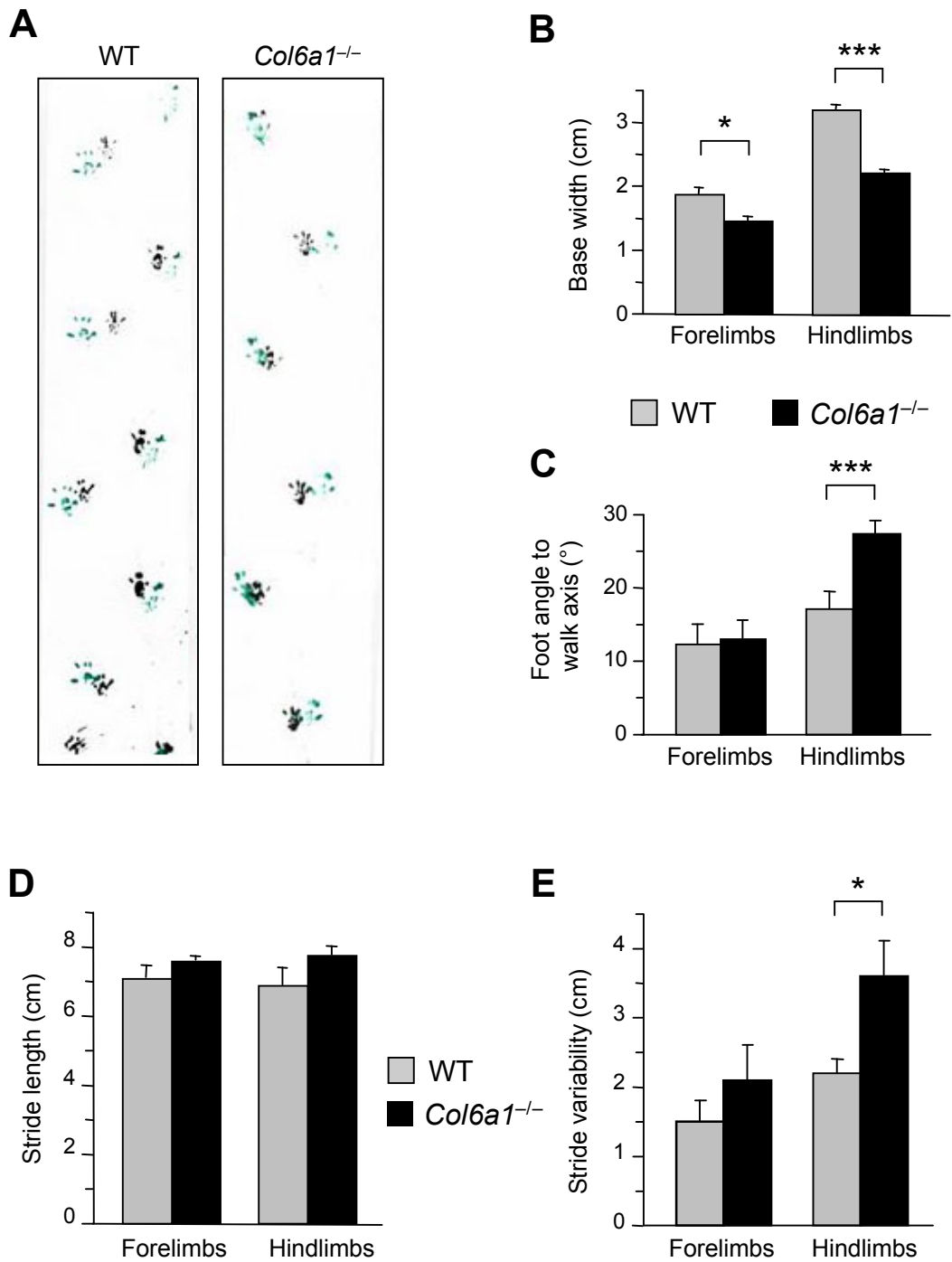


Figure 17. Footprint analysis of wild-type and *Col6a1*^{-/-} mice.

The footprint test was performed on 7-month-old mice (wild-type = 4; *Col6a1*^{-/-} = 4), to assess for the presence of altered behavioural phenotypes.

A. Representative images of footprint tracks from the mice. The forepaws of mice were dipped in atoxic black paint, hindpaws in green.

B. Quantification of base width, measured as the distance between the right and the left forepaw, and the left and right hindlimb respectively (***, $P < 0.001$; *, $P < 0.05$; $n = 4$).

C. Quantification of mean foot angle to walk direction, measured as the angles between foot steps and walking direction. Mean foot angle to walk direction was calculated with the support of ImageJ software (*, $P < 0.05$; $n = 4$).

D. Quantification of stride length, measured as the mean distance between consequent footprints of the same side (not significant; $n = 4$).

E. Quantification of stride variability, calculated by subtracting the shortest stride from the longest stride (*, $P < 0.05$; $n = 4$).

WT, wild-type.

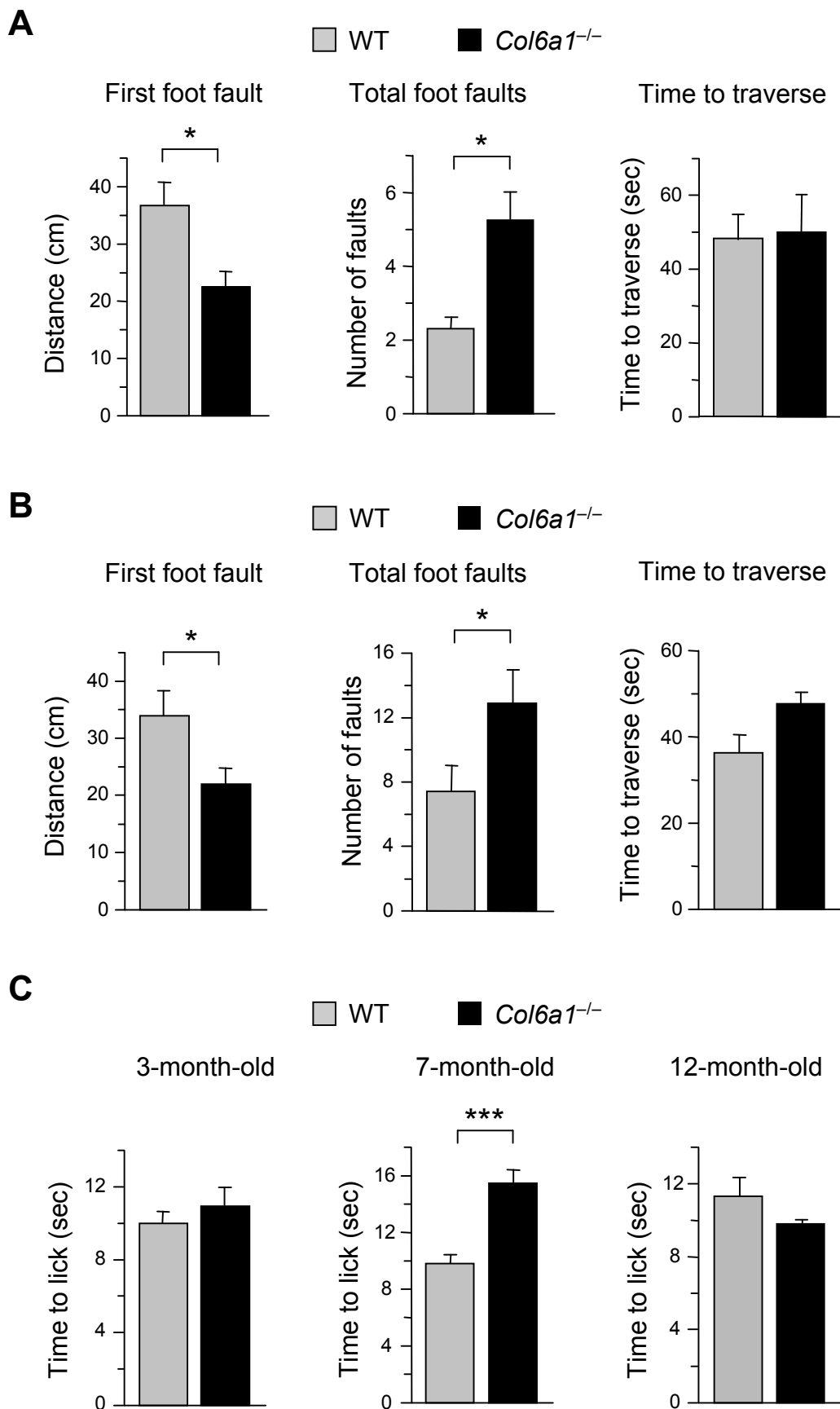


Figure 18. Functional alterations in *Col6a1*^{-/-} mice.

A. Ledged beam test results from 7-month-old wild-type and *Col6a1*^{-/-} mice. The histograms report the mean distance before the initial foot fault, the number of total hindpaw foot faults, and the time spent to reach the end of the beam (*, $P < 0.05$; $n = 4$).

B. Ledged beam test results from 23-month-old wild-type and *Col6a1*^{-/-} mice. The histograms report the mean distance before the initial foot fault, the number of total hindpaw foot faults, and the time spent to reach the end of the beam (*, $P < 0.05$; $n = 4$).

C. Assessment of acute pain perception by hot plate test in 3-month-, 7-month-, and 23-month-old wild-type and *Col6a1*^{-/-} mice. Data are expressed as latency to respond, identified as licking of the paws (***, $P < 0.001$; $n = 14-15$).

References

- Alberio T., Lopiano L., Fasano M., (2012). Cellular models to investigate biochemical pathways in Parkinson's disease. *FEBS Journal*; 279, 1146-1155.
- Allen J.M, Zamurs L., Brachvogel B., Schlotzer-schrehardt U., Hansen U., Lamande S.R., Rowley L., Fitzgerald J., Bateman J.F. (2009). Mice Lacking the Extracellular Matrix Protein WARP Develop Normally but Have Compromised Peripheral Nerve Structure and Function. *J Biol Chem*; 284, 12020-12030.
- Anderson J.L., Head S.I., Rae C., Morley J.W. (2002). Brain function in Duchenne muscular dystrophy. *Brain*; 125, 4-13
- Angelini A., Tiepolo T., Sabatelli P., Grumati P., Bergamin N., Golfieri C., Mattioli E., Gualandi F., Ferlini A., Merlini L., Maraldi N.M., Bonaldo P., Bernardi P. (2007). Mitochondrial dysfunction in the pathogenesis of Ullrich congenital muscular dystrophy and prospective therapy with cyclosporins. *Proc Natl Acad Sci USA*; 104, 991-996.
- Alovskaya A., Alekseeva T., Phillips J.B., King V., Brown R. (2007). Fibronectin, collagen, fibrin-components of extracellular matrix for nerve regeneration. *Topics in Tissue Engineering*; 3, 1-26.
- Bernardi P, Bonaldo P. (2008). Dysfunction of mitochondria and sarcoplasmic reticulum in the pathogenesis of collagen VI muscular dystrophies. *Ann N Y Acad Sci.*; 1147, 303-11.
- Boland B., Kumar A., Lee S., Platt F.M., Wegiel J., Yu W.H., Nixon R.A. (2008). Autophagy induction and autophagosome clearance in neurons: relationship to autophagic pathology in Alzheimer's disease. *The Journal of Neuroscience*; 28, 6926-6937.
- Bonaldo P., Russo V., Bucciotti F., Doliana R., Colombatti A. (1990). Structural and functional features of the alpha 3 chain indicate a bridging role for chicken collagen VI in connective tissues. *Biochemistry*; 29, 1245-1254.
- Bonaldo P., Russo V., Bucciotti F., Doliana R., Colombatti A. (1989). $\alpha 1$ chain of chick type VI collagen. The complete cDNA sequence reveals a hybrid molecule made of one short collagen and three von Willebrand factor type A-like domains. *J Biol Chem*; 264, 5575-5580.
- Bonaldo P., Braghetta P., Zanetti M., Piccolo S., Volpin D., Bressan G.M. (1998). Collagen VI deficiency induces early onset myopathy in the mouse: an animal model for Bethlem myopathy. *Human Molecular Genetics*; 7, 2135-2140.
- Bönnemann C.G. (2011). The collagen VI-related myopathies: muscle meets its matrix. *Nat. Rev. Neurol.*; 7, 379-390
- Braghetta, P., Fabbro, C., Piccolo, S., Marvulli, D., Bonaldo, P., Volpin, D., Bressan, G.M. (1996). Distinct regions control transcriptional activation of the alpha1(VI) collagen promoter in different tissues of transgenic mice. *J. Cell. Biol.* 135, 1163-1177.
- Braunewell K.H., Pesheva P., McCarthy J.B., Furcht L.T., Schmitz B., Schachner M. (1995). Functional involvement of sciatic nerve-derived versican- and decorin-like molecules and other chondroitin sulphate proteoglycans in ECM-mediated cell adhesion and neurite outgrowth. *Eur J Neurosci.*; 7, 805-814.
- Brinas L., Richard P., Quijano-Roy S. (2010) Early onset collagen VI myopathies: genetic and clinical correlations. *Ann Neurol*; 68, 511-520.
- Brückner G. and Grosche J. (2001). Perineuronal nets show intrinsic patterns of extracellular matrix differentiation in organotypic slice cultures. *Exp Brain Res*; 137, 83-93.

- Burg M.A., Tillet E., Timpl R., Stallcup W.B. (1996). Binding of the NG2 proteoglycan to type VI collagen and other extracellular matrix molecules. *J Biol Chem*; 271, 26110–26116.
- Busch S.A., Silver J. (2007). The role of extracellular matrix in CNS regeneration. *Curr. Op. Neurobiol.*; 17, 120-127.
- Caballero B., Coto-Montes A. (2012). An insight into the role of autophagy in cell responses in the aging and neurodegenerative brain. *Histol Histopathol*; 27, 263-275
- Campbell K.P., Stull J.T. (2003). Skeletal muscle basement membrane-sarcolemma-cytoskeleton interaction minireview series. *J Biol Chem.*, 278, 12599-600.
- Carmignac V. and Durbeej M. (2012) Cell-matrix interactions in muscle disease. *J. Pathol*; 226, 200-218.
- Celio M.R., Spreafico R., De Biasi S., Vitellaro-Zuccarello L.(1998). Perineuronal nets: past and present. *Trends Neurosci.*; 21, 510-515.
- Chen H., Chan D.C. (2009). Mitochondrial dynamics—fusion, fission, movement, and mitophagy—in neurodegenerative diseases. *Hu. Mol. Gen.*; 18, R169–R176.
- Chen J. and Herrup K. (2008). Selective vulnerability of neurons in primary cultures and in neurodegenerative diseases. *Rev Neurosci.*; 19, 317-26.
- Cheng I.H., Lin Y.-C., Hwang E., Huang H.-T., Chang W.-H. Liu Y.-L., Chao C.-Y. (2011). Collagen VI protects against neuronal apoptosis elicited by ultraviolet irradiation via an Akt/phosphatidylinositol 3-kinase signaling pathway. *Neurosci.*; 183, 178-188.
- Cheng J.S., Dubal D.B., Kim D.H., Legleiter J., Cheng I.H., Yu G.Q., Tesseur I., Wyss-Coray T., Bonaldo P., Mucke L. (2009). Collagen VI protects neurons against A β toxicity. *Nat Neurosci.*; 12, 119-21.
- Cheung Z.H., Ip N.Y. (2011). Autophagy deregulation in neurodegenerative diseases- recent advances and future perspectives. *J. Neurochem.*; 118, 317-325.
- Christensen S.E., Coles J.M., Zelenski N.A., Furman B.D., Leddy H.A., Zauscher S., Bonaldo P., Guilak F. (2012). Altered trabecular bone structure and delayed cartilage degeneration in the knees of collagen VI null mice. *PLoS One*; 7, e33397.
- Colombatti A., Bonaldo P. (1987). Biosynthesis of chick type VI collagen II. Processing and secretion in fibroblasts and smooth muscle cells. *J. Biol Chem*; 262, 14461-14466.
- Colombatti A., Ainger K., Colizzi F. (1989). Type VI collagen: high yields of a molecule with multiple forms of alpha 3 chain from avian and human tissue. *Matrix Biol.*; 9, 177-185.
- Colombatti A., Mucignat M.T., Bonaldo P. (1995). Secretion and matrix assembly of recombinant type VI collagen. *J Biol. Chem.*; 270, 13105-13111.
- Degli Esposti (2002). Measuring mitochondrial reactive oxygen species. *Methods*; 26, 335–340.
- Di Bartolomeo S., Nazio F., Cecconi F. (2010). The role of autophagy during development in higher eukaryotes, *Traffic*, 1-10.
- Doliana R, Mucignat MT, Segat D, Zanussi S, Fabbro C, Lakshmi TR, Colombatti A.(1998). Alternative splicing of VWFA modules generates variants of type VI collagen alpha 3 chain with a distinctive expression pattern in embryonic chicken tissues and potentially different adhesive function. *Matrix Biol.*; 16, 427-42.
- Eisenberg-Lerner A., Bialik S., Simon H-U., Kimchi A. (2009). Life and death partners: apoptosis, autophagy and the cross-talk between them. *Cell Death Differ.*; 16, 966-75.

- Erlich S., Shohami E. and Pinkas-Kramarski R. (2006). Neurodegeneration induces upregulation of Beclin 1. *Autophagy*; 2, 49-51.
- Ferraro E. e Cecconi F. (2007). Autophagic and apoptotic response to stress signals in mammalian cells. *Archives of Biochemistry and Biophysics*; 462, 210-219.
- Gara S.K., Grumati P., Urciuolo A., Bonaldo P., Kobbe B., Koch M., Paulsson M., Wagener R. (2008). Three novel collagen VI chains with high homology to the $\alpha 3$ chains. *J Biol Chem.*; 283, 10658-70.
- Gara S.K., Grumati P., Squarzone S., Sabatelli P., Urciuolo A., Bonaldo P., Paulsson M., Wagener R. (2011). Differential and restricted expression of novel collagen VI chains in mouse. *Matrix Biology*; 30, 248-257.
- Giamanco K.A., Morawski M., Matthews R.T. (2010). Perineuronal net formation and structure in aggrecan knockout mice. *Neuroscience*; 170, 1314–1327.
- Gillies A.R., Lieber B.S., Lieber R.L. (2011) Structure and function of the skeletal muscle extracellular matrix. *Muscle Nerve*; 44, 318-331.
- Goody M.F. and Henry C.A. (2010). Dynamic interactions between cells and their extracellular matrix mediate embryonic development. *Molecular reproduction & development*; 77, 475-488.
- Grumati P., Coletto L., Sabatelli P., Cescon M., Angelin A., Bertaglia E., Blaauw B., Urciuolo A., Tiepolo T., Merlini L., Maraldi N.M., Bernardi P., Sandri M., Bonaldo P. (2010). Autophagy is defective in collagen VI muscular dystrophies and its reactivation rescues myofiber degeneration. *Nature Medicine*; 16, 1313-1320.
- Gualandi F., Curci R., Sabatelli P., Martoni E., Bovolenta M., Maraldi M.N., Merlini L, Ferlini A. (2011). Macrophages: a minimally invasive tool for monitoring collagen VI myopathies. *Muscle and Nerve*; 44, 80-84.
- Gullberg D., Tiger C.-F. and Velling T. (1999). Laminins during muscle development and in muscular dystrophies. *CMLS, Cell. Mol. Life Sci.*; 56, 442–460
- Han J., Daniel J.C., Lieska N., Pappas G.D. (1994). Immunofluorescence and biochemical studies of the type VI collagen expression by human glioblastoma cells in vitro. *Neurol Res.*; 16, 370-5.
- Han J., Daniel J.C., Pappas G.D. (1995). Expression of type VI collagen during glioblastoma cell invasion in brain tissue cultures. *Cancer Lett.*; 88, 127-32.
- Hara, T., Nakamura, K., Matsui, M., Yamamoto, A., Nakahara, Y., Suzuki-Migishima, R., Yokoyama, M., Mishima, K., Saito, I., Okano, H. and Mizushima, N. (2006) Suppression of basal autophagy in neural cells causes neurodegenerative disease in mice. *Nature*; 441, 885-889.
- Hardingham T.E, Fosang A. (1992). Proteoglycans: many forms and many functions. *The FASEB Journal*; 6, 861-870.
- Hashimoto, T., Wakabayashi, T., Watanabe, A., Kowa, H., Hosoda, R., Nakamura, A., Kanazawa, I., Arai, T., Takio, K., Mann, D. M., and Iwatsubo, T. (2002) . CLAC: a novel Alzheimer amyloid plaque component derived from a transmembrane precursor, CLAC-P/collagen type XXV. *EMBO J.*; 21, 1524-1534
- Huang J., Lam G.Y., Brumell J.H. (2011). Autophagy signaling through reactive oxygen species. *Antioxidants & Redox Signaling*; 14, 2215-2231.
- Hubert T., Grimal S., Ratzinger S., Mechaly I., Grassel S., Fichard-Carroll A.(2007). Collagen XVI is a neural component of the developing and regenerating dorsal root ganglia extracellular matrix. *Matrix Biol.*; 26, 206-10.

- Hubert T., Grimal S., Carroll P. and A. Fichard-Carroll A. (2008). Collagens in the developing and diseased nervous system. *Cell Mol Life Sci.*; 66, 1223-38.
- Hynes R.O. (2009). The Extracellular Matrix: not just pretty fibrils. *Science*; 326, 1216-9.
- Ichimura Y., Komatsu M. (2011). Pathophysiological role of autophagy: lesson from autophagy-deficient mouse models. *Exp. Anim.*; 60, 329-345.
- Ichimura Y., Kominami E., Tanaka K., Komatsu M. (2008). Selective turnover of p62/A170/SQSTM1 by autophagy. *Autophagy*; 4, 1063-1066.
- Ioannou Y.A., Chen F.W. (2006). Quantitation of DNA fragmentation in apoptosis. *Nucleic Acids Research*; 24, 992-993.
- Iozzo R., Sanderson R.D. (2011). Proteoglycans in cancer biology, tumour microenvironment and angiogenesis. *J. Cell. and Mol. Med.*; 15, 1013–1031.
- Irwin W.A., Bergamin N., Sabatelli P., Reggiani C., Megighian A., Merlini L., Braghetta P., Columbaro M., Volpin D., Bressan G.M., Bernardi P., Bonaldo P. (2003). Mitochondrial dysfunction and apoptosis in myopathic mice with collagen VI deficiency. *Nat Genet*; 35, 267–271.
- Iyengar P., Espina V., Williams T.W., Lin Y., Berry D., Jelicks A., Lee H., Temple K. (2005). Adipocyte-derived collagen VI affects early mammary tumor progression in vivo, demonstrating a critical interaction in the tumor/stroma microenvironment. *J. Clin. Invest.*; 115, 1163-1176.
- Jaakkola, S., Peltonen, J., Riccardi, V., Chu, M.-L., Uitto, J., (1989). Type 1 neurofibromatosis: selective expression of extracellular matrix genes by Schwann cells, perineurial cells, and fibroblasts in mixed cultures. *J.Clin. Invest.* 84, 253-261.
- Jaeger P.A., Wyss-Coray T. (2009). All-you-can-eat: autophagy in neurodegeneration and neuroprotection. *Molecular Neurodegeneration*; 4, 16.
- Karbowski M., Lee Y., Gaume B., Jeong S., Frank S., Nechushtan A., Santel A., Fuller M., Smith C.L., Youle R. J. (2002). Spatial and temporal association of Bax with mitochondrial fission sites, Drp1 and Mfn2, during apoptosis. *J.Cell. Biol.*; 159, 931-938.
- Karetko M., Skangiel-Kramska J. (2009). Deverse functions of perineuronal nets. *Acta Neurobiol Exp.*; 69, 564-577.
- Keene, D. R., Engvall, E., Glanville, R. W. (1988) *J. Cell Biol.*; 107, 1995–2006
- Khan T., Muise E.S., Iyengar P., Wang Z.V., Chandalia M., Abate N., Zhang B.B., Bonaldo P., Chua S., Scherer P.E. (2009) Metabolic dysregulation and adipose tissue fibrosis: role of collagen VI. *Mol. Cell. Biol.*; 29, 1575–1591.
- Klionsky *et al.* (2008). Guidelines for the use and interpretation of assays for monitoring autophagy in higher eukaryotes. *Autophagy*; 4, 151-175.
- Komatsu, M., Waguri, S., Chiba, T., Murata, S., Iwata, J., Tanida, I., Ueno, T., Koike, M., Uchiyama, Y., Kominami, E., Tanaka, K. (2006). Loss of autophagy in the central nervous system causes neurodegeneration in mice. *Nature*; 441, 880-884.
- Kovanen V. (2002). Intramuscular extracellular matrix: Complex environment of muscle cells. *Exerc Sport Sci Rev.*; 30, 20-25.
- Krüger U., Wang Y., Kmar S., Mandelkow E.-M. (2011). Autophagic degradation of tau in primary neurons and its enhancement by trehalose. *Neurobiology of Aging*;

- Kubota C., Torii S., Hou N., Saito N., Yoshimoto Y., Imai H., Takeuchi T. (2010). Constitutive reactive oxygen species generation from autophagosome/lysosome in neuronal oxidative toxicity. *J. Biol. Chem.*; 285, 667–674.
- Kuo H.J., Maslen C.L., Keene D.R., Glanville R.W. (1997). Type VI collagen anchors endothelial basement membranes by interacting with type IV collagen. *J. Biol. Chem.*; 272, 26522-29.
- Lee J.-A. (2009). Autophagy in neurodegeneration: two sides of the same coin. *BMB reports*; 42, 324-330.
- La Marca R., Cerri F., Horiuchi K., Bachi A., Feltri M.L., Wrabetz L., Blobel C.P., Quattrini A., Salzer J.L., Taveggia C. (2011). TACE (ADAM17) inhibits Schwann cell myelination. *Nature Neuroscience*; 14, 857-867.
- Lampe A.K., Bushby K.M. (2005). Collagen VI related muscle disorders. *J. Med. Genet.*; 42, 673-685.
- Luther D.J., Thodeti C.K., Shamhart P.E., Adapala R.K., Hodnichak C., Weihrauch D., Bonaldo P., Chilian W.M., Meszaros J.G. (2012) Absence of type VI collagen paradoxically improves cardiac function, structure, and remodeling after myocardial infarction. *Circ Res.*; 110, 85.
- Ma Q., Qiang J., Gu P., Wang Y., Geng Y., Wang M. (2011). Age-related autophagy alterations in the brain of senescence accelerated mouse prone 8 (SAMP8) mice. *Experimental Gerontology*; 46: 533–541
- Maertens B., Hopkins D., Franzke C.W., Keene D.R., Bruckner-Tuderman L., Greenspan D.S., Koch M. (2007). Cleavage and oligomerization of gliomedin, a transmembrane collagen required for node of ranvier formation. *J Biol Chem.*; 282, 10647-59.
- Maiuri M.C., Zalekvar E., Kimchi A., Kroemer G. (2007). Self- eating and self-killing: crosstalk between autophagy and apoptosis. *Nature Reviews*; 8, 741-752.
- Malicdan, M.C., Noguchi, S., Nonaka, I., Saftig, P. & Nishino, I. (2008). Lysosomal myopathies: an excessive build-up in autophagosomes is too much to handle. *Neuromuscul. Disord.*; 18, 521–529.
- Mammucari, C., Milan G., Romanello V, Masiero E, Rudolf R, Del Piccolo P, Burden SJ, Di Lisi R, Sandri C, Zhao J, Goldberg AL, Schiaffino S, Sandri M. (2007). FoxO3 controls autophagy in skeletal muscle in vivo. *Cell Metab.*; 6, 458–471.
- Mariño G., Ugalde A.P., Salvador-Montoliu N., Varela I., Quiros P.M., Cadinanos J., van der Pluijm I., Freije J.M., Lopez-Otin C. (2008). Premature aging in mice activates a systemic metabolic response involving autophagy induction. *Hum. Mol. Genet.*; 17, 2196-2211.
- Mariño G., Fernandez A.F. and Lopez-Otin C. (2010). Autophagy and aging: lessons from progeria models. *Adv. Exp. Med. Biol.*; 694: 61-68.
- Marvulli, D., Volpin, D., Bressan, G.M., (1996). Spatial and temporal changes of type VI collagen expression during mouse development. *Dev. Dyn.* 206, 447-454.
- Matusica D., Fenech M.P., Rogers M.-L., Rush R.A. (2008). Characterization and use of the NSC-34 cell line for study of neurotrophin receptor trafficking. *Journal of Neuroscience Research*; 86, 553-565.
- McCray B.A., Taylor J.P. (2008). The role of autophagy in age-related neurodegeneration. *Neurosignals*; 16, 75-84.
- McGarvey ML, Baron-Van Evercooren A, Kleinman HK, Dubois-Dalcq M (1984) Synthesis and effects of basement membrane components in cultured rat Schwann cells. *Dev Biol*; 105, 18-28.

- Menazza S., Blaauw B., Tiepolo T., Toniolo L., Braghetta P., Spolaore B., Reggiani C., Di Lisa F., Bonaldo P., Canton M. (2010). Oxidative stress by monoamine oxidases is causally involved in myofiber damage in muscular dystrophy. *Hum Mol Genet.*; 19, 4207-15.
- Merlini L., Angelin A., Tiepolo T., Braghetta P., Sabatelli P., Zamparelli A., Ferlini A., Maraldi N.M., Bonaldo P., Bernardi P. (2008a). Cyclosporin A corrects mitochondrial dysfunction and muscle apoptosis in patients with collagen VI myopathies. *Proc. Natl. Acad. Sci. USA*; 105, 5225-9.
- Merlini L., Martoni E., Grumati P., Sabatelli P., Squarzoni S., Urciuolo A., Ferlini A., Gualandi F., Bonaldo P. (2008b). Autosomal recessive myosclerosis myopathy is a collagen VI disorder. *Neurology*; 71, 1245-53.
- Milner R. (1997) Understanding the molecular basis of cell migration; implications for clinical therapy in multiple sclerosis. *Clin Sci (Lond)*; 92,113-122.
- Mizushima N. (2004). Methods for monitoring autophagy. *IJBCB*; 36, 2491-2502.
- Mizushima N., Yamamoto A., Matsui M., Yoshimori T., Ohsumi Y. (2004) In vivo analysis of autophagy in response to nutrient starvation using transgenic mice expressing a fluorescent autophagosome marker. *Mol Biol Cell*; 15, 1101-1111.
- Mizushima N., Levine B., Cuervo A.M., Klionsky D.J. (2008) Autophagy fights disease through cellular self-digestion. *Nature*; 451, 1069-75.
- Mizushima N., Yoshimori T., Levine B., 2010. Methods in mammalian autophagy research. *Cell*; 140, 313-326.
- Moscat J., Diaz-Meco M.T. (2009). P62 at the crossroads of autophagy, apoptosis and cancer. *Cell*, 137, 1001-1004.
- Nishimura S., Tabata S., Nakamura Y.N., Okano K., Iwamoto H. (2004). Three dimensional architecture and distribution of collagen components in the goat hypophysis. *Anat Rec A Discov Mol Cell Evol Biol.*, 277(2), 275-86.
- Novak U., Kaye A.H. (2000). Extracellular matrix and the brain: components and function. *J. Clin. Neurosci.*; 7,280-290.
- Perini G.I., Menegazzo E., Ermani M., Zara M., Gemma A., Ferruzza E., Gennarelli M., Angelini C. (1999). Cognitive impairment and (CTG)_n expansion in myotonic dystrophy patients. *Biol Psychiatry*; 46, 425-31.
- Perris, R., Kuo, H.-J., Glanville, R.W., Bronner-Fraser, M., (1993). Collagen type VI in neural crest development: distribution in situ and interaction with cells in vitro. *Dev. Dyn.*; 198, 135-149.
- Piccioni F., Simeoni S., Andriola I., Armatura E., Bassanini S., Pozzi P., Poletti A. (2001). Polyglutamine tract expansion of the androgen receptor in a motoneuronal model of spinal and bulbar muscular atrophy. *Brain Res Bull*; 56, 215-20.
- Pickford F., Masliah E., Britschgi M., Lucin K., Narasimhan R., Jaeger P.A., Small S., Spencer B., Rockenstein E., Levine B., Wyss-Coray T. (2008). The autophagy-related protein beclin 1 shows reduced expression in early Alzheimer disease and regulates amyloid beta accumulation in mice. *J. Clin. Invest.*; 118, 2190-2199.
- Probstmeier R., Nellen J., Gloor S., Wernig A., Pesheva P. (2001) Tenascin-R is expressed by Schwann cells in the peripheral nervous system. *J Neurosci Res*; 64,70-78.
- Pujol A., Hindelang C., Callizot N., Bartsch U., Schchner M., Mandel J.L. (2002). Late onset neurological phenotype of the X-ALD gene inactivation in mice: a mouse model for adrenomyeloneuropathy. *Human Molecular Genetics*; 11, 499-505.

- Quarto R., Dozin B., Bonaldo P., Cancedda R., Colombatti A. (1993). Type VI collagen expression is upregulated in the early events of chondrocyte differentiation. *Development*; 117, 245-251.
- Ray B., Bailey J.A., Sarkar S., Lahiri D.K. (2009). Molecular and immunocytochemical characterization of primary neuronal cultures from adult rat brain: Differential expression of neuronal and glial protein markers. *J Neurosci Methods*; 184, 294-302.
- Roediger B., Armati P.J. (2003). Oxidative stress induces axonal beading in cultured human brain tissue. *Neurobiol Dis*; 13, 222-9.
- Rubinsztein D.C., Gestwicki J.E., Murphy L.O., Klionsky D.J. (2007). Potential therapeutic applications of autophagy. *Nat. Rev. Drug Discov*; 6, 304–312.
- Rühl M., Sahin E., Johannsen M., Somasundaram R., Manski D., Riecken E.O., Schuppan D. (1999). Soluble collagen VI drives serum-starved fibroblasts through S phase and prevents apoptosis via down-regulation of Bax. *J Biol Chem*; 274, 34361-8.
- Rutka J.T., Apodaca G., Stern R., Rosenblum M. (1988). The extracellular matrix of the central and peripheral nervous systems: structure and function. *J Neurosurg*; 69, 155-70.
- Sabatelli P., Bonaldo P., Lattanzi G., Braghetta P., Bergamin N., Capanni C., Mattioli E., Columbaro M., Ognibene A., Pepe G., Bertini E., Merlini L., Maraldi N.M., Squarzone S. (2001). Collagen VI deficiency affects the organization of fibronectin in the extracellular matrix of cultured fibroblasts. *Matrix Biol*; 20, 475–486.
- Saitta B., Stokes D.G., Vissing H., Timpl R., Chu M.L. (1990). Alternative splicing of the human alpha 2(VI) collagen gene generates multiple mRNA transcripts which predict three protein variants with distinct carboxyl termini. *J Biol Chem*; 265, 6473–80.
- Sánchez-Danés A., Richaud-Patin Y., Carballo-Carbajal I., Jiménez-Delgado S., Caig C., Mora S., Di Guglielmo C., Ezquerro M., Patel B., Giralto A., Canals J.M., Memo M., Alberch J., López-Barneo J., Vila M., Cuervo A.M., Tolosa E., Consiglio A., Raya A. (2012). Disease-specific phenotypes in dopamine neurons from human iPS-based models of genetic and sporadic Parkinson's disease. *EMBO Mol Med*; 4, 380-95.
- Sanes J.R. (2003). The basement membrane/basal lamina of skeletal muscle. *J Biol Chem*; 278, 12601–12604.
- Scorrano L. (2005). Proteins that fuse and fragment mitochondria in apoptosis: con-fissioning a deadly con-fusion? *Journal of Bioenergetics and Biomembranes*; 37(3), 165-170.
- Seibenhener, M. L., Wooten, M. W. (2012). Isolation and Culture of Hippocampal Neurons from Prenatal Mice. *J. Vis. Exp.*; 65, e3634.
- Seppänen A., Autio-Harmainen H., Alafuzoff I., Sarkioja T., Veijola J., Hurskainen T., Bruckner-Tuderman L., Tasanen K., Majamaa K. (2006). Collagen XVII is expressed in human CNS neurons. *Matrix Biol*; 25, 185–188.
- Seppänen A., Pikkarainen M., Hartikainen P., Hofmann S.C., Majamaa K., Alafuzoff I. (2009). Expression of collagen XVII and ubiquitin-binding protein p62 in motor neuron disease. *Brain Research*; 1247, 171-177.
- Shastri P., Basu A., Rajadhyaksha M.S. (2001). Neuroblastoma cell lines: a versatile in vitro model in neurobiology. *Int J Neurosci*; 108, 109-26.
- Sievers J., Pehlemann F.W., Gude S., Berry M. (1994). Meningeal cells organize the superficial glia limitans of the cerebellum and produce components of both the interstitial matrix and the basement membrane. *J. Neurocytol*; 23, 135-149.

- Son J.H., Shim J.H., Kim K.-H., Ha J.-L., Han J.Y. (2012). Neuronal autophagy and neurodegenerative diseases. *Experimental and molecular medicine*; 44, 89-98.
- Soontornniyomkij V., Risbrough V.B., Young J.W., Soontornniyomkij B., Jeste D.V., Achim C.L. (2012). Increased hippocampal accumulation of autophagosomes predicts short-term recognition memory impairment in aged mice. *Age*; 34, 305–316.
- Stallcup W.B. (2002). The NG2 proteoglycan: past insights and future prospects. *Journal of Neurocytology*; 31, 423-435.
- Stokin G.B., Lillo C., Falzone T.L., Brusch R.G., Rockenstein E., Mount S.L., Raman R., Davies P., Masliah E., Williams D.S., Goldstein L.S.B. (2005). Axonopathy and Transport Deficits Early in the Pathogenesis of Alzheimer's Disease. *Science*; 307, 1282.
- Sund M., Väisänen T., Kaukinen S., Ilves M., Tu H., Autio-Harminen H., Rauvala H., Pihlajaniemi T. (2001). Distinct expression of type XIII collagen in neuronal structures and other tissues during mouse development. *Matrix Biol.*; 20, 215-31.
- Svineng, G., Ravuri, C., Rikardsen, O., Huseby, N.E., Winberg, J.O. (2008). The role of reactive oxygen species in integrin and matrix metalloproteinase expression and function. *Connect. Tissue Res.*; 49, 197–202.
- Ughrin YM, Chen ZJ, Levine JM (2003) Multiple regions of the NG2 proteoglycan inhibit neurite growth and induce growth cone collapse. *J Neurosci*; 23, 175-186.
- Taddei, M.L., Parri, M., Mello, T., Catalano, A., Levine, A.D., Raugei, G., Ramponi, G., Chiarugi, P. (2007). Integrin-mediated cell adhesion and spreading engage different sources of reactive oxygen species. *Antioxid.Redox Signal.*; 9, 469–481.
- Takeda, T., Matsushita, T., Kurozumi, M., Takemura, K., Higuchi, K., Hosokawa, M., (1997). Pathobiology of the senescence-accelerated mouse (SAM). *Exp. Gerontol*; 32, 117–127.
- Tan S., Wood M., Maher P. (1998). Oxidative stress induces a form of programmed cell death with characteristics of both apoptosis and necrosis in neuronal cells. *Journal of Neurochemistry*; 71, 95-105.
- Terman A, Gustafsson B, Brunk UT. (2006). The lysosomal-mitochondrial axis theory of postmitotic aging and cell death. *Chem Biol Interact.*; 27, 29-37.
- Tsang KY., Cheung MC., Chan D., Cheah KS. (2010). The developmental roles of the extracellular matrix: beyond structure to regulation. *Cell Tissue Res.*; 339, 93-110.
- Vitale P. Braghetta P., Volpin D., Bonaldo P., Bressan G.M. (2001). Mechanisms of transcriptional activation of the col6a1 gene during Schwann cell differentiation. *Mechanisms of development* 102, 145-156.
- Wojcik-Stanaszek L., Gregor A., Zalewska T. (2011). REgulation of neurogenesis by extracellular matrix and integrins. *Acta Neurobiol. Exp.*; 71, 103-112.
- Wood M.D., Kemp S.W.P., Weber C., Borschel G.H., Gordon T. (2011). Outcome measures of peripheral nerve regeneration. *Annals of Anatomy*; 193, 321-333.
- Xu Y.Z., Deng X.H., Bentivoglio M. (2007). Differential response of apoptosis-regulatory Bcl-2 and Bax proteins to an inflammatory challenge in the cerebral cortex and hippocampus of aging mice. *Brain Res Bull.*; 74, 329-35.
- Yamamoto A., Cremona M.L., Rothman J.E. (2006). Autophagy-mediated clearance of huntingtin aggregates triggered by the insulin-signaling pathway. *Journal of Cell Biology*; 172, 719-731.
- Yang P., Baker K.A., Hagg T. (2006). The ADAMs family: coordinators of nervous system

development, plasticity and repair. *Prog. Neurobiol.*; 79, 73–94.

You W.K., Bonaldo P., Stallcup W.B. (2012). Collagen VI ablation retards brain tumor progression due to deficits in assembly of the vascular basal lamina. *Am. J. Pathol.*; 180, 1145-58.

Young J.E., Martinez R.A., La Spada A.R. (2009). nutrient deprivation induces neuronal autophagy and implicates reduced insulin signaling in neuroprotective autophagy activation. *The Journal Of Biological Chemistry*; 284, 2363–2373.

Yu W.H., Cuervo A.M., Kumar A., Peterhoff C.M., Schmidt S.D., Lee J.H., Mohan P.S., Mercken M., Farmery M.R., Tjernberg L.O., Jiang Y., Duff K., Uchiyama Y., Na˚slund J., Mathews P.M., Cataldo A.M., Nixon R.A. (2005). Macroautophagy—a novel beta-amyloid peptide-generating pathway activated in Alzheimer’s disease. *J Cell Biol*; 171, 87–98.

Yue J., Zhang K., Chen J.F. (2012). Role of Integrins in Regulating Proteases to Mediate Extracellular Matrix Remodeling. *Cancer Microenvironment*; 5, 275–283.

Zeng M., Zhou J.N. (2008). Roles of autophagy and mTOR signaling in neuronal differentiation of mouse neuroblastoma cells . *Cell Signal.*; 20, 659-6.

Zhang KZ., Westberg JA., Hölttä E., Andersson LC. (1996). BCL2 regulates neural differentiation. *Proc Natl Acad Sci USA*; 93, 4504-8.

Zimmermann D.R., Dours-Zimmermann M.T. (2008). Extracellular matrix of the central nervous system: from neglect to challenge. *Histochem Cell Biol.*; 130, 635-653.